UNIVERSITÀ DEGLI STUDI DI MILANO

Dottorato in Scienze Farmacologiche Biomolecolari, Sperimentali e Cliniche

XXXV Ciclo

Dipartimento di Scienze Farmacologiche e Biomolecolari

UNRAVELLING SEX-DEPENDENT MECHANISMS IN CALCIFIC AORTIC VALVE STENOSIS

BIO/14

Dott. Donato MOSCHETTA

Matricola R12600

TUTOR: Chiar.ma Prof.ssa Marina Camera

COTUTOR: Dott. Paolo Poggio

COORDINATORE: Chiar.mo Prof. Giuseppe Danilo Norata

A.A.

2021 - 2022

Index

List of included papers

I. Sex-specific differences in age-related aortic valve calcium load: A systematic review and meta-analysis.

Myasoedova V.A., Di Minno A., Songia P., Massaiu I., Alfieri V., Valerio V., Moschetta D., Andreini D., Alamanni F., Pepi M., Trabattoni D., Poggio P.

Ageing Research Reviews, 2020 Aug; 61:101077

II. Sex-Specific Features of Calcific Aortic Valve Disease.

Summerhill V.I., Moschetta D., Orekhov A.N., Poggio P., Myasoedova V.A.

International Journal of Molecular Sciences, 2020 Aug; 6;21(16):5620

III. Evaluation of Oxford Nanopore MinION RNA-Seq Performance for Human Primary Cells.

Massaiu I., Songia P., Chiesa M., Valerio V., Moschetta D., Alfieri V., Myasoedova V.A., Schmid M., Cassetta L., Colombo G.I., D'Alessandra Y., Poggio P.

International Journal of Molecular Sciences, 2021 Jun; 12;22(12):6317

IV. Sex-Specific Cell Types and Molecular Pathways Indicate Fibro-Calcific Aortic Valve Stenosis.

Myasoedova V.A., Massaiu I., Moschetta D., Chiesa M., Songia P., Valerio V., Alfieri V., Capoulade R., Trabattoni D., Andreini D., Mass E., Parisi V., Poggio P.

Frontiers in Immunology, 2022 Feb; 24;13:747714

V. Purinergic Receptor P2Y2 Stimulation Averts Aortic Valve Interstitial Cell Calcification and Myofibroblastic Activation.

Moschetta D., Di Maria E., Valerio V., Massaiu I., Bozzi M., Songia P., D'alessandra Y., Myasoedova V.A., Poggio P.

Biomedicines, 2022 Feb; 16;10(2):457

ABSTRACT

Calcific aortic valve stenosis (CAVS) is the most common form of heart valve disease and affects about 3% of the population. Its prevalence increases with age, without a causal relation between ageing and CAVS development. To date, CAVS is a slow, progressive, multifactorial disorder considered to be actively driven by several cellular and molecular processes. Its natural history consists of a long clinically silent phase of non-uniform leaflet thickening with or without minimal calcification, known as aortic valve sclerosis (AVSc), without significant obstruction of blood flow, followed by the symptomatic stage, the aortic valve stenosis (AS). Currently, there is no pharmacological therapy preventing CAVS progression nor treating patients with AS. As a result, surgical or percutaneous aortic valve replacement remain the only treatments for severe AS, leaving the pathological molecular and cellular mechanisms unsolved.

One of the first trigger of the pathology due to the oxidative stress is the endothelial dysfunction, followed by local inflammation and interstitial cells (VIC) differentiation into myofibroblasts and osteoblasts.

Activated valve endothelial cells, undergoing endothelial to mesenchymal transition (EndMT), begin to express mesenchymal adhesion molecules and facilitate monocytes infiltration and local inflammation. These environmental changes induce VIC trans-differentiation into myofibroblast- and osteoblast-like cells. Activated VICs carry out a progressive extracellular matrix (ECM) pathological rearrangement characterized by the activation of fibrosis and calcification processes, which ultimately drive to fibro-calcific deposit formation.

In the last years different studies reported sex-related difference in molecular mechanisms in the context of CAVS. In particular, it was shown that men with AS show a higher aortic valve calcium (AVC) load than women. Recently, it has been described that woman aortic valve leaflets were more fibrotic than man ones. Hence, it has been hypothesized that the mechanisms underlying CAVS progression could be different between the two sexes.

We confirmed the evidence on sex-related calcium load in a meta-analysis performed on almost three thousand AS patients. Based on our results, AVC load, evaluated by computed tomography, is higher in man AS patients than in woman ones, even normalizing the data for the state of the pathology and for the aortic

annulus area. By the CT scan images analysis, we confirmed also the higher prevalence of fibrotic tissue in woman AS patients, than in men.

In silico analysis of whole tissue RNA microarray revealed that the cellular composition of the aortic valve was different between men and women with CAVS. In particular, women showed a prevalence of mesenchymal cells, while in men there was a prevalence of inflammatory cells. This finding was in line with the analysis of circulating cytokines: pro inflammatory cytochines such as IL1β, TNFα, INFβ, and INFγ were upregulated in men CAVS patients.

Based on these premises, we isolated and characterized VICs from AS patients and performed RNA sequencing to evaluate the differentially expressed molecular mechanisms. Among pathways overactivated in men there was the mitochondrial gene expression and this finding was confirmed by the higher mitochondrial damage in AS VICs from men respect to the one from women. We hypothesized that the mitochondrial damage caused a lower ATP production, therefore we evaluated the effects of a synthetic ATP equivalent, the 2ThioUTP, on the extracellular calcification of VICs from CAVS men. The *in vitro* 2ThioUTP administration showed indeed lower extracellular calcification of CAVS VICs both in normal and pro-calcifying conditions.

All these data, taken together with robust literature evidences, shed light on the influence of sex in the development and progression of CAVS disease. Further studies are needed to better define the sexual dimorphism of this detrimental pathology. The recognition of sex-specific molecular mechanisms, linked to AS onset, may help in the identification of a gender-specific targeted therapy. In this direction, novel pharmacological therapies intended to reduce or even halt CAVS progression could be discovered, providing the basis for a personalized medicine approach in the context of CAVS.

RIASSUNTO

La stenosi calcifica della valvola aortica (CAVS) è la forma più comune di malattia delle valvole cardiache e colpisce circa il 3% della popolazione. La sua prevalenza aumenta con l'età, senza una relazione causale tra l'invecchiamento e lo sviluppo della CAVS. Ad oggi, la CAVS è considerata una patologia lenta, progressiva e multifattoriale, il cui sviluppo è provocato da diversi processi cellulari e molecolari. La sua storia naturale consiste in una lunga fase clinicamente silente di ispessimento non uniforme del lembo con o senza micro-calcificazioni, nota come sclerosi della valvola aortica (AVSc), senza ostruzione significativa del flusso sanguigno, seguito dalla fase sintomatica, la stenosi valvolare aortica (AS). Attualmente non esiste una terapia farmacologica che prevenga la progressione della CAVS o in grado di revertire il fenotipo patologico dei pazienti con AS. Di conseguenza, la sostituzione chirurgica o transcatetere della valvola aortica rimane l'unico trattamento per la AS grave, lasciando irrisolti i meccanismi patologici molecolari e cellulari.

Uno dei primi fattori scatenanti della patologia è l'aumento dello stress ossidativo che causa la disfunzione endoteliale, seguita dallo sviluppo dell'infiammazione locale e dal differenziamento delle cellule interstiziali (VIC) in miofibroblasti e osteoblasti.

Le cellule endoteliali valvolari attivate, in fase di transizione endotelio-mesenchimale (EndMT), esprimono molecole di adesione di origine mesenchimale e facilitano l'infiltrazione di monociti e lo sviluppo dell'infiammazione locale. Questi cambiamenti ambientali inducono la trans-differenziazione delle VIC in cellule simili a miofibroblasti e/o osteoblasti. Le VIC attivate portano avanti un progressivo riarrangiamento patologico della matrice extracellulare (ECM) caratterizzato dall'attivazione di processi di fibrosi e calcificazione.

Negli ultimi anni diversi studi hanno riportato differenze legate al sesso nei meccanismi molecolari nel contesto della CAVS. In particolare, è stato dimostrato che gli uomini con AS presentano un accumulo di calcio della valvola aortica (AVC) più elevato rispetto alle donne. Recentemente, è stato descritto che i foglietti della valvola aortica delle donne sono più fibrotici di quelli degli uomini. Si è quindi ipotizzato che i meccanismi alla base della progressione della CAVS possano essere diversi tra i due sessi.

Abbiamo confermato l'evidenza sul carico di calcio dipendente dal sesso in una meta-analisi condotta su quasi tremila pazienti affetti da AS. In base ai nostri risultati, il carico di AVC, valutato mediante tomografia computerizzata, è più elevato nei pazienti AS di sesso maschile rispetto a quelli di sesso femminile, anche normalizzando i dati per lo stato della patologia e per l'area dell'anulus aortico. L'analisi delle immagini della TAC ha confermato anche la maggiore prevalenza di tessuto fibrotico nei pazienti AS di sesso femminile rispetto a quelli di sesso maschile.

L'analisi in silico del microarray di RNA dell'intero tessuto ha rivelato che la composizione cellulare della valvola aortica è diversa tra uomini e donne con CAVS. In particolare, le donne hanno mostrato una prevalenza di cellule mesenchimali, mentre negli uomini c'era una prevalenza di cellule infiammatorie. Questo risultato è in linea con l'analisi delle citochine circolanti: le citochine pro-infiammatorie come IL1β, TNFα, INFβ e INFγ sono risultate sovra-espresse negli uomini affetti da CAVS.

Sulla base di queste premesse, abbiamo isolato e caratterizzato le VIC dei pazienti con AS e abbiamo eseguito il sequenziamento dell'RNA per valutare i meccanismi molecolari differenzialmente espressi. Tra le vie iperattivate negli uomini c'era l'espressione genica mitocondriale e questo dato è stato confermato dal danno mitocondriale più elevato nelle VICs degli uomini rispetto a quelle delle donne con AS. Abbiamo ipotizzato che il danno mitocondriale causasse una minore produzione di ATP, pertanto abbiamo valutato gli effetti di un equivalente di ATP sintetico, il 2ThioUTP, sulla calcificazione extracellulare delle VIC di uomini affetti da CAVS. La somministrazione in vitro di 2ThioUTP ha mostrato effettivamente una minore calcificazione extracellulare delle VIC di pazienti con CAVS sia in condizioni normali che pro-calcifiche.

Tutti questi dati, insieme alle solide evidenze della letteratura, gettano luce sull'influenza del sesso nello sviluppo e nella progressione della CAVS. Sono necessari ulteriori studi per definire meglio il dimorfismo sessuale di questa patologia invalidante. Il riconoscimento dei meccanismi molecolari sesso-specifici, legati all'insorgenza della CAVS, può contribuire all'identificazione di una terapia mirata specifica per il sesso. In questa direzione, potrebbero essere scoperte nuove

terapie farmacologiche destinate a ridurre o addirittura ad arrestare la progressione della CAVS, fornendo le basi per un approccio di medicina di genere nel contesto della CAVS.

PURPOSE

Although calcific aortic valve stenosis is a debilitating disease, no pharmacological treatments are available. Surgical or transcatheter aortic valve substitution are the only available options to arrest the disease progression. For this reason, the search for pharmacological targets is of critical importance to reduce the costs for the national health system and to have an alternative to the surgery. In the last decade, several studies reported sex dimorphism in the progression of the pathology.

Hence, the aim of this project is to deeply investigate sex-differences in CAVS onset and progression at molecular and cellular level. The recognition of sex-specific molecular mechanisms, linked to AS onset, may help in the identification of patients at high-risk. In this direction, novel pharmacological therapies intended to reduce or even halt CAVS progression could be discovered, providing the basis for a personalized medicine approach in the context of CAVS.

1. INTRODUCTION

1.1. The heart

The heart is a hollow organ situated under the rib cage in the anterior mediastinum. It is the main organ of the cardiovascular system that, acting as a pump, lets the blood to reach all the body's districts. It is mainly constituted by muscular tissue, but it has also districts able to generate and conduct the contractile impulse. Anatomically, it is divided by a septum into a left and a right side. Each side is composed of two chambers known as the atrium and the ventricle. Each atrium is connected to the respective ventricle, which is separated by a valve. In particular, the right atrium pumps the blood into the right ventricle, by opening the tricuspid valve. Then, the right ventricle pumps deoxygenated blood into the pulmonary artery by the pulmonary valve. The pulmonary artery brings the blood into the lung (pulmonary or small circulation), where it could be oxygenated. From the lung, the blood goes back to the heart by the pulmonary vein and reaches the left atrium. After the contraction of the left atrium, the mitral (or bicuspid) valve is forced to

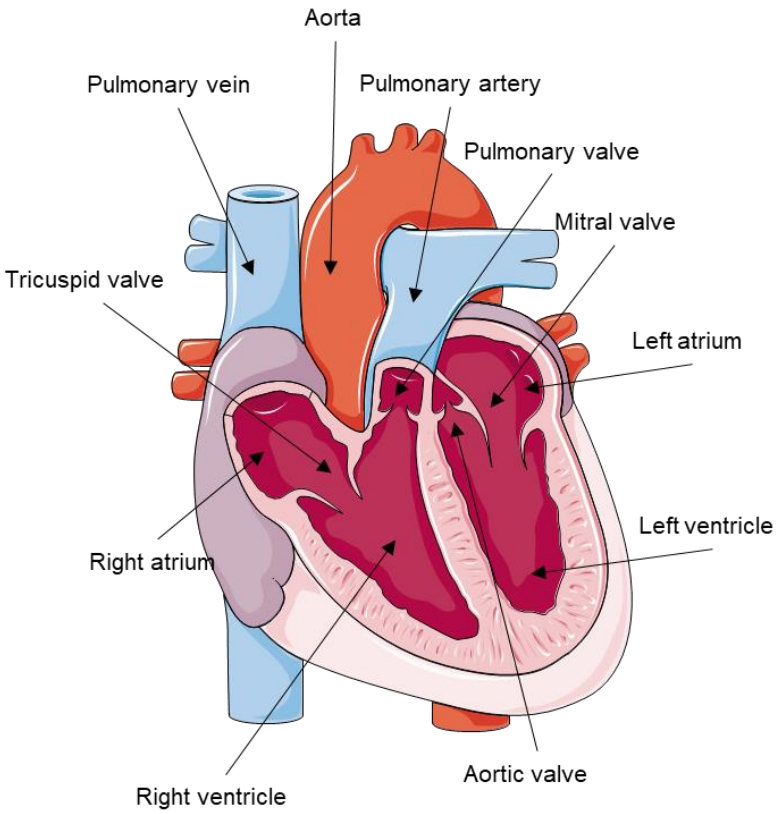

Figure 1: Heart anatomy. The heart is a pump composed by four chambers, two atria (right and left) and two ventricles (right and left). Each atrium is connected with the corresponding ventricle bi a semilunar valve: the tricuspid in the right and the mitral in the left. The right ventricle pumps the blood into the pulmonary artery by the pulmonary valve, the left ventricles pumps it into the aorta by the aortic valve.

open, and the blood reaches the left ventricle. The latter delivers blood into the aorta, by the aortic valve, towards the systemic circulation (big or systemic circulation). All valves ensure unidirectional blood flow (**Figure 1**).

1.1.1. The cardiac cycle

The cardiac cycle is the sequence of mechanical and electrical events that allow blood circulation. It is characterized by a fine regulation of the heart chambers' contraction and relaxation (**Figure 2**). During a cardiac cycle, systole and diastole phases alternate. The former refers to the ventricle contraction when the blood is pumped in the pulmonary and systemic circles by the opening of the semilunar valves (pulmonary and aortic valves). The latter is characterized by ventricular relaxation when they could be filled by the blood coming from the respective atria by the opening of the atrioventricular valves (tricuspid and mitral valves). The average duration of the cardiac cycle is about 800 ms. The entire cycle is allowed by the proper functioning of the heart valves. The point subjected to the highest pressure in the entire circle is the aortic valve. For this reason, the aortic valve is a common breaking point of the circle, because of its malfunctioning [1].

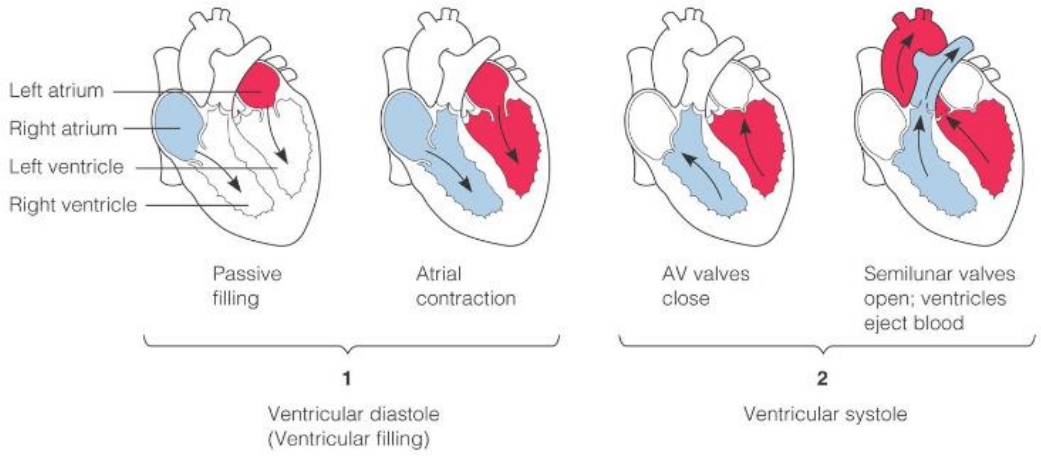

Figure 2: The cardiac Cycle. FROM: biology-pictures.blogspot.co.uk

1.1.2. The aortic valve

The aortic valve is the semilunar valve that separates the left ventricle from the proximal part of the ascending aorta. It is fundamental to maintain the unidirectional blood flow from the left ventricle to the aorta and to prevent blood regurgitation during the diastole. The aortic valve opens when the left ventricle

contracts due to the blood pressure and it closes mechanically when the pressure in the aorta exceeds the one in the left ventricle.

Anatomically, the aortic valve is normally composed of three leaflets, which are in continuity with the aortic root in a semilunar manner, ascending to the commissures ad descending to the basal attachment of each leaflet to the aortic wall (**Figure 3**; [2]).

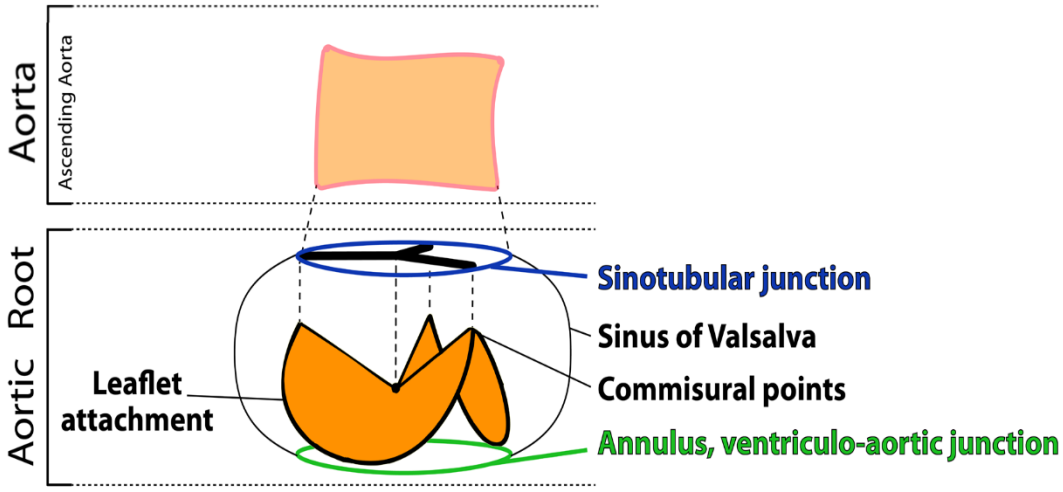

Figure 3: Aortic valve anatomy. Upper side: the ascending aorta. Lower side: the aortic root components: the sinotubular junction of aortic root with ascending aorta; the aortic valve leaflets; the ventriculo-aortic junction of aortic root and left heart ventricle. From Perrucci et al., Pathophysiology of Aortic Stenosis and Mitral Regurgitation.

Each leaflet in physiological conditions is less than 1 mm thick and it is characterized by a three-layer structure, appreciable in the histological transversal section of the valve (**Figure 4**) [3].

Starting from the ventricular side, the first lamina is the ventricularis: it is mainly composed of elastic fibres, radially oriented, useful to help the opening of the valve in systole by their extension and the valve closure by their recoil. The internal layer is called spongiosa lamina, rich in glycosaminoglycans, which facilitate the outer layers to slide over one another during leaflets motion, dampening shear forces acting on aortic valve leaflets during the cardiac cycle. The fibrosa layer is the last one. It is composed of collagen fibres densely packed, that facilitate valve contraction during systole and relaxation during diastole due to their circumferential disposition which gives strength and stiffness to the leaflet [4].

The leaflets are covered by a monolayer of valve endothelial cells on both sides, while in the middle of the extracellular matrix reside valve interstitial cells, the most representative cell population.

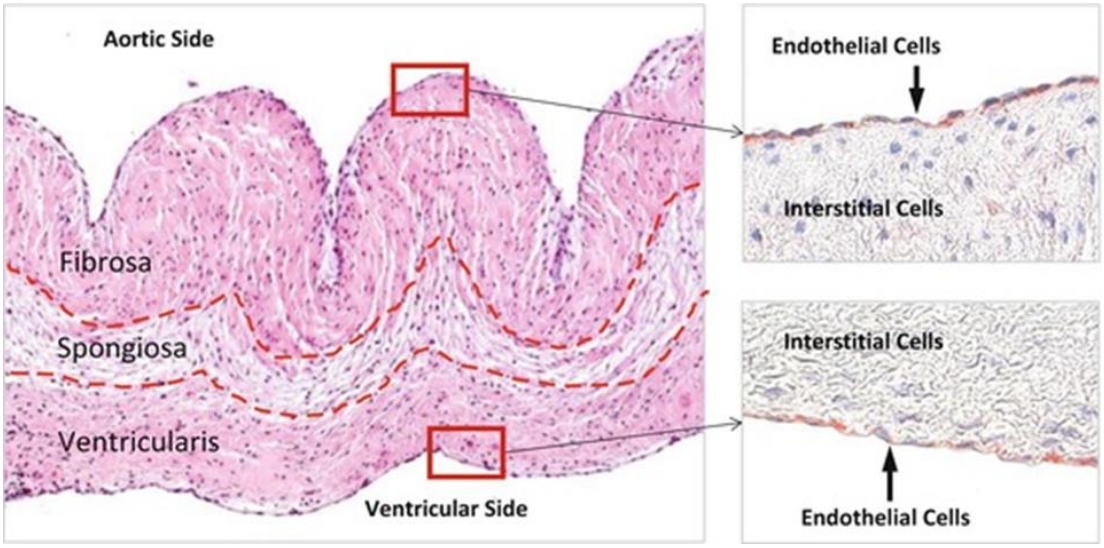

Figure 4: Aortic valve histology. Left side: transversal section of a healthy aortic valve with the typical three layers structure. From the aortic side there is the lamina fibrosa rich in collagen, the lamina spongiosa made by glycosaminoglycan, and the lamina ventricularis composed by elastin. Right side: focus on the cell types; the endothelial cells cover each leaflet; the interstitial cells reside into the tissue. Modified from Zhong A et al., Heart Valve Mechanobiology in Development and Disease.

1.1.2.1. Valve endothelial cells

Valve endothelial cells (VEC) are fundamental to preserve valve integrity, although the high shear stress to which the valve leaflets are exposed [5]. Their principal role is valve homeostasis establishment and maintenance [6, 7]. To absolve these functions, VECs cover the entire area of valve leaflets, regulating permeability, mediating inflammation, and preventing thrombosis [8]. VECs are highly specialized endothelial cells. VECs are oriented perpendicular to the blood flow direction, and they are exposed to different shear stress, depending on the surface they are covering: the ventricular side is exposed to high-velocity flow resulting in high laminar shear stress, while the aortic side is subjected to low velocity oscillatory and consequently low shear stress [9]. For this reason, the transcriptome and the phenotypes of VECs of the aortic and ventricular sides are highly specialized (**Figure 5**).

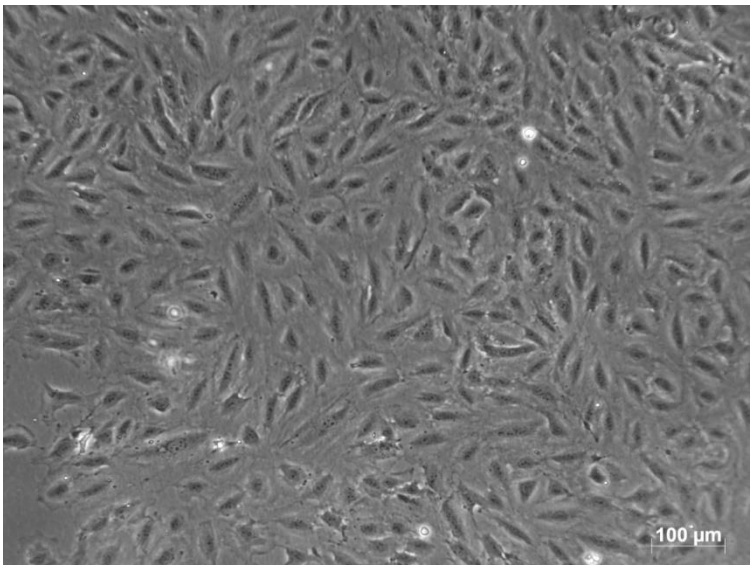

Figure 5: Isolated valve endothelial cells. Phase-contrast image. Magnification 10X. Scale bar: 100 uM.

1.1.2.2. Valve interstitial cells

Valve interstitial cells (VIC) are the most representative cell population of the entire valve leaflets and resides within the entire valve tissue [10]. VICs are composed by a heterogeneous cell population of mesenchymal origin. The main role of VICs is the deposition and the regeneration of the extracellular matrix, to maintain the inner layers architecture previously described (**Figure 6**).

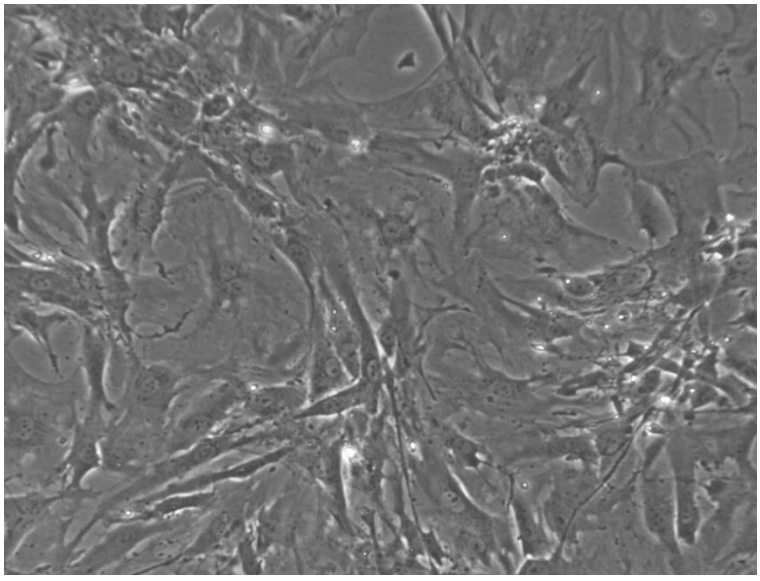

Figure 6: Isolated valve interstitial cells. Phase-contrast image. Magnification 10X.

To date, among VICs different cell types have been reported: fibroblasts, smooth muscle cells, osteoblast- and myofibroblastic- like cells, and embryonic progenitor of endothelial/mesenchymal cells, as confirmed by different single-cell studies on VICs [11-13]. All these cells contribute to the pathophysiological status; indeed, the VIC phenotype is believed to be plastic and reversible. In particular, in healthy subjects, VICs are almost quiescent cells, but in response to injury or disease, these cells are able to activate. Among the stimuli able to activate VICs, there are oxidative stress, inflammation, pro-fibrotic/calcific stimuli (such as TGF- β1 and BMPs) [13, 14], the biochemical and biomechanical properties of the ECM [15, 16], and mechanical stimuli induced by hemodynamic forces [17, 18]. Once activated, VICs acquire a secretory myofibroblast-like phenotype, characterized by the expression of α-smooth muscle actin (SMA) [19] or they differentiate into osteoblasts and begin to produce bone matrix [20-23].

1.1.3. Calcific Aortic Valve Stenosis

Calcific aortic valve stenosis (CAVS) is the most common heart valve disease in Western countries and affects about 3% of the population over than 65 years of age [3, 24]. Considering the progressive population aging, CAVS prevalence, the missing of pharmacological therapy, and the cost sustained by the national health system per single hospitalization (about € 30 000), the research of therapeutic targets for CAVS will tackle down this important socio-economic burden [25, 26].CAVS consists of a long clinically silent phase of non-uniform leaflet thickening, aortic valve sclerosis (AVSc), without significant obstruction of blood flow. In 10% of AVSc, it evolves in aortic valve stenosis (AS), with aortic valve area restriction and obstruction to blood flow [27]. AS is characterized by a progressive rearrangement of the extracellular matrix (ECM), due to fibrosis and calcification of the ECM. Originally, valve calcification was considered an inevitable consequence of aging with clinical relevance when symptoms due to valve obstruction occur.

To date, CAVS is a slow, progressive, multifactorial disorder considered to be driven by cellular and molecular processes' activation (**Figure 7**) [27].

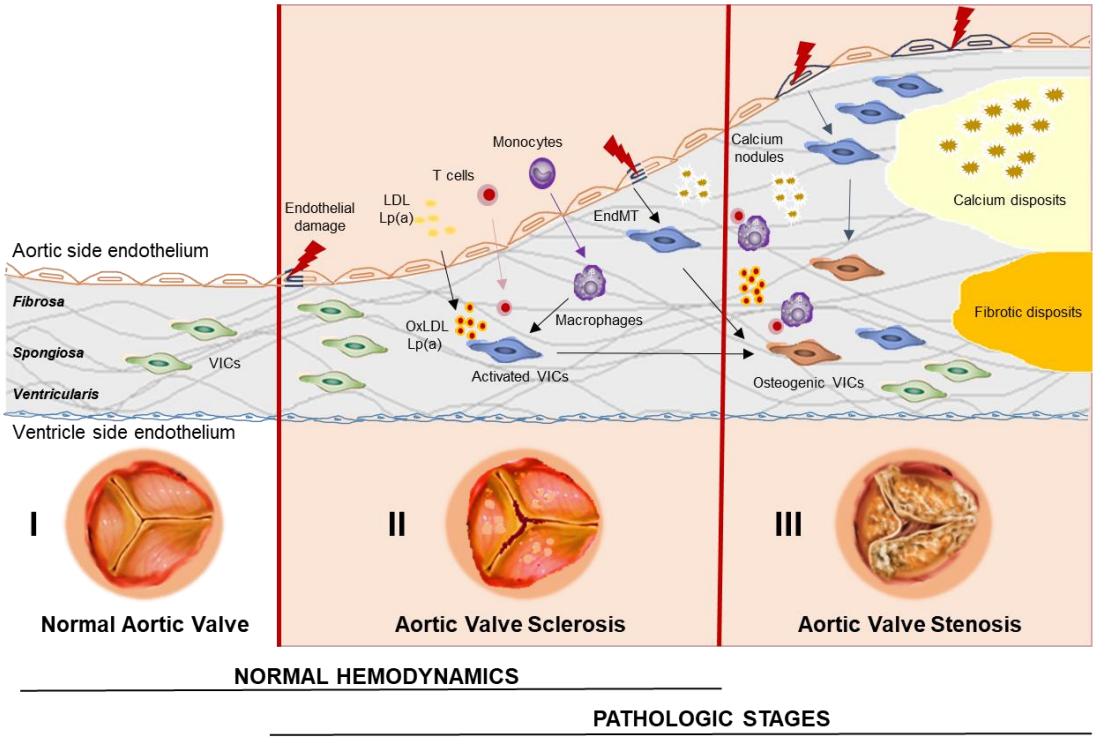

Figure 7: Molecular and cellular mechanisms activated in calcific aortic valve stenosis progression. I) normal aortic valve leaflet covered by a monolayer of valve endothelial cells (VECs) and with valve interstitial cells (VICs) localized in all the three layers of the extracellular matrix. **II**) aortic valve sclerosis: characterized by normal hemodynamics (aortic jet velocity < 2,5 m/s) and endothelial damage (due to oxidative stress), endothelial to mesenchymal transitions (EndMT), low-density lipoprotein (LDL) and lipoprotein a (Lp(a)) infiltration and oxidation, monocytes infiltration and macrophages differentiation. **III**) aortic valve stenosis: characterized by pathological hemodynamics (aortic jet velocity>4.0 m/s, mean gradient > 40 mmHg, aortic valve area < 1.0 cm^2, and aortic valve area index to body surface < 0.60 cm^2/m^2) and VICs activation, and fibro-calcific nodules deposition. Modified from Myasoedova et al. Novel pharmacological targets for calcific aortic valve disease: Prevention and treatments.

Oxidative stress is among the first triggers of the pathology, leading to endothelial damage and endothelial to mesenchymal transition (EndMT) [26, 28]. EndMT paves the way for the development of local inflammation, by monocyte infiltration [29] and the consequent activation of VICs [3, 26, 29]. Activated VICs phenotypically switch to osteoblast- and myofibroblast-like cells and subsequently deposit fibro-calcific nodules [23, 27, 30]. This process leads to a vicious cycle in which fibro-calcific nodule accumulation causes an increase in leaflet stiffness that, in turn, boosts VIC activation [31]. Activated VICs carry out a progressive ECM rearrangement, characterized by fibro-calcific deposit formation [3]. Despite the huge number of studies aimed at defining the molecular effectors of CAVS progression, they are not yet fully discovered.

1.1.3.1. Symptoms and diagnosis

As previously described, the initial phase of CAVS, AVSc, is clinically silent, whit no symptoms. However, in this stage of pathology, echocardiography can provide detail regarding tissue characterization without the definition of histological properties. Nevertheless, this type of examination in this stage is subject to instrumentation and artifact variables common to ultrasound imaging. AVSc is difficult to diagnose, also due to the lack of a universal definition of the pathology [32, 33]. The symptomatic stage is the last one, the aortic valve stenosis. The main symptoms of this phase are angina, dyspnoea, congestive heart failure, presyncope, or syncope. Consequently, after left ventricular dysfunction and reduction in cardiac output, symptoms of congestive heart failure appear [34].

To date, different risk factors of CAVS development have been reported: male gender, aging, smoking habits, hypertension, hypercholesterolemia, renal disease, and metabolic syndrome [35-38].

In addition to the environmental risk factors, also some genetic factors could be associated with the pathology. The most important one is the presence of a bicuspid aortic valve (BAV) [28]. Patients with BAV develop aortic valve calcification at an earlier age compared with degenerative tricuspid aortic valve (TAV).

The gold standard to diagnose CAVS in clinical practice is echocardiography. Typically, echocardiography is performed via transthoracic, however, when the transthoracic examination is deemed insufficient or uninterpretable, technicians perform transoesophageal echocardiography (even if it is more invasive) [39]. This type of examination provides information on the anatomy of the valve (tricuspid, bicuspid, or others very rare) and the presence of calcium deposits and their extension (**Figure 8**).

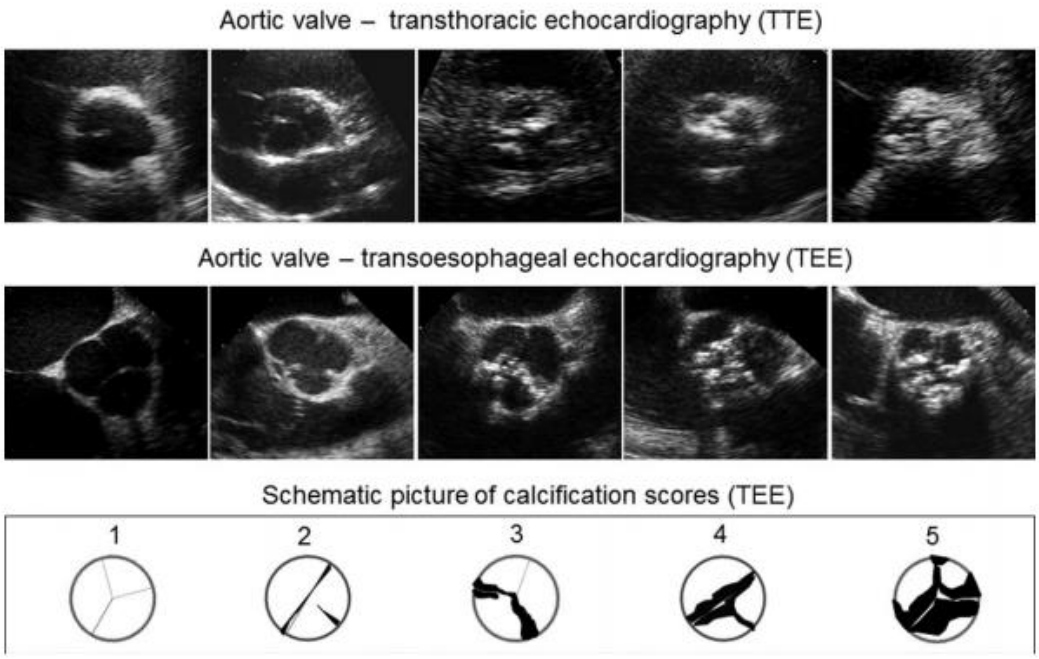

Figure 8: Representative images of echocardiographic examination of different grades of aortic valve stenosis. Transthoracic (TTE, upper panel) and transesophageal (TEE, lower panel) echocardiographic scoring of aortic valve calcification and relative pictures of calcium deposition. Image from Yousry M. et al. Aortic valve type and calcification as assessed by transthoracic and transesophageal echocardiography.

In clinical practice, Echo-Doppler is used to calculate other parameters such as the mobility of the cusps, the maximum velocity (Vmax) across the stenotic valve, the mean transaortic pressure gradient (ΔPmean), and the effective aortic valve area (AVA) using the standard continuity equation (**Table 1**).

	Aortic valve sclerosis	**Aortic valve stenosis**		
		Mild	Moderate	Severe
Aortic jet velocity (m/s)	≤ 2,5	2,6 – 2,9	3,0 – 4,0	> 4,0
Mean gradient (mmHg)	-	< 20* (< 30**)	20 – 40* (30 – 50**)	> 40* (> 50**)
AVA (cm^2)	-	> 1,5	1,0 – 1,5	< 1,0

Table 1: Echo-Dopler criteria for definition of aortic sclerosis and stenosis. *AHA/ACC Guidelines; **ESC guidelines

All these indicators contribute to the diagnosis of the severity of CAVS and the prediction of the clinical outcome and for clinical decision-making (**Figure 9**) [40].

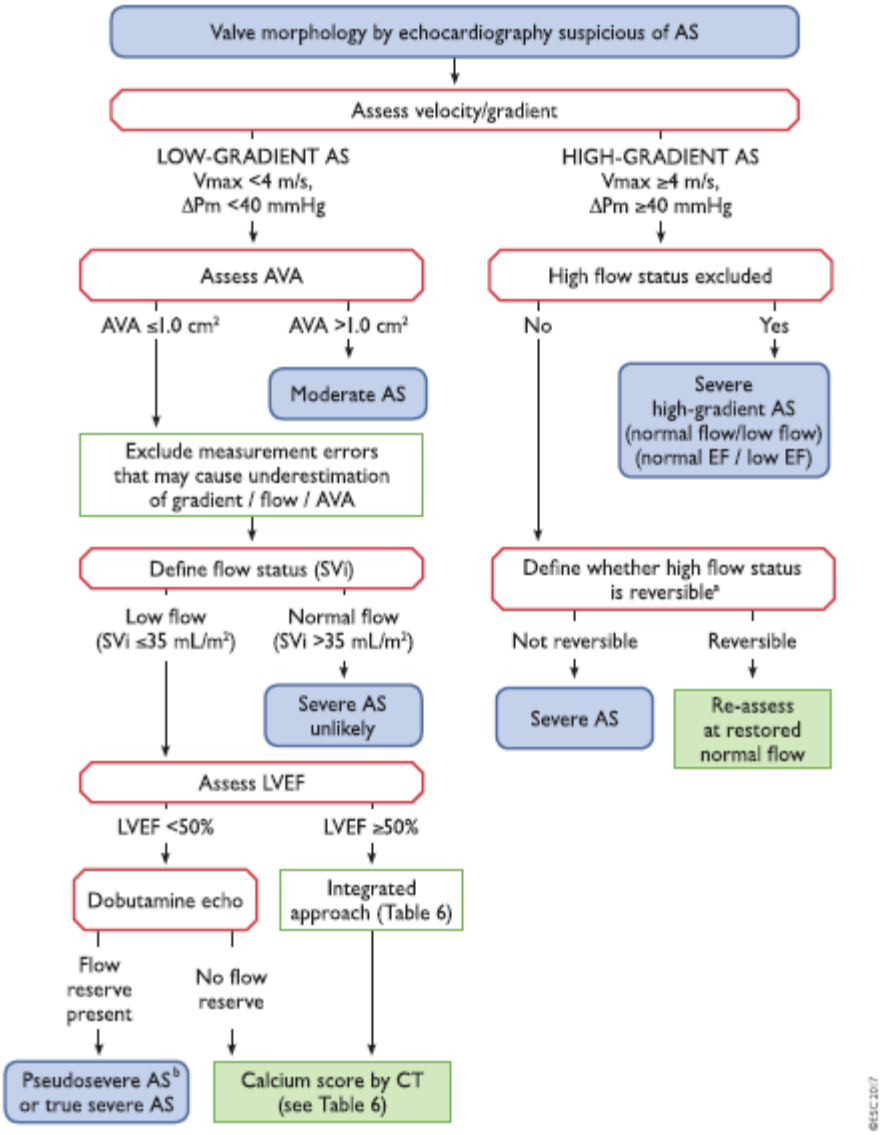

Figure 9: ESC/EACTS recommendations on echocardiographic assessment of aortic valve stenosis. AS: aortic stenosis; ΔPi: mean transvalvular pressure gradient; Vmax: peak transvalvular velocity; AVA: aortic valve area; EF: ejection fraction; SVi: stroke volume index; LVEJ: left ventricular ejection fraction.

1.1.3.2. Therapeutic options

Although the increasing number of studies aimed at defining the pathological molecular mechanisms activated in CAVS, to date, there isn't a pharmacological treatment able to target the detrimental molecules and arrest/revert the pathology progression. As a result, surgical aortic valve replacement (AVR) or percutaneous, via transcatheter, aortic valve implantation (TAVI) remain the only treatments for symptomatic CAVS, leaving the pathological mechanisms unsolved [41]. The need of

an AVR or TAVR surgery became when CAVS shows its symptoms, therefore during the last stage, the aortic valve stenosis [27, 42].

1.1.3.2.1. AVR and TAVI

Aortic valve replacement is a surgical therapy that implies the removal of the damaged valve leaflets and the replacement with a new valve made of synthetic materials or animal tissue. AVR procedure is highly invasive as it involves open-heart surgery, via sternotomy, with the use of extracorporeal circulation, under general anesthesia (AHA/ACC GUIDELINE). The surgical substitution of the valve is different from patient to patient. Ideally, the prosthetic valve should mimic the natural one: it could be mechanical and biological [43]. The formers are mainly of three types: caged-ball, tilting disc valve, and bi-leaflets heart valve (the most used today; **Figure 10**) [44]. Unfortunately, mechanical valves are prone to thrombus formation due to high shear stress, stagnation, and flow separation. For this reason, patients receiving this type of valve are forced to take oral anticoagulants, and thus, they show a higher risk of bleeding with respect to the biological prosthesis [45]. Elective patients for this type of valve are younger than 60 years of age, because of the extreme durability of these valves and the higher incidence of major adverse cardiovascular events than those receiving biological prostheses [46, 47]. Moreover, it was observed that patients between 60 and 69 years of age receiving mechanical prostheses have a higher risk of bleeding than patients who underwent TAVI [48]. The bioprosthetic valves are made with glutaraldehyde-fixed porcine aortic valves or constructed with glutaraldehyde-fixed bovine pericardium and most of the time mounted on stents [49]. Other types available are pulmonary autograft and aortic valve homograft. Bioprosthetic valves do not require anticoagulant therapy and are less long-lasting than mechanical ones [43]. For these reasons, they are recommended in patients older than 70 years of age and in patients with high bleeding risk and contra-indications for prolonged anticoagulation treatment. Moreover, those types of valves are recommended for women with pregnancy wishes [46].

For patients between 60 and 70 years of age there are no strong evidence of the benefits deriving from the use of mechanical or biological valves, so clinicians decide case per case the elective operative strategy [46].

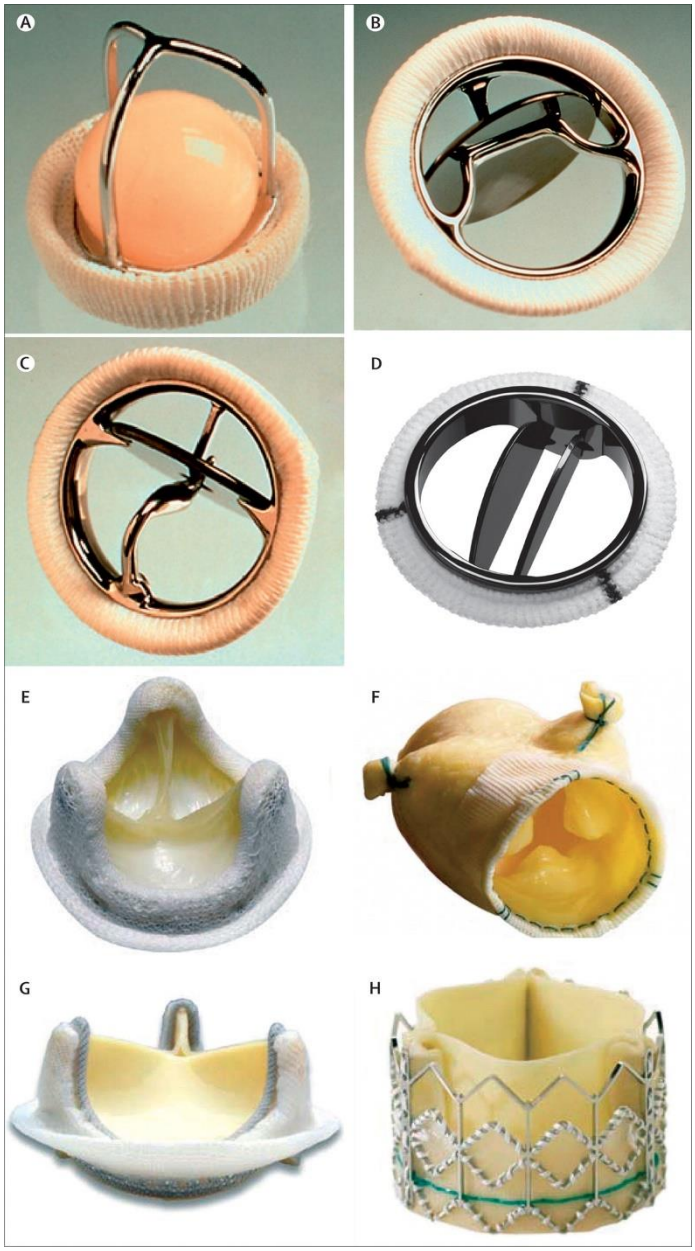

Figure 10: Mechanical and biological prosthesis. (A) Starr-Edwards caged-ball valve; (B) Bjork-Shiley tilting-disk valve; (C) Medtronic Hall tilting-disk valve; (D) St Jude Medical Regent bileaflet valve; (E) Medtronic HK II ultra-porcine valve; (F) Medtronic Freestyle porcine valve; (G) Carpentier-Edwards Perimount bovine pericardial valve; (H) Edwards SAPIEN transcatheter pericardial aortic valve. Image from: Sun J et al. Antithrombotic management of patients with prosthetic heart valves: current evidence and future trends.

Despite technical improvement, mechanical and biological prosthesis degenerate as the naïve aortic valve, due to thrombosis, endocarditis, pannus growth, and leaflets calcification and regeneration (**Figure 11**). For these reasons, often surgical reintervention is required for those patients [45, 50]. Although the disadvantages, AVR remains the elective strategy of care for CAVS treatment. Indeed, thanks to the progress in surgical and postoperative care driving, perioperative mortality is down to 1%-3%. The main perioperative complications include conduction disease requiring permanent pacemaker insertion (1.5%–8.6%) [51], cerebrovascular accidents (2.4%– 8.1%) [52, 53], cognitive decline (due to perioperative cerebral hypoperfusion micro-emboli or anesthetic agent neurotoxicity) [54].

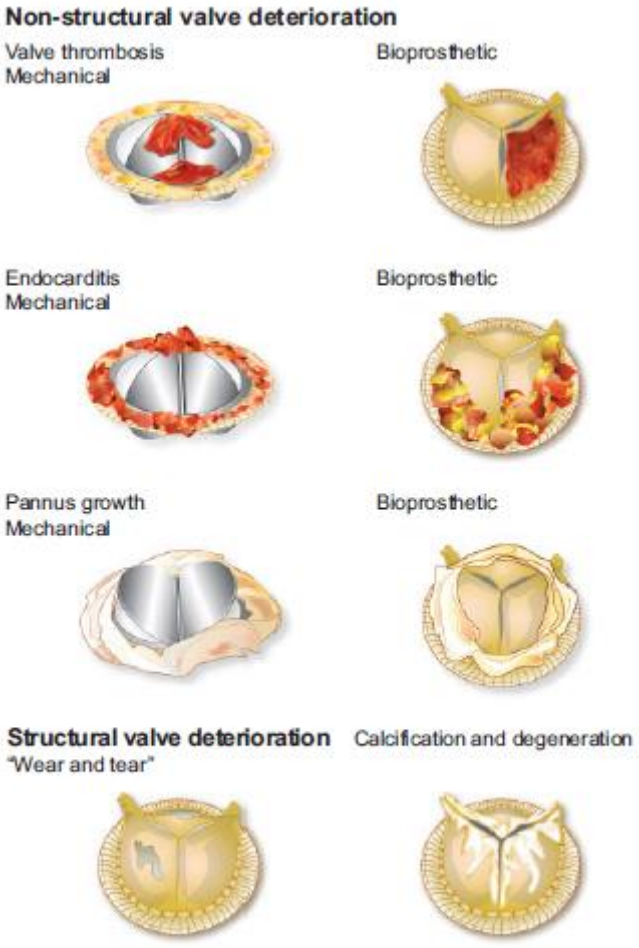

Figure 11: Example of structural and non-structural prosthesis degeneration. Image from: Head S. et al. Mechanical versus bioprosthetic aortic valve replacement

In the last ten years, however, the introduction of minimally invasive transcatheter aortic valve insertion (TAVI) drastically changed the scenario of surgical intervention for CAVS. TAVI is a less invasive technique, developed by Nielsen [55]. It provides the implantation of stent-valve via transcatheter for patients at high risk for AVR. TAVI is associated with a reduction in all-cause mortality and stroke for up to 2 years irrespective of baseline surgical risk and type of transcatheter heart valve system [56]. The widespread implementation of this technique in the last decade brings to its introduction in the ESC/EACS guidelines for the management of CAVS (**Figure 12**).

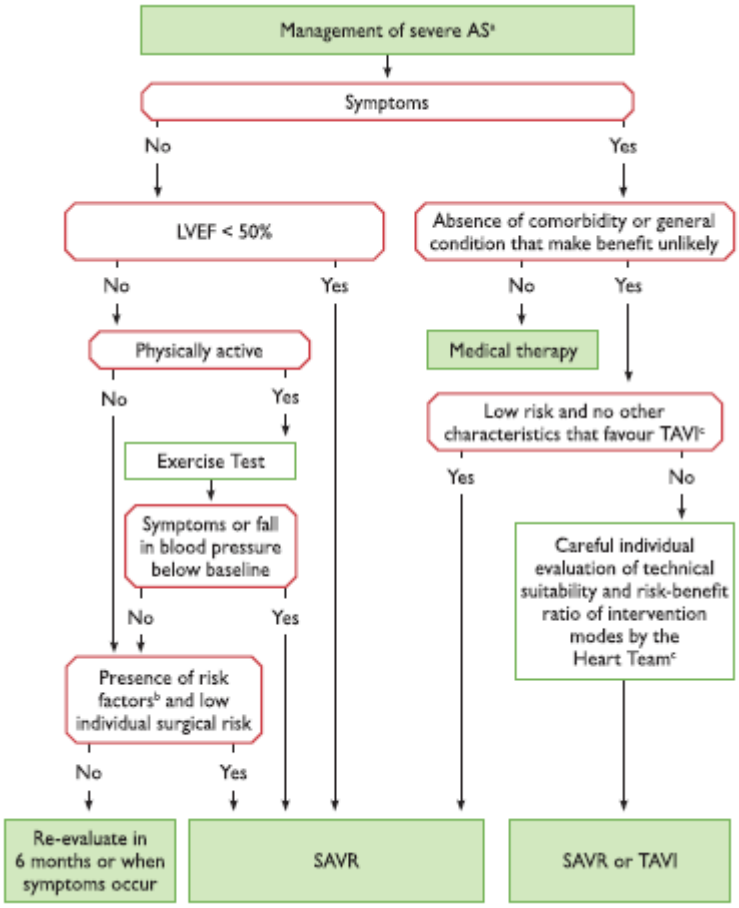

Figure 12: ESC/EACTS guidelines for the management of severe aortic stenosis. AS: aortic stenosis; LVEF: left ventricular ejection fraction; SAVR: surgical aortic valve replacement; TAVI: transcatheter

1.1.3.3. Pharmacological treatments

Despite the increasing efforts in the identification of molecular mechanisms involved in CAVS, currently, there is no approved pharmacological therapy act to prevent or treat CAVS [27, 42]. Symptoms such as heart failure, syncope, and angina, occur only when AS becomes severe. Therefore, an effective

pharmacological treatment is difficult to carry out. For this reason, the research for a pharmacological therapy to treat AS patients is actually a challenge still open. In the last decades, several therapeutic targets have been proposed for CAVS treatment. Considering that circulating lipid levels are associated with aortic valve calcification (AVC) and AS incidence [57], several randomized clinical trials have been performed to investigate the effects of statins on AS. All these trials failed, demonstrating the drug's ineffectiveness to prevent or halt AS progression [58-61]. Different studies investigated the effects of angiotensin receptor blockers (ARBs) and angiotensin-converting enzyme inhibitors (ACEi) on AS progression [62]. All these studies provided evidence that ARBs or ACEi therapies induced a reduction of AS progression rate, but did not revert the phenotype of the pathology [63, 64].

In the last years, new pharmacological targets have been identified to reduce or at least slow down AS progression. Proprotein convertase subtilisin/kexin type 9 (PCSK9) inhibitors and niacin, provoking the lowering of circulating levels of LDL and lipoprotein (a), respectively, have been hypothesized to be a potential pharmacological treatment for AS [27]. Dipeptidyl peptidase 4 (DPP-4) inhibitors have been used on mouse and rabbit models and they seem to reduce VIC osteoblastic differentiation and improve echocardiographic characteristics [65]. Bouchareb et al. reported a reduction of calcium extracellular deposits due to pharmacological stimulation of purinergic receptor 2Y2 both *in vitro* on healthy controls and *in vivo* on a mouse model [66].

1.1.3.3.1. P2Y2 receptor

P2Y2 receptor is a membrane protein with seven transmembrane domains connected by three extracellular loops (EL) and three intracellular loops. It is a G coupled receptor, associated with a Gq protein [67].

Like all P2Y receptors, also P2Y2 has four cysteine domains in the ELs (**Figure 13**). Thanks to the cysteine domains, the receptor is able to form homo- and hetero-dimers by disulfide bridges [68].

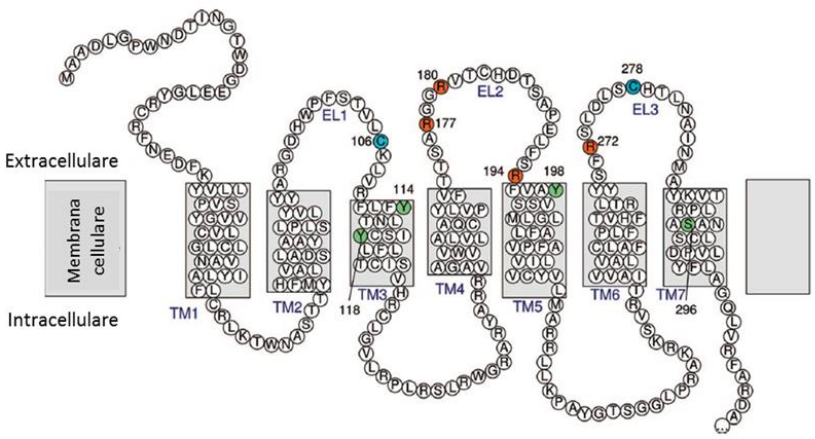

Figure 13: Purinergic receptor 2 type 2 structure (P2RY2). P2RY2 is a transmembrane (TM) receptor with seven TM domains and three extracellular loops (EL) and three intracellular loops (IL). Image modified from: Hillmann P et al., Key Determinants of Nucleotide-Activated G Protein-Coupled P2Y2 Recept Receptor Function Revealed by Chemical and Pharmacological Experiments, Mutagenesis and Homology Modeling.

P2RY2 is activated by adenosine triphosphate (ATP), uridine triphosphate (UTP), and their analogues ATPγS ed UTPγS. It was reported to be expressed by different cell types: nervous and immunity cells of the central nervous system, smooth muscle cells, cardiomyocytes, osteoblasts, leucocytes, epithelial, and endothelial cells [69]. For this reason, it is reported to be involved in many physiological mechanisms among which the inhibition of bone formation by the osteoblasts. In particular, P2Y2 is involved in the ion transport regulation [70], chloride secretion negative regulation in the P2Y2(-/-) mouse model [71], chronic renal disease [72], and the reduction of vasodilatory responses [73] and the effects post-myocardial infarction [74]. Moreover, immunity cells of P2Y2(-/-) mice showed a reduced migration capacity and immune response [75].

To date, several synthetic compounds have been synthesized to pharmacologically activate P2RY2: poli-phosphate dinucleotides, in particular diadhenosine and diuridine tetra-phosphate and the 2-tiouridine-5'-triphosphate (2-ThioUTP) and its analogues [76-78].

It has been reported that the activation of P2RY2 by 2-ThioUTP could reduce the extracellular calcification of VICs from healthy controls. In particular, the authors hypothesized that the activation of P2RY2 could promote the translocation of the carbonic anhydrase XII on the cell membrane and activate the condensation of water and carbonic anhydrase to carbonic acid (H_2CO_3). H_2CO_3, in physiological pH

conditions, dissociates into H+ ions and bicarbonate (HCO_3-). The acid produced could dissolve the calcium deposits in the extracellular space [66].

1.1.3.4. Sex-differences in calcific aortic valve stenosis

During the last decade, even more, studies have reported evidence of sex-related differences in the pathobiology, clinical phenotypes, and outcomes of CAVS patients. Sex-related differences may be significant in the development and progression of CAVS. Different studies reported that the quantification of aortic valve calcium load (AVC) measured by echocardiography or multidetector computed tomography (MDTC; a largely recognized technique used to evaluate calcium load with accurate and reproducible data) [79], is higher in men than in women with AS, even correcting data for cross-sectional aortic annulus area and body surface area [80-82]. Moreover, aortic valve calcium load has been reported to be associated with hemodynamic severity of AS both in men and women, supporting the hypothesis that women develop hemodynamically more severe AS for an equal amount of AVC compared with men [83, 84]. To investigate the reason why, even with low AVC, women showed similar haemodynamic progression, some studies explored the contribution of pathological extracellular matrix remodelling in the AS progression. They reported that women have less valvular calcification, but more fibrosis and dense connective tissue compared with men with similar hemodynamic AS degree [85-87]. Taken together, these data suggest that sex can influence not only the likelihood of CAVS development but also its nature (**Figure 14**), paving the way for sex-specific management and treatment of CAVS.

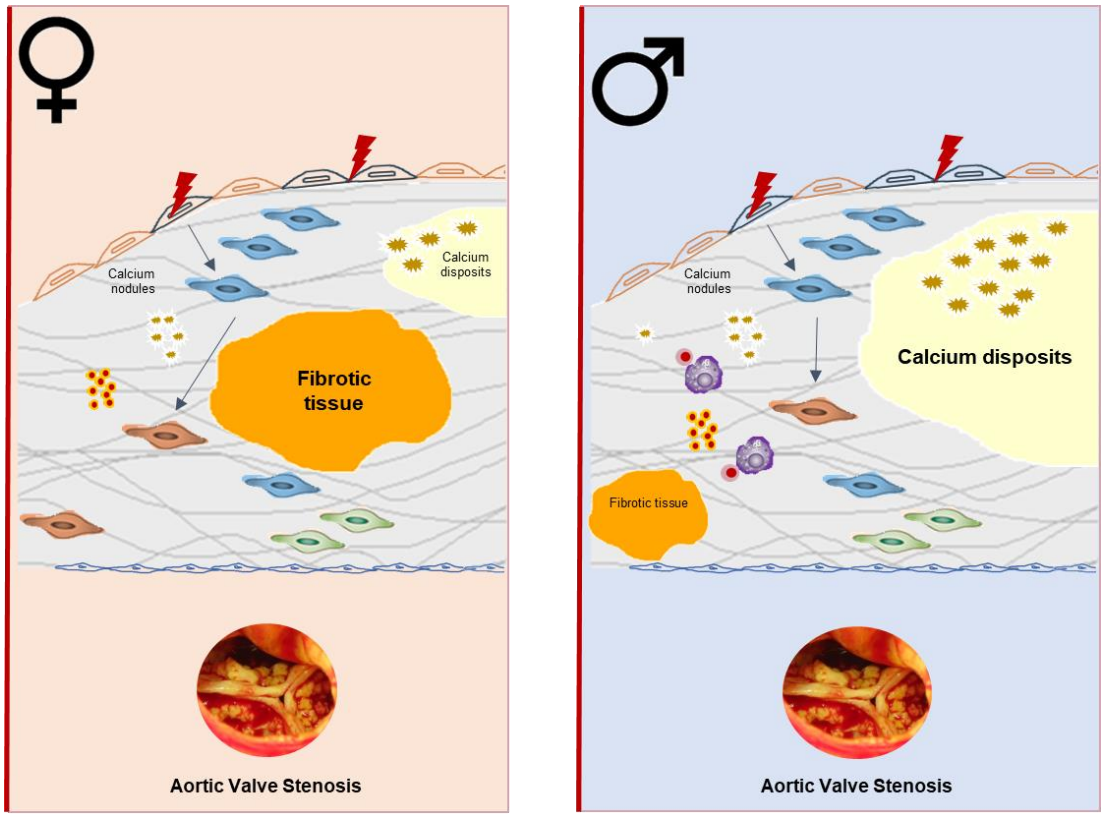

Figure 14: Sex specific features of aortic valve stenosis. In women with aortic valve stenosis there is a prevalence of fibrotic tissue, in men there is more calcium deposition. Image modified from: Summerhill V. et al., Sex-Specific Features of Calcific Aortic Valve Disease.

Starting from these data, the need to deepening the molecular pathological mechanisms activated in a sex-dependent way during CAVS development and progression is crucial. Some studies investigated some of these both in vitro and in vivo on animal models (**Figure 14**) [88]. In particular, it has been reported that in men with CAVS the janus kinase (JAK) - signal transducer and activator of transcription (STAT) and the extracellular signal-regulated kinase (ERK) pathways are upregulated, causing a higher calcification through tissue nonspecific alkaline phosphatase (TNAP) [88], an enzyme involved in the extracellular calcification of CAVS patients [89]. Whereas, in women with AS interferon α (INFα) expression blocked the apoptosis and the mineralization processes, favoring fibrosis (**Figure 15**) [88].

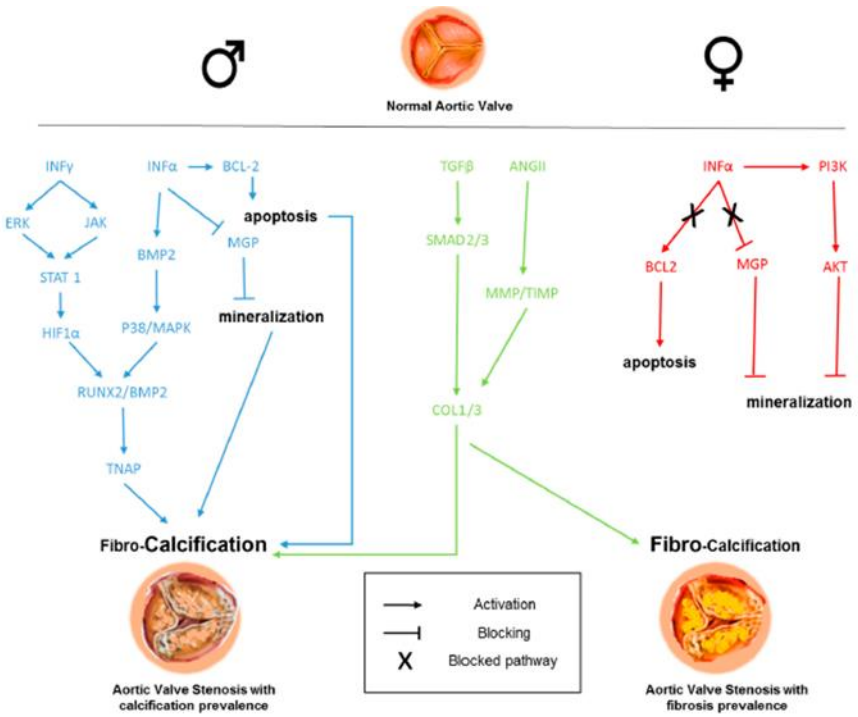

Figure 15: Sex-dependent cellular and molecular processes involved in CAVS fibro-calcification. The diagram represents the known sex differences observed in the signaling pathways implicated in calcific aortic valve stenosis (CAVS) pathogenesis and progression. Blue lines: male specific signaling pathway; red lines: female specific signaling pathways; green lines: generic signaling pathways. Image from: Summerhill V. et al., Sex-Specific Features of Calcific Aortic Valve Disease.

Despite the actual evidence, the role of sex-related pathways in driving CAVS are not yet fully investigated. Some authors investigated this field, as reported in the **Appendix A**. This type of knowledge could pave the way for a new scenario of gender-specific management and therapy for CAVS patients.

2. MATERIAL AND METHODS

2.1. Patients enrollment

2.1.1. Specimens collection

We prospectively enrolled patients affected by calcific aortic valve stenosis in all stages of the pathology who undergo to aortic valve replacement (AVR) at Centro Cardiologico Monzino IRCCS (CCM). This study was approved by the Institutional Review Board and by the Ethical Committee of CCM according to the principles outlined in the Declaration of Helsinki (1964). Each enlisted patient read and signed informed consent to use the removed aortic valve leaflets for research purpose. In particular, we enrolled patients with tricuspid aortic valve (TAV) intended for surgery because they suffer from aortic valve sclerosis (AVSc) and severe stenosis (AS). We evaluated the morphology and functionality of the aortic valve pre-operatively by echocardiography.

The inclusion criteria were: i) elective and isolated surgical procedure; ii) over 18 years of age; iii) ejection fraction >30%; and iv) normal sinus rhythm. Patients were excluded from the study due to: previous cardiac surgery, rheumatic heart disease, endocarditis, active malignancy, chronic liver or kidney diseases, calcium regulation disorders (hyperparathyroidism, hyperthyroidism, and hypothyroidism), and chronic or acute inflammatory states (sepsis, autoimmune disease, and inflammatory bowel disease).

Blood samples for research purposes were obtained the day before surgery (for patients) and after their adhesion to the study (for healthy subjects).

After the surgical procedure, the aortic valve leaflets removed were collected and processed within 30 minutes.

2.1.2. Echocardiographic Evaluation

Pre-operative echocardiographic evaluation with M-mode, two-dimensional and pulsed, continuous and colour-flow Doppler capabilities were performed for all patients. Morphology and function of the aortic valve were assessed. Specifically, the presence of AVSc was recognized as non-uniform thickening with or without spotty calcified areas of the aortic valve leaflets without a significant transvalvular gradient (maximum aortic velocity < 2.5 m/s).

2.1.3. Computed tomography examination

Cardiac computed tomography (CT) was performed with the following parameters: section configuration 256x0.625 mm, voxel size 0.625 mm, spatial resolution along the X-Y planes 0.23 mm, gantry rotation time 280 msec, and iterative reconstruction. A BMI-adapted scanning protocol (tube voltage and current) was used [90]. All patients received a 50-mL bolus of contrast (Iomeprol 400 mg/mL).

2.2. Meta-analysis

2.2.1. Studies collection

To identify all available studies, a systematic search was evaluated in the electronic databases (PubMed, Web of Science, and Scopus). A detailed search relating to AVC load, measuring by CT scan, and the gender-specific difference was conducted according to PRISMA guidelines [91]. Following search, terms were used in all possible combinations: gender difference, sex difference, aortic valve calcification (AVC), aortic valve stenosis (AS), calcific aortic valve stenosis (CAVS), computed tomography (CT), calcium score, MDCT. Elective studies for this meta-analysis have been published before April 2020. Data were expressed as mean difference (MD) and standard error (SE); analyses were performed with random effect. The reference lists of all retrieved articles were manually reviewed. Two independent operators analyzed each article and performed the data extraction independently. In case of disagreement, a third investigator was consulted. Discrepancies were resolved by consensus.

2.2.2. Data extraction and quality assessment

All studies evaluating the AVC load and AVC density in men and women with aortic valve stenosis, and the impact on cardiovascular risk factors were included. Case-reports, case-series without a control group, reviews and animal studies were excluded. Values needed for the analysis were means with standard deviation of at least one variable among the following: AVC load, AVC density in men and women, separately. We included the studies where AVC scores were quantified with the Agatston scoring method and all AVC data were expressed with AU (Agatston Units). AVC density (AU/cm2) was calculated by indexing AVC load to the cross-

sectional area of aortic valve annulus (the echocardiographic measurement of the left ventricular outflow tract; LVOT) [92]. In each study, data regarding major clinical, demographic and echocardiographic variables, values of AVC, AVC density and prevalence of cardiovascular risk factors in men and women were extracted.

The quality analysis for each included study was performed accordingly to Newcastle-Ottawa Scale (NOS).

2.2.3. Statistical analysis and risk of bias assessment

Statistical analysis was performed using Comprehensive Meta-analysis Version 3 (Biostat, Englewood, NJ 2013). AVC differences between men and women were expressed as mean difference (MD) and standard error (SE).

The overall effect was tested using Z scores and significance was set at $p < 0.05$. Statistical heterogeneity among studies was assessed with chi-square Cochran's Q test and with I2 statistic, which measures the inconsistency across study results and describes the proportion of total variation in study estimates, that is due to heterogeneity rather than sampling error. In detail, I2 values of 0 % indicate no heterogeneity, 25 % low, 25–50 % moderate, and 50 % or more high heterogeneity [93].

Publication bias was assessed by Egger's test. The value $p < 0.10$ was considered statistically significant. In order to be as conservative as possible, the random-effect method was used for all analyses to consider the variability among the included studies. In the case of significant publication bias, the Duval and Tweedie's trim and fill method was used to allow for the estimation of adjusted effect size.

2.3. Imaging acquisition and deep learning workflow

Images were post-processed using dedicated software for aortic valve calcium load (AVC) assessment (3Mensio Valves™, 3Mensio Medical Imaging, Maastricht, The Netherlands) [94] with manual correction. Contrast attenuation values (Hounsfield Units, HU) and contrast-to-noise ratio were measured at the level of the ascending aorta. Total aortic valve fibrosis (AVF) was assessed based on HU ranging between 30 and 350, adjusting the upper threshold by increments of 25 HU in either direction until blood pool was not highlighted. The calcium and fibrosis volumes

were assessed and quantified using the ImageJ (Java-based image processing program developed at the National Institutes of Health) thresholding method [95]. Indexed contrast-enhanced CT calcium volume and fibrosis volume were calculated by dividing the volume by the aortic annular area for each patient (measured by ImageJ, Java-based image processing program developed at the National Institutes of Health).

Each CT scan is composed of 256 or 224 slices (512 x 512 pixels) and stored in a DICOM object. In order to remove useless anatomical structures, such as aorta or ventricles, we selected the consecutive slices containing the aortic valve, which allows decreasing the computational burden and improving the overall network performances. Each selected slice was then used to perform a manual segmentation in order to generate the 'ground truth' images. Thirty-eight out of 56 randomly selected samples were then used to train a U-Net model, with a default parameter, to segment the aortic valve. The remaining 20 samples served as the test set. The U-Net model was implemented with default hyperparameters, using the 'Keras' package; concerning the training step, we set the 'Root Mean Squared (RMS) propagation' optimizer to minimize the 'binary cross-entropy (BCE) dice' loss function, the number of epochs = 50 and the batch size = 10. The Dice Score was used to assess the segmentation accuracy, comparing the predicted mask and the ground truth. Finally, the predicted masks were combined with the corresponding starting frames in order to extract the pixel intensity (Hounsfield Unit) of the aortic valve and, then, calculate the fibrosis and calcium volumes. The Pearson's correlation index (rp) allowed assessing the consistency between the automatic predictions and the calculations of fibrosis and calcium volumes, made by human operators.

2.4. Blood Sampling and Biochemical Measurement

Serum sample: 5 mL of peripheral blood sample was drawn from patients and healthy subjects while fasting, into tubes Vacutainer Z (Vacutainer Systems, Becton Dickinson, Franklin Lakes NJ, USA). Whole blood was incubated for two hours at 37°C in a thermostat-controlled bath to promote coagulation. Then blood

was centrifuged at 2000 g for 10 min at room temperature. Serum sample in the supernatant was separated and aliquots were stored at -80 °C until analysis.

2.5. Human cytokine evaluation

Circulating cytokine levels were assessed by human XL cytokine magnetic luminex performance assay 44-plex fixed panel (Bio-techne, Minneapolis, MN, USA). Briefly, each serum sample were centrifuged for five minutes at 4°C at 16000 rcf after defrosting. Then they were diluted 1:2, as per manufacturer's instructions and analyzed as per manufacturer's instructions. Briefly, each sample and standard were loaded in duplicate in the96-well plate, whit the 50 µL of microparticle cocktail and incubated 2 hours shacking at 850 rpm at room temperature. The plate was placed on a magnet, to retain beads with antibodies and protein bounded, washed three times and incubated with 50 µL of diluted Biotin-Antibody Cocktail for 1 hour shacking at room temperature. Following this passage, each well was washed three times and incubated with streptavidin for 30 minutes shacking at room temperature. Controls and samples were then washed three times, resuspended in wash buffer and read within 90 minutes using Bio-plex 200 system (BioRad, Hercules, CA, USA) setting the following acquisition protocol: at least 50 beads per region, with a sample time out of 45 seconds. All analytes with less than 10 beads were excluded by the analysis.

2.6. Whole tissue gene expression data processing

Gene expression data were retrieved from Gene Expression Omnibus (GEO) public repository (GEO accession number: GSE102249) [96]. This dataset includes the transcriptomic analysis (performed by microarray technology) of 240 aortic valve tissues, coming from 120 men and 120 women whit aortic valve stenosis. We reannotated the Illumina probe ID, using the Ensembl human gene annotation (GRCh38, version 97), removed outliers and normalized data by log2 transformation and quantile normalization. The analysis was performed by R (v. 3.6.3).

2.7. Pathways' and cell types' enrichment analysis

Gene set enrichment analysis (GSEA) was conducted using GSEA pre-ranked tool (v 4.0.3) [97] and the biological functions were inferred by taking advantage of gene

ontology biological processes (GO-BP), Reactome, WikiPathways, and BioCarta databases. To reduce redundancy and visually interpret GSEA results, the most significant GO-BP/Reactome/BioCarta pathway gene sets were identified by a false discovery rate (FDR) < 0.1. The network was drawn through the Enrichment Map software v.3.3.2 [98] implemented as a plugin in Cytoscape v.3.8.2 [99]. Cell-Type Enrichment Analysis Cellular composition of stenotic aortic valve tissue in women and men was inferred by the xCell R package [100], starting from the gene expression dataset of 240 samples. xCell raw scores were generated and transformed applying the spill-over compensation. Then, we assessed the association between the xCell scores and sex by Wilcoxon rank-sum test. The log2 foldchange (logFC) of each cell type scores between men and women was computed and the pValues were adjusted with FDR correction. It is important to note that xCell results are expressed in terms of enrichment scores. Therefore, any inference on the cell counts or proportion of cell types is not provided.

2.8. Isolation of aortic valve endothelial and interstitial cell

Aortic valve interstitial cells (VICs) were isolated by aortic valve leaflets within 30 minutes by the surgical resection. Each leaflet was incubated for 20 min at 37 °C in 2 mg/mL type II collagenase (Worthington Biochemical Corp., Lakewood, NJ, USA) in cell culture medium (advanced Dulbecco's modified Eagle's medium (Ad DMEM, Life Technologies, Carlsbad, CA, USA) containing 10% fetal bovine serum (FBS, Microtech, Naples, Italy), 1% penicillin (Life Technologies, Carlsbad, CA, USA), 1% streptomycin (Life Technologies, Carlsbad, CA, USA), and 1% l-glutamine (Life Technologies, Carlsbad, CA, USA)). This step was implied to remove the endothelial cells. Then, leaflets were moved away in new fresh medium and finely shredded with a scalpel, before incubating overnight in 2 mg/mL type II collagenase in cell culture medium at 37 °C to process the extracellular matrix proteins. At the end of incubation, the resulting valve interstitial cells (VIC) were plated in tissue culture plates in complete Ad DMEM and maintained at 37°C and 5% CO2. All the experiments were performed on cultured cells between the second and fifth passage.

2.9. Cell treatments

2.9.1. Calcium assay

Thirty thousand of cells were seeded in a 24 well plate (Merck, Darmstadt, Germany) in cell culture medium. After two days (when the confluence was about 80%) media was changed and the treatments were added. We use pro-osteogenic medium (β-glycerophosphate 10 mM and ascorbic acid 50 µg/mL; βGAA) and pro-calcific medium (inorganic phosphate 2 mM (Pi) with or without ascorbic acid (AA)). 2-thiouridine-5'-triphosphate (2ThioUTP; 10 µM) was added when necessary. Treatments and media were changed every other day for seven or fourteen days.

After removing the culture media, extracellular calcium crystals were dissolved with 0.6 M hydrochloric acid (HCl) for 5 h in gentle agitation. Subsequently, HCL samples were recovered and stored +4°C; meanwhile, the layer of cells present in each well was treated with 0.1 M sodium hydroxide (NaOH) and 0.1% sodium dodecyl sulfate (SDS) to ensure cellular lysis necessary for total protein quantification. Extracellular calcium quantification was performed using a colorimetric assay kit (BioVision Inc., Milpitas, CA, USA) following the manufacturing company's protocol. The absorbance was read off at the Infinite® 200pro (TECAN) spectrophotometer. Raw data on calcium concentration were normalized on the total protein measured by the bicinchoninic acid (BCA) protein assay kit (Thermo Fisher Scientific, Waltham, MA, USA).

2.9.2. Pro-fibrotic assay

For the fibrosis assays, one hundred thousand cells were seeded in a 6 well plate (Merck, Darmstadt, Germany) in cell culture medium. When adherent cell culture medium was changed with serum free medium and cells were treated with TGFβ1 (PeproTech, London, UK) every other day or 2ThioUTP (10 µM) every day without changing media for 5 days. At the end of the assay, media were collected, centrifuged at 500 g, for 5 minutes, at +4°C to pellet cellular debris and stored at -80°C until the analysis. Total mRNA and protein were extracted and preserved at −80°C until analyzed.

2.10. Nucleic acids handling

2.10.1. RNA Isolation from VICs

RNA extraction was performed from valve VECs using Total RNA Purification Plus Kit (Norgen Biotek Corp., Thorold, ON, Canada) according to the manufacurer's instructions. RNA quantification was determined with a spectrophotometer (ND-1000, NanoDrop®, EuroClone®).

2.10.2. Reverse Transcription and Real Time PCR

Reverse transcription was performed by LunaScript® RT SuperMix Kit (New England Biolabs, County Road Ipswich, MA, USA) following the manufacturer's instructions.

Real time PCR was performed on 25 ng of cDNA using Luna® Universal qPCR Master Mix (New England Biolabs, County Road Ipswich, MA, USA) following the manufacturer's instructions.

2.10.3. RNA sequencing by Oxford Nanopore Minion

2.10.3.1. Sample and library preparation

We prepared cDNA libraries following the recommendations of the Nanopore cDNA-Seq protocol for the SQK-PCS109 kit. Briefly, we employed RT primers to convert only poly-adenylated RNA into cDNA. For the multiplex run, we used six different ad hoc designed barcoded sequences. cDNA synthesis was performed using 50 ng of total RNA per sample. RT and strand-switching primers were provided by ONT with the SQK-PCS109 kit. Following RT, PCR amplification was performed using the LongAmp Taq 2X Master Mix (New England Biolabs, Ipswich, MA, USA) and the following cycling conditions: 1 cycle (95 °C for 30 s), 18 cycles (95 °C for 15 s, 62 °C for 15 s, and 65 °C for 3 min), and 1 last cycle (65 °C for 15 min). PCR products were purified using Agencourt AMPure XP beads (Beckman Coulter, Brea, CA, USA). The cDNA sequencing libraries were prepared using a total of 200 fmol of cDNA each.

2.10.3.2. MinION sequencing

Nanopore libraries were sequenced using a MinION Mk1B sequencing device with R9.4 flow cells. Sequencing was controlled and data were generated using ONT

MinKNOW software (v3.4.12). Runs were terminated after 48 h and FAST5 files were generated.

2.10.3.3. Data processing

DNA bases were called from FAST5 files using ONT Guppy GPU (v3.4.5) in high accuracy mode (31234903). Reads with an average Phred quality score, which measures the confidence based on the estimated error rate, lower than 7 were discarded. Reads were aligned to the 22 diploid chromosomes of the GRCh38 human genome reference with minimap2 (v2.1, default parameters except for -ax splice) [101]. SAM-to-BAM format conversion as well as an assessment of the alignment quality were performed using Samtools (v 1.10) [102]. The FeatureCounts software (v2.0.0) [103], included in the Subread package, was used to count the mapped reads.

2.10.3.4. Gene expression and functional analysis

The raw counts were processed using the R software environment (v 3.6.0). In particular, the genes were annotated based on the ENSEMBL ID and log2 counts per million mapped reads (CPM) were computed) [104]. For the multiplex run, the quality-checked reads were de-multiplexed and trimmed for barcodes using the Cutadapt function (v1.15) [105], before the alignment and counting procedures. Genes with a read count greater than 3 were deemed as expressed.

Differential expression analysis between male and female samples was performed through the limma R/Bioconductor package [106]. The genes with absolute value of log2 fold-change (|logFC|) > 1 and FDR-adjusted pValue < 0.05 were considered as differently expressed. The robustness of the differential expression analysis results was assessed by exploring the histogram of the pValue distribution.

Gene set enrichment analysis (GSEA) was conducted using GSEA pre-ranked tool (v 4.0.3) [97] and the biological functions were inferred by taking advantage of gene ontology biological processes (GO-BP), Reactome, WikiPathways, and BioCarta databases. To reduce redundancy and visually interpret GSEA results, the most significant GO-BP/Reactome/BioCarta pathway gene sets were identified by a false

discovery rate (FDR) < 0.1. The network was drawn through the Enrichment Map software (v.3.3.2) [98] implemented as a plug-in in Cytoscape v.3.8.2 [99].

2.11. Protein expression

2.11.1. Protein extraction

Protein extraction was performed in RIPA buffer (Merck, Darmstadt, Germany) with protease and phosphatase inhibitors (Sigma-Aldrich, St Louis, MO, USA). Cells were scraped in the RIPA buffer, moved in a 1,5 ml tube, and sonicated for 5 minutes for two cycles. Between one cycle and the other cells were placed on ice for five minutes to avoid sample degradation due to high temperature. Samples were put into rotation at +4°C for 1 hour, to facilitate mechanical disruption of cell membrane. At the end, samples were centrifuged at +4°C, for 20 minutes at 14000 g, to pellet cell membranes. Protein sample in the supernatant have been moved into fresh tubes, quantified by with BCA kit (Thermo Fisher Scientific, Waltham, MA, USA), following manufacturer's instructions and stored at -80°C until analysis.

2.11.2. Western blot

10 µg of total protein separation was performed using Bolt™4–12% Bis-Tris Plus Gels (Thermo Scientific, Waltham, MA, USA); after the run, we transferred proteins onto a nitrocellulose membrane and blocked them with 5% skim milk (Sigma-Aldrich, St. Louis, MO, USA). To detect target proteins, we incubated membrane overnight at 4 °C with specific primary antibodies: α-smooth muscle actin (αSMA; Abcam, Cambridge, UK) and α-tubulin (Novus Biologicals, Minneapolis, MN, USA). Then, the membranes were washed with TBS plus 0.1% Tween-20 and incubated with IRDye-conjugated secondary antibody (LI-COR Biosciences) for 20 min. Finally, the membranes were washed to remove any excess secondary antibody and acquired using an Odyssey Infrared Imaging System (LI-COR Biosciences). Densitometric analysis was performed using the software ImageJ (Version 1.48v– National Institute of Health).

2.11.3. Capillary western blot

The capillary Western blot was performed using WES for Simple Western (Protein Simple, BioTechne). Briefly, a total of 2 µg of protein was diluted in fluorescent

master mix 5×, sample buffer 10×, and DTT, following the manufacturer's instructions. Then, samples were thermically reduced at 95 °C for 5 min and loaded in a separation module 12–230 kDa (Protein Simple, Minneapolis, MN, USA). The running protocol was the standard one. To detect P2RY2 expression, we used anti-P2RY2 (Santa Cruz Biotechnology, Dallas, TX, USA) and anti-rabbit HRP-conjugated antibody (Protein Simple, Minneapolis, MN, USA). To normalize data, anti-GAPDH (Cell Signalling, Danvers, MA, USA) was used. Image analysis was performed using Compass for Simple Western software.

2.11.4. Sircol assay

Collagen secretion was evaluated in cell culture supernatant by sircol assay (BioColor, Carrickfergus, UK) following manufacturer's instructions. Briefly, collagen in medium samples were precipitated, stained with sircol dye reagent, washed, and resuspended in alkali reagent to be quantified. The absorbance at 555 nm was read by Infinite® 200pro (TECAN) spectrophotometer.

2.12. Imaging Flow Cytometry Analyses

2.12.1. P2RY2 staining

VIC characterization was performed by an ImageStream X flow cytometer, which combines flow cytometry with microscopy technology (ImageStream X Mark II, Amnis). VICs were detached through TripLE Select (Gibco, Carlsbad, CA, USA), an enzymatic method useful to preserve the extracellular epitopes of proteins on the cell surface. Then, we incubated cells in NH_4Cl 50 mM to break down cell auto-fluorescence, and resuspended in 100 µL of PBS with 5 mM ethylenediaminetetraacetic acid (EDTA), 1% bovine serum albumin (BSA). Then, cell samples were incubated for 30 min at room temperature using specific conjugated-antibodies against P2RY2 (Santa Cruz Biotechnology, Dallas, TX, USA) for 30 min, and conjugated with an anti-rabbit–AlexaFluor 647 for 30 min. Samples were then washed with FACS buffer (PBS con-taining 5 mM EDTA and 1% BSA) by centrifugation for 5 min at 600× g. Finally, cells were resuspended in FACS buffer and analyzed. A total of 30,000 events were acquired in the single cells and focus gated area. Image analysis was performed using the IDEAS 6.2 software.

2.12.2. Mitotracker and mitoSOX staining

Mitotracker and mitoSOX staining were performed using Mitotracker Green (Life Technologies, Carlsbad, CA, USA) and MitoSOX (Life Technologies, Carlsbad, CA, USA) probes following manufacturer's instructions.,

2.13. Statistical Analysis

Data were analyzed using Graph Pad Prism software (version 7). Quantitative variables with normal or skewed distribution were reported as mean ± SD or median and interquartile range, respectively. Variables were analyzed by Student's t-test or one-way ANOVA. A p-value <0.05 was deemed statistically significant.

3. RESULTS

3.1. Sex-specific differences in aortic valve calcium load: a systematic review and meta-analysis

3.1.1. Meta-analysis workflow and patient population description

In order to validate the hypothesis of sex-related outcomes in patients with calcific aortic valve stenosis, we performed a systematic review and meta-analysis evaluating sex differences in age-related AVC.

The search strategy, reported in the Material & Methods section, identifies 73 articles (**Figure 16**). Ones obtained the article list, we excluded duplicates and performed a screening of titles and abstracts to evaluate the eligibility of the study for the meta-analysis. A total of thirty-four articles were selected for the full-text evaluation. The revision of full-length papers allows the exclusion of twenty-seven articles due to wrong study design (n = 11) or lacked data of interest (n = 16). Thus, seven studies were included in the qualitative and quantitative synthesis [80, 83-85, 107-109].

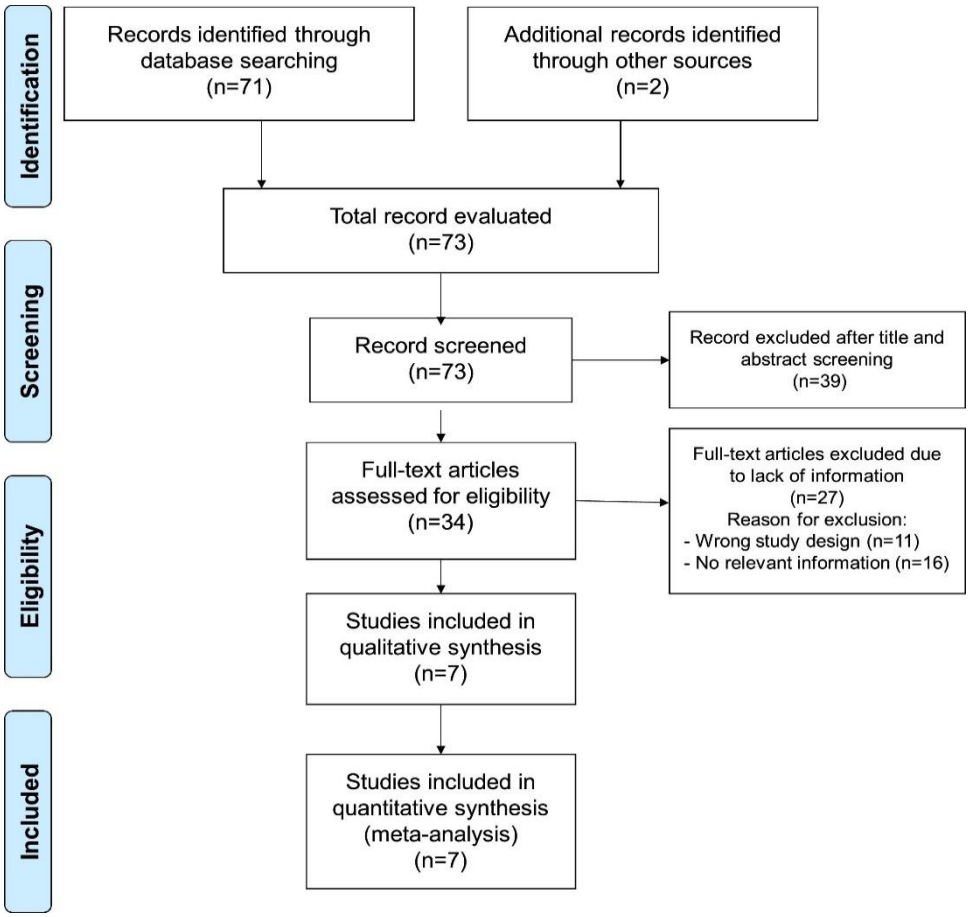

Figure 156: PRISMA flow diagram of meta-analysis.

All the patients' demographic and clinical characteristics are reported in the **Table 2**. All the included studies had a prospective design. The total number of enrolled patients was 2914 (1859 men and 1055 women), with a mean patient age ranges from 70 to 81 years. The number of participants in each single study varied from 103 to 794, with male gender prevalence between 57 % and 74 %, and mean AVC load ranging between 436 AU and 4062 AU. The presence of cardiovascular risk factors was carried out from each study, and it results to be: hypertension 67–89 %, dyslipidemia 58–69 %, diabetes in 17–38 %, and known coronary artery disease 35–66 % of cases. Furthermore, echocardiographic characteristics such as peak aortic jet velocity (3.0–4.4 m/s) and body surface area (1.82- 1.91 m^2) were reported in four studies. In six studies, mean value of aortic valve gradient varied from 22 mmHg to 55 mmHg, aortic valve area (AVA) from 0.66 cm2 to 1.39 cm^2, indexed aortic valve area (iAVA) from 0.39 cm^2/m^2 to 0.73 cm^2/m^2, and left ventricular ejection fraction (LVEF) from 56 % to 65 %.

Author, year	Sex	n	AVC, AU	AVC density, AU/cm^2	Age, year	HT, (%)	DM, (%)	Dys, (%)	BMI, kg/m^2	CAD, (%)	PAJV, m/s	MG, mmHg	AVA, cm^2	AVAi, cm^2/m^2	LVEF, %	BSA, m^2
Abramowitz *et al.* 2017	Men	354	4062±2029	-	81±8	507 (89)	176 (35)	-	27.5±6.2	366 (66)	-	42±12	0.66±0.15	-	56±15	-
	Women	209	1278±485	-												
Aggarwal *et al.* 2013	Men	427	2694±1628	633±399	75±11	453 (68)	158 (24)	444 (67)	28.3±6.1	279 (42)	3.97±0.94	39±19	1.05±0.35	0.55±0.19	60±13	1.91±0.24
	Women	238	1703±1321	520±384												
Clavel *et al.* 2013	Men modAS	102	1241±824	290±303	72±12	121 (70)	31 (17)	100 (58)	27.2±4.8	61 (35)	-	-	1.29±0.15	0.71±0.08	65±5	1.82±0.21
	Women modAS	72	487±473	142±218												
	Men sevAS	162	2695±2190	877±644	75±12	192 (67)	65 (23)	190 (66)	28.7±6.5	119 (42)	-	-	0.81±0.17	0.43±0.07	64±6	1.89±0.25
	Women sevAS	124	2100±1581	629±543												
Clavel *et al.* 2014	Men nsAVC	262	1070±708	257±263	72±12	121 (70)	31 (17)	100 (58)	27.2±4.8	61 (35)	3.0±0.7	22±11	1.29±0.15	0.71±0.08	65±5	1.82±0.21
	Women nsAVC	122	436±423	127±172												
	Men sevAVC	258	3403±1330	790±544	75±12	192 (67)	65 (23)	190 (66)	28.7±6.5	119 (42)	4.1±0.8	47±17	0.81±0.17	0.43±0.07	64±6	1.89±0.25
	Women sevAVC	152	1879±1051	553±522												
Nguyen *et al.* 2016	Men	152	1256±969	-	73±9	139 (68)	50 (25)	-	29±5	73 (36)	3.03±0.6	23±11	1.39±0.37	0.73±0.19	63±5	1.91±0.22
	Women	51	906±989	-												
Simard *et al.* 2017	Men	64	2741±1496	670±614	75±9	90 (87)	39 (38)	-	28.3±5.3	64 (62)	4.1±0.8	41±18	0.77±0.24	0.41±0.12	61±9	-
	Women	39	1279±765	400±375												
Thaden *et al.* 2016	Men	78	3606±1632	-	75±9	-	-	-	-	-	-	55 ±15	-	0.39±0.07	-	-
	Women	48	2520±1199	-												

Table 2: Demographic and clinical characteristics of patients. - data not available; AS: aortic stenosis; AVC: aortic valve calcification; AU: Agatston Units; AVA: aortic valve area; AVAi: indexed aortic valve area; BMI: body mass index; BSA: body surface area; CAD: coronary artery disease; ns: non severe; sevAS: severe aortic stenosis; modAS: moderate aortic stenosis; HT: hypertension; DM: diabetes mellitus; Dys: dyslipidemia; LVEF: left ventricle ejection fraction; PAJV: peak aortic jet velocity; MG: mean gradient.

3.1.2. Aortic valve calcium load difference in men and women with aortic valve stenosis

The meta-analysis of AVC load data showed a significant AU mean difference (MD) between men and women in AVC load (MD: 1131±243 AU; 95 %CI: 655, 1606; p<0.0001; **Figure 17A**) with a corresponding odds ratio (OR) of 5.2 (95 %CI: 3, 9; p<0 0.0001). The heterogeneity among studies was significant (I2: 96.5; p<0.001), but, even after the exclusion of each study from the analysis, it was not reduced. Similar results were obtained considering only the subpopulation of patients with severe aortic valve stenosis (MD: 1214±415 AU; 95 % CI: 400, 2028; p<0.001; **Figure 17B**). This meta-analysis confirmed that men with AS have a higher AVC load than women with an OR of 4.4 (95 %CI: 2, 11; p<0 0.001).

3.1.3. Indexed aortic valve calcium density difference in men and women with calcific aortic valve stenosis

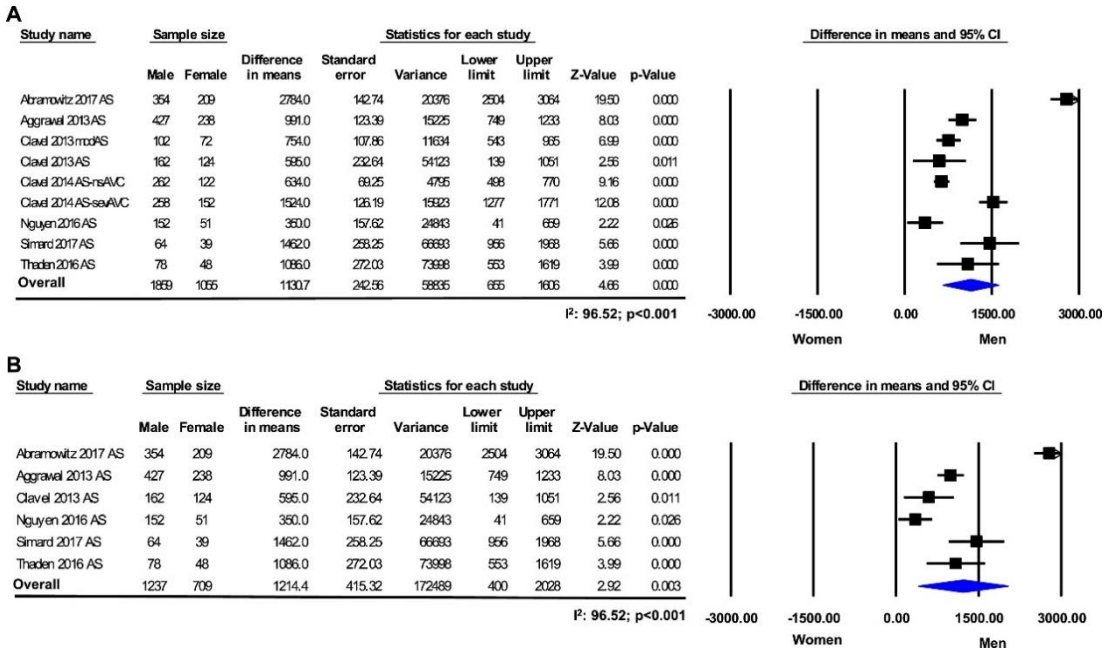

Figure 17: Forest plot of aortic valve calcium (AVC) load in men and women. (**A**) Studies including patients with different degree of aortic stenosis (AS). (**B**) Studies including only patients with severe AS. Calcification was evaluated with the difference in means (MD) with standard error between men and women, expressed as continuous variable in AU. The diamond represents the estimated overall effect, while the squares represent each study with 95 %CI.

Studies that reported data on AVC density showed a significant difference between men and women with AS in AVC density (MD: 159±20 AU/cm2; 95 %CI: 119, 200, p<0.0001, **Figure 18A**) with a corresponding OR of 2.2 (95 %CI: 2, 3; p<0 0.0001). In this case, no heterogeneity among studies have been resulted (I^2: 23.5; p = 0.3). Considering the studies with severe CAVS only, the

AVC density remain significantly higher in men (MD: 185±47 AU/cm2; 95 %CI: 92, 278, p<0.0001; **Figure 18B**) with OR of 2.0 (95 %CI: 2, 2; p<0 0.0001) compared to women.

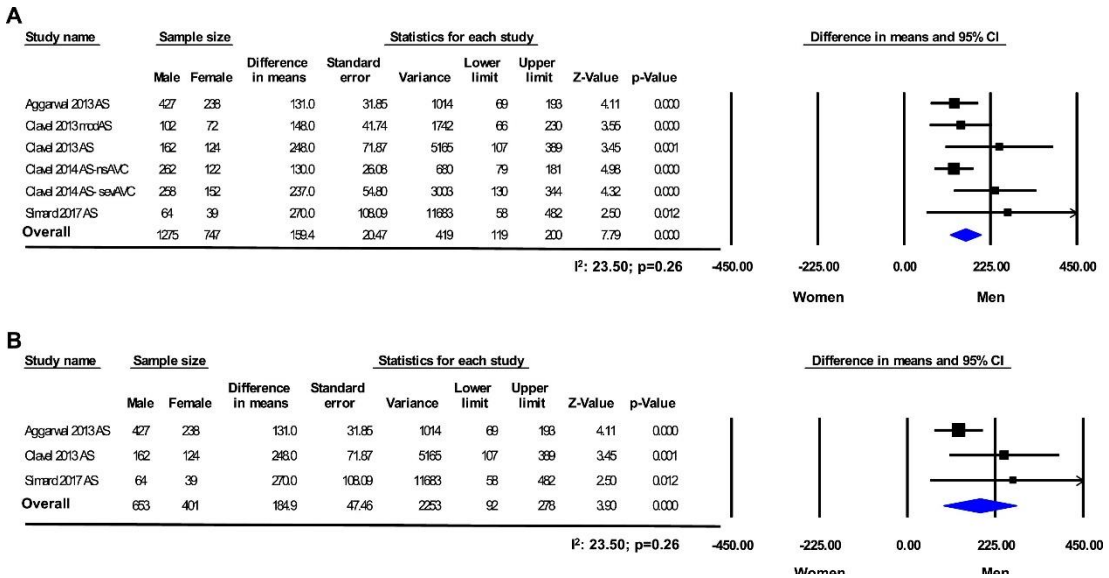

Figure 18: Forest plot of aortic valve calcium (AVC) load in men and women. (**A**) Studies including patients with different degree of aortic stenosis (AS). (**B**) Studies including only patients with severe AS. Calcification was evaluated with the difference in means (MD) with standard error between men and women, expressed as continuous variable in AU. The diamond represents the estimated overall effect, while the squares represent each study with 95 %CI.

3.2. Sex-specific analysis of cellular and molecular pathways activated in CAVS patients' aortic valve leaflets and in the periphery

3.2.1. Contrast computed tomography evaluation of indexed aortic valve calcium and fibrosis

Fifty-six age-matched patients with severe AS (28 men and 28 women; age: 71± 11 years) were enrolled for this analysis. All patient characteristics are summarized in the **Table 3**.

Variables	**Men** **n = 28**	**Women** **n = 28**	**Total** **p-Value**
Age, years	71.4±10.8	71.5±11.1	0.961
Diabetes, n (%)	7 (25)	5 (18)	0.515
Hypertension, n (%)	22 (79)	21 (75)	0.752
Dyslipidaemia, n (%)	22 (79)	16 (57)	0.086
Smoking, n (%)	9 (32)	8 (27)	0.771
Body mass index, kg/m^2	26.9±3.8	26.2±6.0	0.588
eGFR, mL/min/1.73m^2	72.3±17.6	80.1±16.3	0.053
BSA, m^2	1.89±0.14	1.67±0.17	**< 0.001**

LVEF, n (%)	64.0±7.8	64.5±7.2	0.798
Peak aortic jet velocity, m/s	4.4±0.6	4.4±0.7	0.916
Mean gradient (mmHg)	46.7±11.8	48.0±15.2	0.726
Aortic valve area, cm^2	0.91±0.21	0.74±0.23	**0.007**
Aortic valve area indexed (cm^2/m^2)	0.48±0.12	0.45±0.15	0.365
Antiplatelet agents, n (%)	17 (61)	13 (46)	0.284
ACE -inhibitors, n (%)	8 (27)	11 (39)	0.397
Angiotensin Receptor Blockers, n (%)	10 (36)	7 (25)	0.383
Beta-blockers, n (%)	17 (61)	18 (64)	0.783
Calcium channel blockers, n (%)	6 (21)	7 (25)	0.752
Diuretics, n (%)	11 (39)	7 (25)	0.252
Anti-diabetic drugs, n (%)	4 (14)	4 (14)	1.000
Lipid-lowering drugs, n (%)	18 (64)	11 (39)	0.061

Table 3: Characteristics of sex and age-matched aortic stenosis (AS) patients that underwent contrast-enhanced cardiac computed tomography. ACE: angiotensin converting enzyme; eGFR: estimated glomerular filtration rate; LVEF: left ventricular ejection fraction. p-value <0.05 are reported in bold.

In brief, there was no difference between men and women in major cardiovascular risk factors, valve phenotype (17 BAV and 39 TAV in total), nor pharmacological treatment. As expected, men had higher body surface area and annulus diameter than women (1.89 ± 0.14 *vs.* 1.67 ± 0.17 m^2, respectively; $p < 0.001$) and (36.1 ± 3.0 *vs.* 31.9 ± 2.8 mm, respectively; $p < 0.001$), while women had lower aortic valve area than men (AVA; 0.74 ± 0.2 *vs.* 0.91 ± 0.2 cm^2, respectively; pValue = 0.007), but similar indexed AVA (0.44 ± 0.15 *vs.* 0.48 ± 0.12 cm^2/m^2, respectively; pValue = 0.262). As described in the Material & Methods section, we implemented images analysis to evaluate the indexed AVC (iAVC) and fibrosis (iAVF), using CT scan examination performed on patients with severe AS (**Figure 19A-H**). The iAVC resulted higher in men compared to women (72 [95% CI: 48-114] mm^3/cm^2 *vs*. 36 [95% Confidence Interval (CI): 27-49], respectively; pValue = 0.011; **Figure 19I**); the we (iAVF) of the valve leaflets was significantly higher in women compared to men (83 [95% CI: 65-111] vs. 63 [95% CI: 45-82] mm3/cm2, respectively; pValue = 0.026; **Figure 19J**). Finally, the fibro-calcific ratio, which indicates the predominance of valve fibrosis if > 1.0, was significantly higher in women compared to men (2.57 [95% CI: 1.16-3.62] *vs.* 0.78 [95% CI: 0.43-1.95], respectively; pValue = 0.0018).

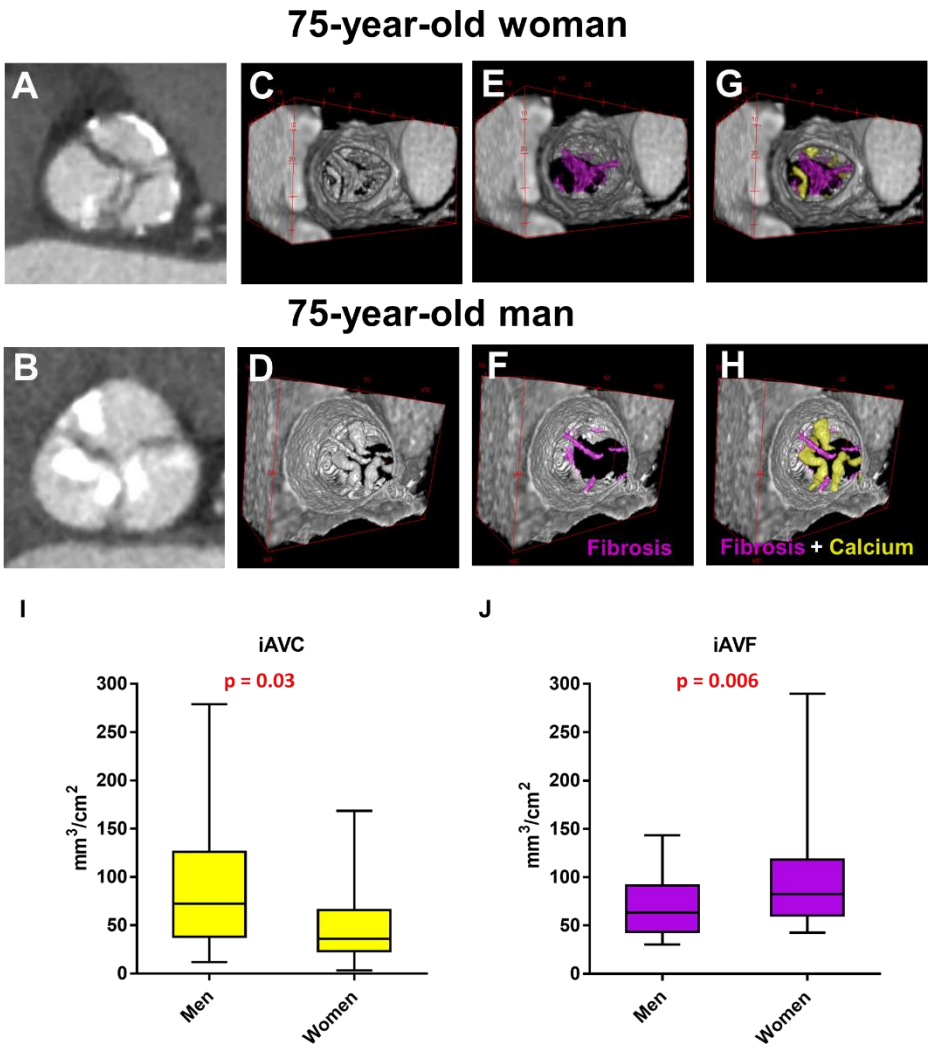

Figure 19: Manual analysis of aortic valve calcium and fibrosis by contrast-enhanced computed tomography in men and women. (**A, B**) Computed tomography images reoriented into en face aortic valve view from a woman and a man with severe aortic stenosis. (**C–H**) Representative 3D contrast-enhanced volume rendered views of aortic valve from a woman and a man with fibrotic tissue enhanced in violet and calcium in yellow. Box plots showing the difference in indexed aortic valve calcium (**I**) and fibrosis (**J**) volume between men (n = 28) and women (n = 28) with severe AS. Unpaired non-parametric Mann-Witney test was used to evaluate differences.

As the identification of valve in CT scans is a crucial step and could depend on the human operator experience, we validated our findings training a deep learning model (U-Net) to automatically recognize valve area in each frame without prior knowledge and calculate calcium and fibrosis volumes (**Figures 20A–C**). As shown in **Figure 20D**, we observed a high level of overlapping (Dice Score = 0.93+-0.09) between 400 predictions of valve area, performed by a human operator and

the U-Net. Moreover, a Pearson's correlation index rp = 0.82 in 10 females and rp = 0.93 in 10 males was gained comparing the calcium volume calculated by human (x-axis) and obtained by the deep learning automatic framework on the test set (i.e., the dataset containing images never seen by U-net during training), while a rp = 0.96 in 10 females and rp = 0.93 in 10 males was gained comparing the fibrosis volume calculated by human (x axis) and obtained by the deep learning automatic framework on the test set (**Figures 20E–H**).

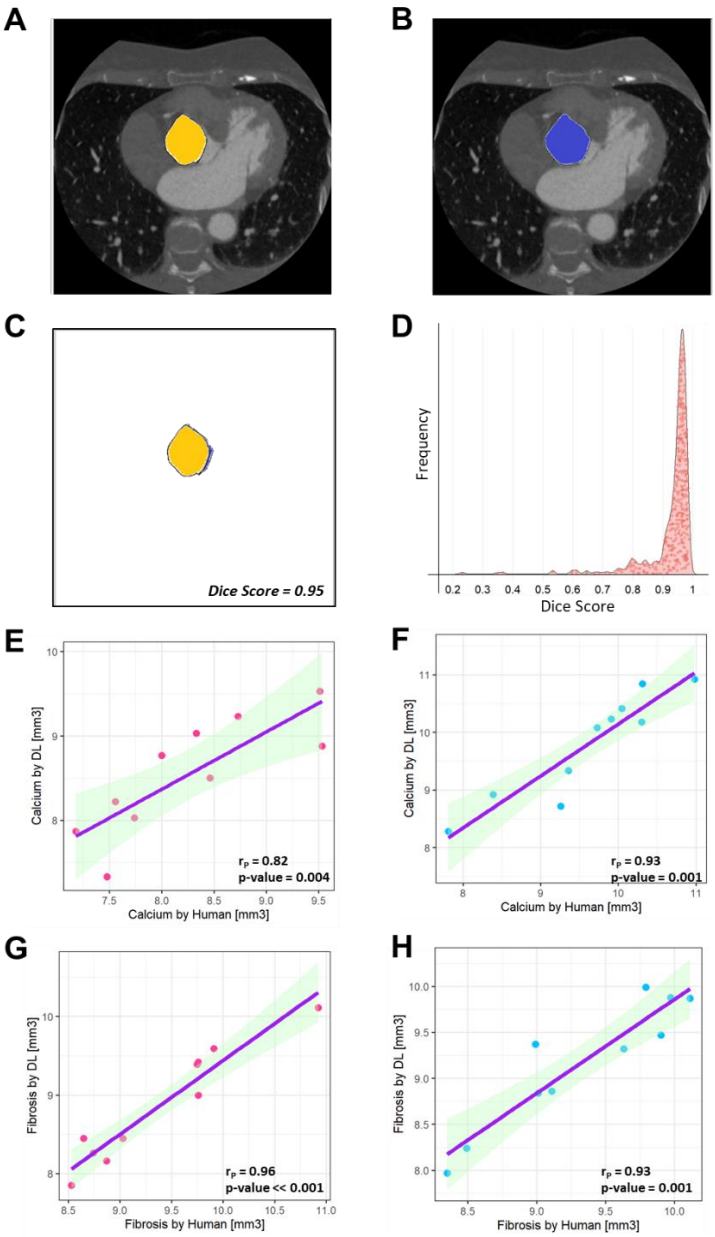

Figure 20: U-net performances. (**A**) An example of mask designed by the human operator ('Ground truth') is highlighted in yellow and combined with the original frame. (**B**) An example of mask predicted by U-Net is highlighted in blue and combined with the original frame. (**C**) The high overlapping level between A and B is assessed by the Dice Score (0.95). (**D**) Distribution of Dice Scores shows that a higher level of overlapping (Dice score = 0.93 +- 0.09) was obtained between the learned U-Net model and the human operator. (**E**) A Pearson's correlation index rP = 0.82 was gained comparing the calcium volume in 10 female patients calculated by human (x-axis) and obtained by the deep learning automatic framework on the test set. (**F**) A Pearson's correlation index rP = 0.93 was gained comparing the calcium volume in 10 male patients calculated by human (x-axis) and obtained by the deep learning automatic framework on the test set. (**G**) A Pearson's correlation index rP = 0.96 was gained comparing the fibrosis volume in 10 female patients calculated by human (x-axis) and obtained by the deep learning automatic framework on the test. (**H**) A Pearson's

correlation index rP = 0.93 was gained comparing the fibrosis volume in 10 male patients calculated by human (x-axis) and obtained by the deep learning automatic framework on the test set.

3.2.2. Circulating cytokines evaluation in control, sclerotic and stenotic subjects

In order to evaluate the systemic inflammation during CAVS progression, we decided to measure the circulating cytokine expression in the peripheral blood. We enrolled 238 subjects age and sex mached (80 healthy subjects, 78 AVSc patients, and 80 AS patients). In the **Table 4** are summarized demographical and clinical characteristics of all subjects. Subjects enrolled for serum cytokines evaluation were sex- and age- matched. The groups differed for the presence of hypertension, dyslipidaemia, and body mass index, all factors associated with CAVS. As per diagnosis the peak aortic jet velocity was higher in AS patients than in control subjects and AVSc patients.

Variables	**CTRL** **n = 80**	**AVSc** **n = 77**	**AS** **n = 81**	**P value**
Sex, male	39 (48.7)	41 (53.2)	50 (61.7)	0.25
Age, years	63.3 ± 4.3	64.2 ± 5.7	62.7 ± 6.8	0.27
Diabetes, n (%)	4 (5.0)	8 (10.4)	11 (13.6)	0.18
Hypertension, n (%)	30 (37.5)	39 (50.6)	62 (76.5)	**<0.0001**
Dyslipidaemia, n (%)	15 (18.7)	25 (32.5)	33 (40.7)	**0.009**
Smoking, n (%)	9 (11.2)	13 (16.9)	10 (12.3)	0.55
Body mass index, kg/m^2	24.6 (4.1)	25.5 (4.5)	28.1 (5.1)	**<0.0001**
Ejection fraction, %	61.5 (5.9)	61.2 (9.4)	63.0 (7.5)	0.29
Peak aortic jet velocity, m/s	1.3 ± 0.2	1.4 ± 0.3	4.4 ± 0.7	**<0.0001**

Table 4: Characteristics of sex and age-matched control (CTRL), sclerotic (AVSc) and stenotic (AS) subjects enrolled for the evaluation of serum cytokines. ANOVA p-value <0.05 are reported in bold.

The differential analysis showed that there were some cytokines differential expressed by the three groups (with a log(FC) over or equal to the threshold of 0.3). In particular, there was an upregulation of growth-regulated α protein (GROα; log(FC) = 0.47; p = 0.003) and interleukin 1β (IL-1β; log(FC) = 0.30 p = 0.046; **Figure 21A**) in AVSc, and of tumor necrosis factor α (TNFα; log(FC) = 0.30; p = 0.03; **Figure 21B**) in AS patients compared to controls. Furthermore, we found that

monocyte chemoattractant protein 1 (MCP-1; log(FC) = -0.62; p < 0.001), fms related receptor tyrosine kinase 3 ligand (Flt3-Ligand; log(FC) = -0.40; p = 0.004), epidermal growth factor (EGF; log(FC) = -0.31; p = 0.036), Eotaxin (log(FC) = -0.32; p = 0.036), and TNF-related apoptosis inducing ligand (TRAIL; log(FC) = -0.31; p = 0.046; **Figure 21B**) were upregulated in controls compared to AS patients, while Flt3-Ligand (log(FC) = -0.56; p < 0.001), MCP-1 (log(FC) = -0.52; p = 0.001), IL-1β (log(FC) = -0.46; p = 0.002), IL-1α (log(FC) = -0.40; p = 0.011); interferon α (INFα; log(FC) = -0.21; p = 0.012), Eotaxin (log(FC) = -0.37; p = 0.020), TRAIL (log(FC) = -0.35; p = 0.029), and macrophage inflammatory protein 1-β (MIP-1β; log(FC) = -0.34; p = 0.034; **Figure 21C**) were upregulated in AVSc respect to AS patients.

To explore if there were differences between sexes, we perform the same differential analysis for sex in each group. The analysis reported that control men expressed more IL-1β and platelet derived growth factor subunit AB/BB (PDGF-AB/BB) than women controls (**Figure 22A**); among AVSc patients, men expressed more INFγ, MIP-3α, IL-10, CD274 molecule (PD-L1/B7-H1), IL-1β, TNFα, IL-1α, and IL-13 and less GROα, GROβ, and RANTES compared to women (**Figure 22B**); AS women showed a higher amount of RANTES and a lower amount of TNFα, MIP-1α, and INFβ respect to AS men (**Figure 22C**).

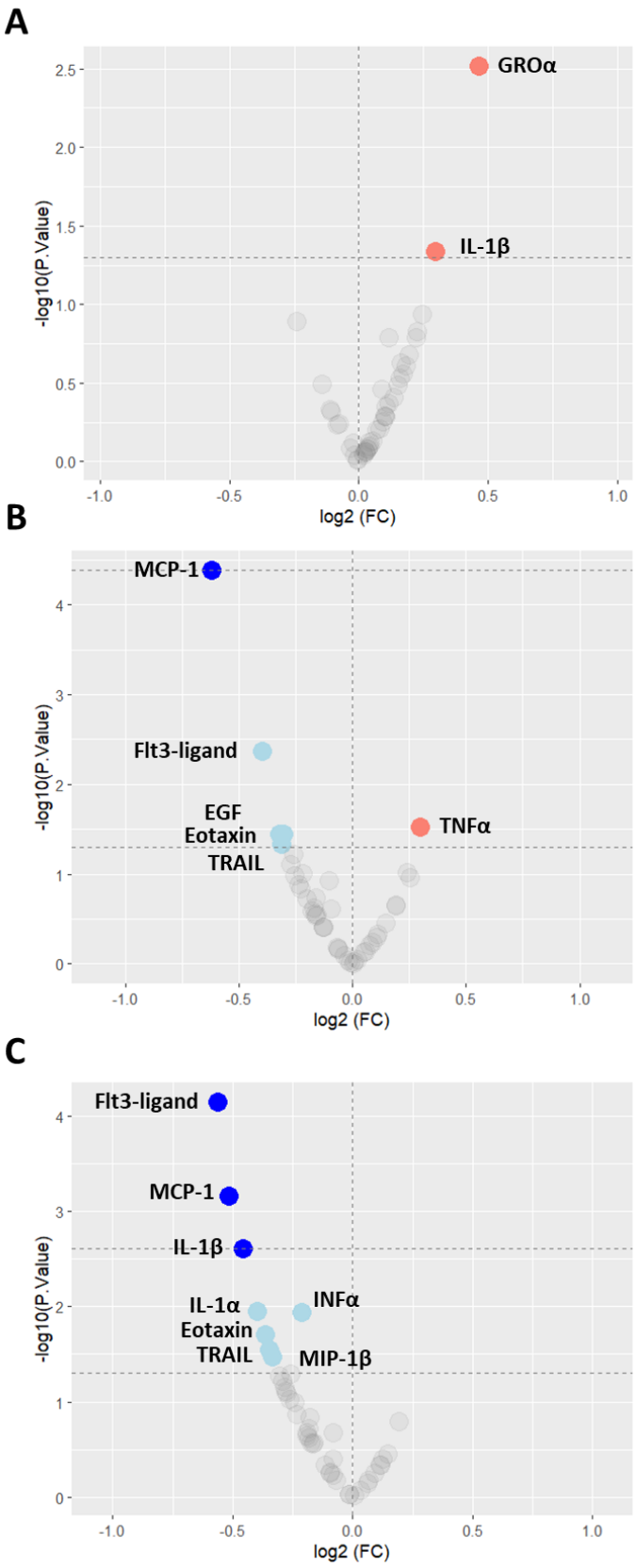

Figure 21: Volcano plots showing differential expression of human serum cytokines. (**A**) AVSc *vs*. controls; (**B**) AS *vs*. controls (**C**) AS *vs*. AVSc. Dark (adjusted $p < 0.05$) and light ($p < 0.05$) blue dots represent downregulated cytokines; light red dots represent upregulated cytokines ($p < 0.05$).

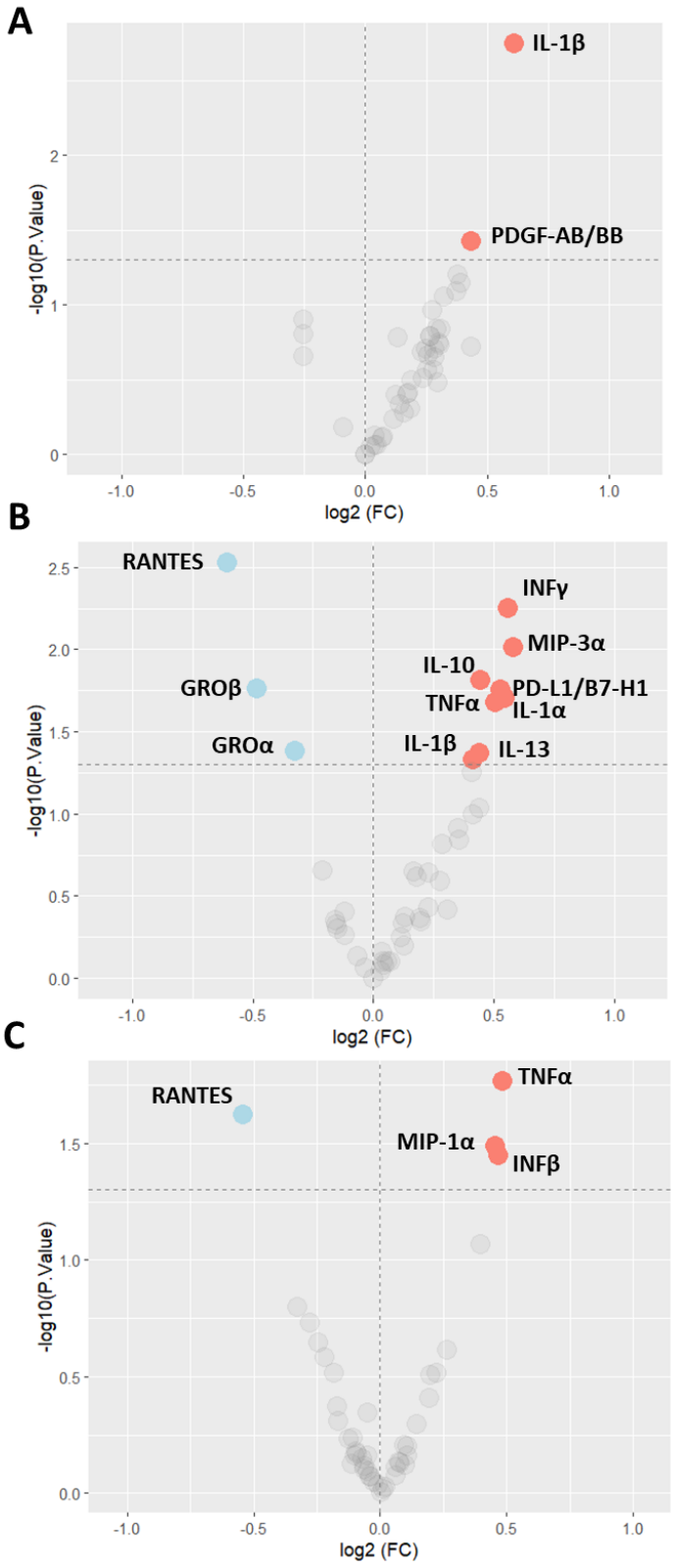

Figure 22: Volcano plots showing sex differential expression of human serum cytokines. (**A**) Controls; (**B**) AVSc (**C**) AS. Blue dots represent upregulated cytokines in women ($p < 0.05$); red dots represent upregulated cytokines in men ($p < 0.05$).

3.2.3. Stenotic aortic valve sex-specific gene expression and functional enrichment analysis

To better define the influence of CAVS disease in the regulation of circulating cytokines levels, we took advantage of a public microarray dataset of whole valve tissue explanted by 240 AS patients. We analysed a public microarray-based gene expression dataset of 240 human stenotic aortic valves specimens to identify the genes and the biological pathways differentially expressed between women and men with severe AS. The sex classification for each sample was performed based on the expression levels of XY-linked genes. In particular, ribosomal protein S4 Y-linked 1 (RPS4Y1) and X inactive specific transcript (XIST) genes were considered sex-specific markers. The identification of one transcript or the other let us identify the sex of the specimens. During the differential expression analysis, the XY-linked genes and pseudogenes were filtered out.

We observed that 3105 genes were significantly regulated by sex (**Figure 23**). In particular, 80 genes upregulated in women and 173 genes upregulated in men, were over the threshold of 0.2 log2 fold-change (logFC; **Figure 23A**). Plotting these 253 genes in the heatmap (**Figure 23B**) we found a clear separation of the specimens by sex.

Using GSEA, we found a total of 4979 pathways characterizing women and men's stenotic aortic valves. To enhance the interpretation of the results, we clustered the most significant pathways (FDR qValue < 0.1) into 33 macropathways (8 related to women and 25 related to men; **Figure 24**). The most representative pathways associated with women were related to the regulation of mRNA splicing, intraflagellar transport, post-translational modification (i.e., mannosylation), elastin fibres formation, insulin-like growth factor 1 pathway, and regulation of tyrosine kinase receptor. In contrast, the most representative pathways associated with men belonged to the immune system response (innate and adaptive immunity), cell migration, and chemotaxis, constituting the wider groups of highly interconnected gene sets. Other molecular pathways enriched in men are inflammation (interleukin 1, 2, 4, 6, 8, 10, and 12), bone remodelling, cell proliferation, endothelial cell differentiation, cellular senescence, lipoprotein metabolism, reactive oxygen species, and reactive nitrogen species production, and regulation of platelet aggregation.

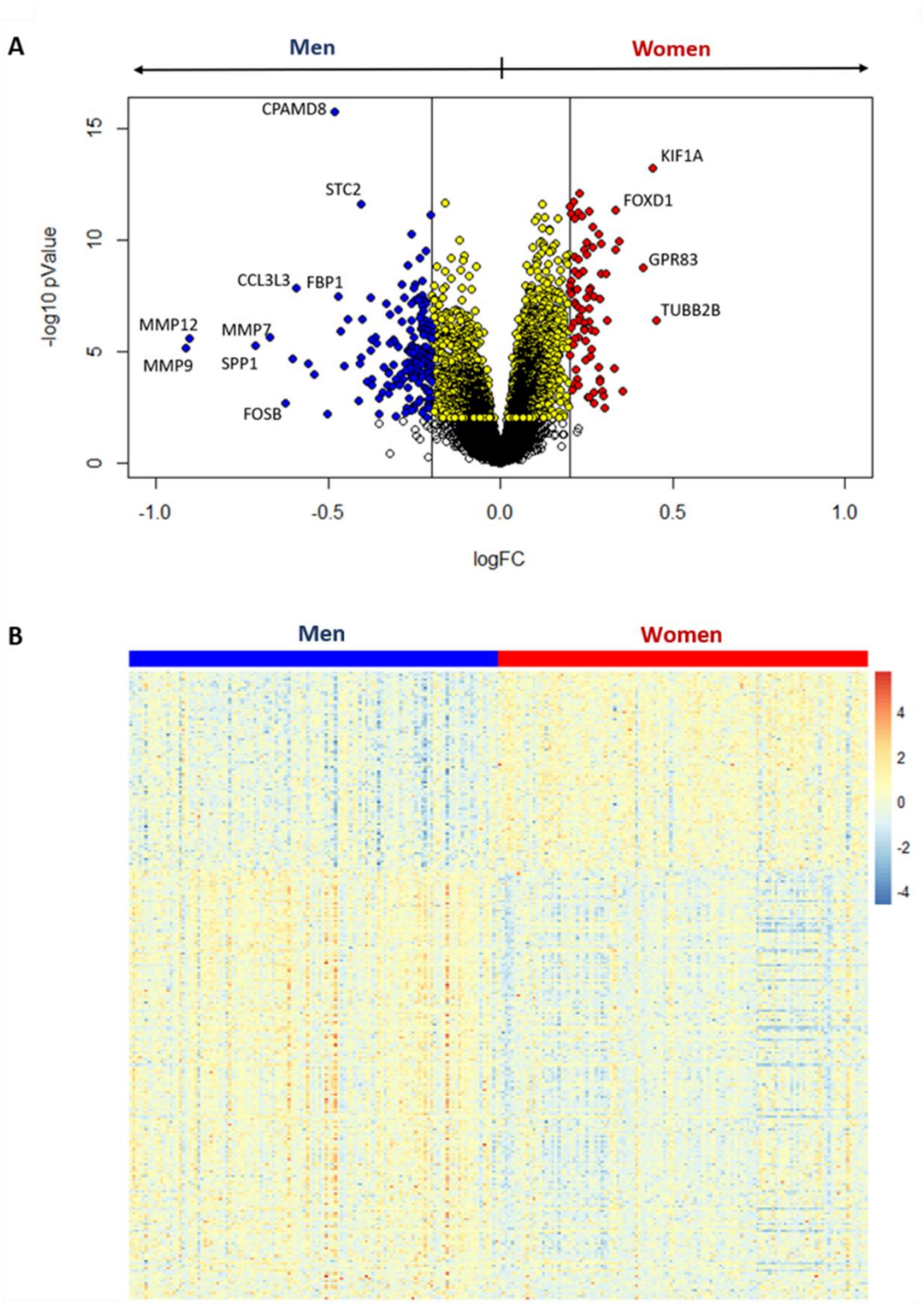

Figure 23: Differential expression analysis between women and men stenotic aortic valves. (**A**) Volcano plot of the differentially expressed genes. Yellow dots represent significant differentially expressed genes at adjusted pValue < 0.05, whereas red and blue dots represent upregulated genes in women and men, respectively, with both the adjusted pValue < 0.05 and the absolute log2 fold change (logFC) > 0.2. (**B**) The heatmap shows the expression levels for the significantly upregulated genes with logFC > 0.2 in women (red) and men (blue).

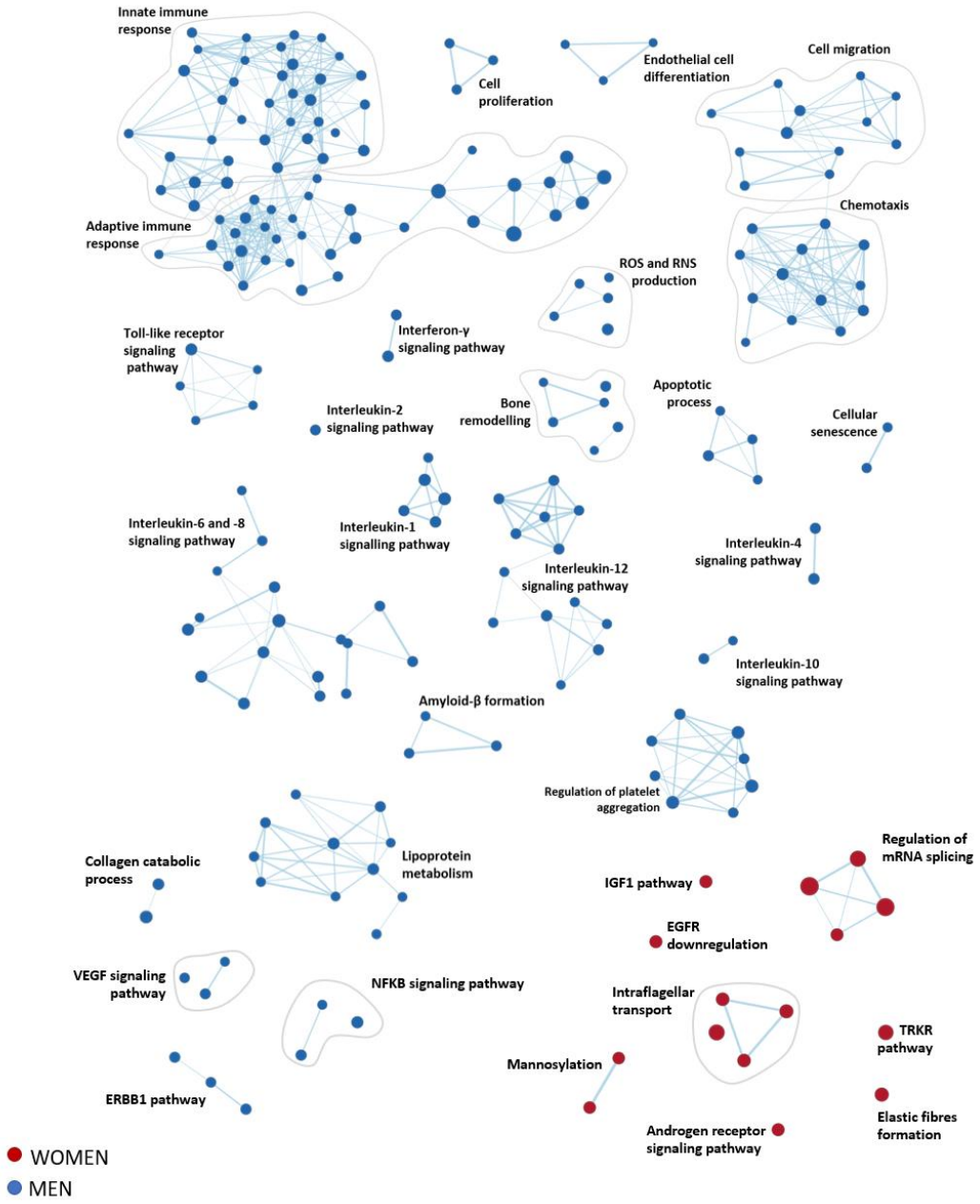

Figure 24: Functional inferences from gene expression analysis of women and men stenotic aortic valves. The enrichment network shows the pathway nodes that are associated (FDR qValue < 0.1) with women (red) and men (blue), where the node size is proportional to the gene-set size.

3.2.4. Enrichment analysis of sex-specific cell types in stenotic aortic valve tissues

We used the microarray dataset to analyse the cellular composition of stenotic aortic valve, in order to visualize sex-differences. To this purpose we employed the xCell method to convert the gene expression profile to enrichment scores of several immune and stromal cell types across specimens (32124326). As expected, aortic valve leaflets showed a heterogeneous cell population (33086873). The cell-type enrichment analysis showed that 14 cell types significantly differed

between women and men (adjusted pValue < 0.05, **Figure 25A**). In particular, 4 cell types were identified as over-represented in women (logFC > 0) and 10 in men (logFC < 0; **Figure 25B**).

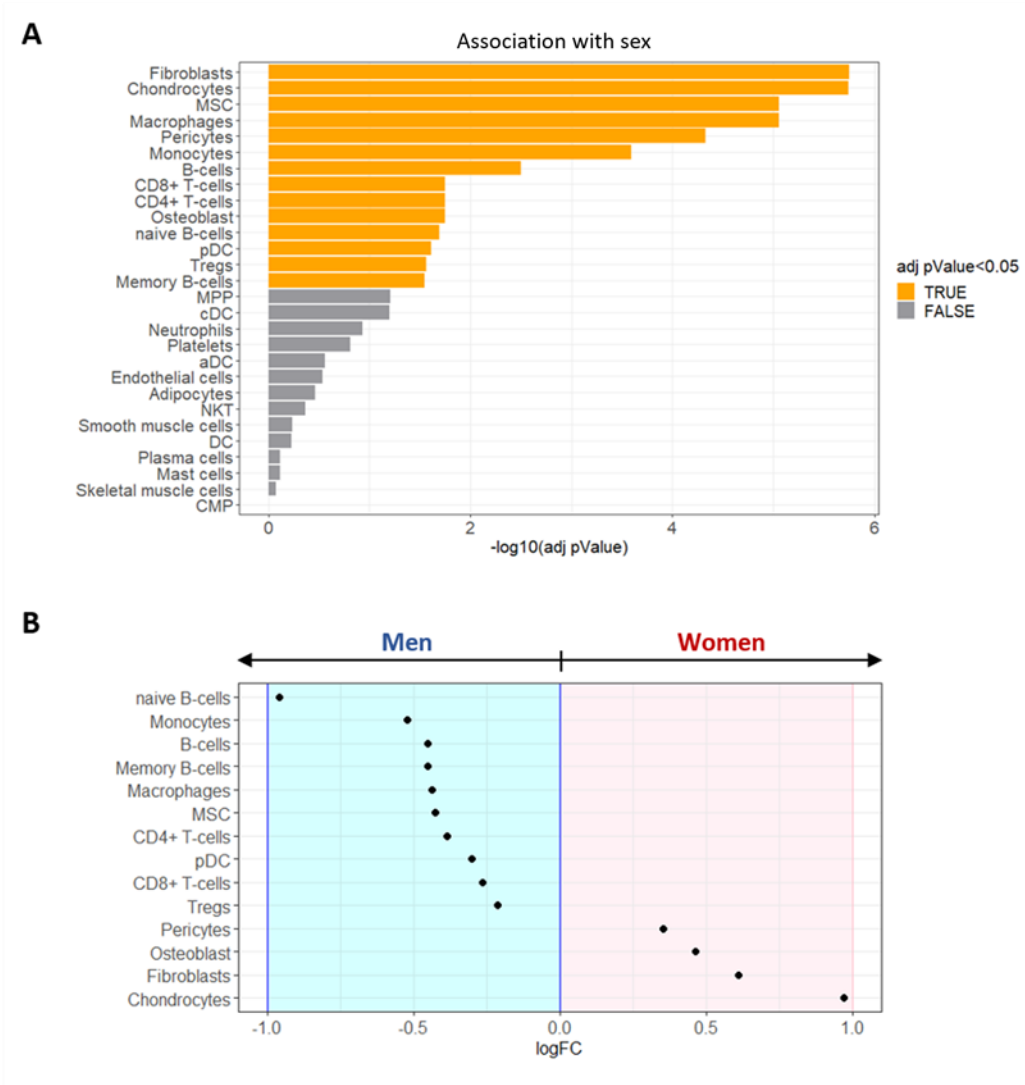

Figure 25: Enrichment analysis of sex-specific cell types in stenotic aortic valve tissues. (**A**) Bar graph showing the sex-related association of xCell scores, performed by Wilcoxon rank-sum test. The cell types with FDR adjusted pValue < 0.05 (orange) were considered significantly associated with one of the two sexes. (**B**) The dot plot shows the log2 fold change (logFC) of xCell scores, being associated with women (logFC > 0; pink background) or with men (logFC < 0; light blue background).

The most representative cell types in women's stenotic aortic valve leaflets were chondrocytes, fibroblasts, osteoblasts, and pericytes. Conversely, men's stenotic aortic valve leaflets were characterized by the presence of i) innate immune system cells (monocytes, macrophages, and dendritic cells), ii) adaptive immune system cells (B and T lymphocytes), and iii) mesenchymal stem cells.

3.3. In vitro evaluation of extracellular calcification potential and fibrosis of VICs isolated from AS patients

In order if VICs in vitro recapitulate the differences in fibro-calcification seen *in vivo*, we implemented calcification and fibrosis assays.

3.3.1. In vitro sex-dependent calcification of VICs isolated from CAVS valve

The calcification potential of VICs was evaluated by a colorimetric kit after 7 days of culture in basal, pro-osteoblastic (β-glycerophosphate and ascorbic acid) and pro-calcific (inorganic phosphate) conditions. The analysis showed that in basal conditions man AVSc VICs calcified more than VICs from women (3.47 ± 0.79 *vs*. 0.30 ± 0.12 ng (calcium)/ µg (total protein), respectively; p = 0.002), while AS VICs from men calcified less than VICs from women (17.96 ± 2.20 *vs*. 25.32 ± 2.67 ng (calcium)/ µg (total protein), respectively; p = 0.037; **Figure 26A**). In pro-osteoblastic conditions, we found no differences in terms of calcification in AVSc VICs (men: 34.79 ± 5.10 *vs*. women: 37.18 ± 6.84 ng (calcium)/ µg (total protein); p = 0.78) and AS VICs (men: 29.63 ± 1.99 *vs*. women: 30.67 ± 3.83 ng (calcium)/ µg (total protein); p = 0.83; **Figure 26B**) between sexes. When we boost calcification with inorganic phosphate 2 mM, AVSc VICs from men calcified less then VICs from women (155.00 ± 24.62 *vs*. 579.60 ± 35.03 ng (calcium)/ µg (total protein), respectively; p < 0.0001), while AS VICs from men calcified more than AS VICs from women (237.80 ± 23.48 *vs*. 125.80 ± 12.65 ng (calcium)/ µg (total protein), respectively; p = 0.0002; **Figure 26C**).

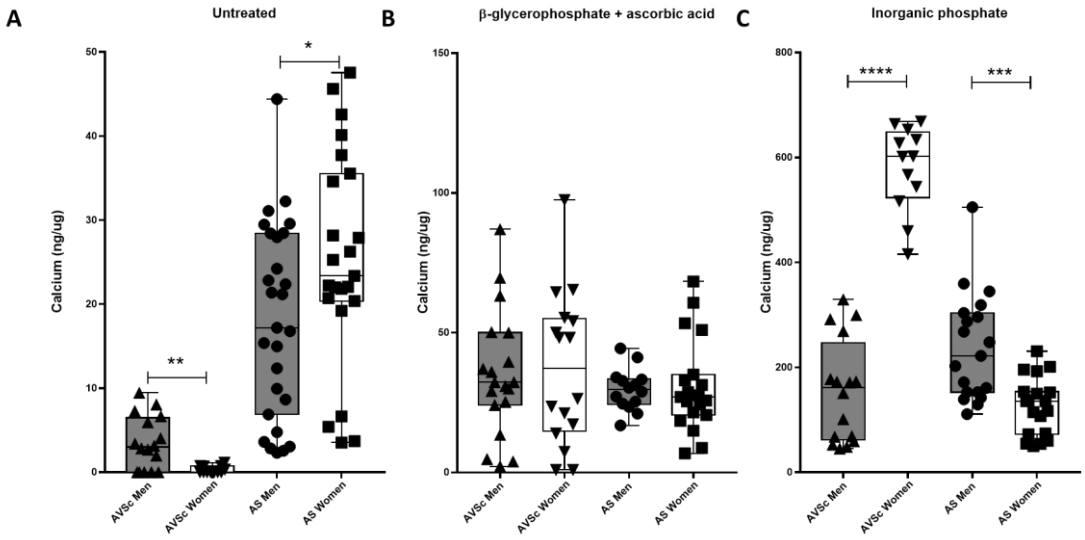

Figure 26: Extracellular calcification of VICs isolated from sclerotic (AVSc) and stenotic (AS) valve leaflets. Box plots showing the difference in extracellular calcification of AVSc (n = 5 men vs. 4 women) and AS (7 men vs. 6 women) VICs in basal (A), pro-osteoblastic (B) and pro-calcific (C) conditions. * = p < 0.05; ** = p < 0.01; *** = p < 0.001; **** = p < 0.0001.

3.3.2. In vitro evaluation of sex-dependent fibrosis processes activated by VICs

We evaluated the production of collagen, as marker of fibrosis activation, both in terms of mRNA transcription (**Figure 27A**) and secretion by Sircol assay (**Figure 27B**).

As shown in the **Figure 27**, women AS VICs expressed more collagen type I α 1 chain (Col1A1) than AS men (0.50 ± 0.13 Log2(FC) *vs*. 0.00 ± 0.09 Log2(FC), respectively; **Figure 27A**) and they secrete also more collagen than men VICs when exposed to tissue growth factor β1 (TGFβ1), a strong pro-fibrotic stimulus (1.22 ± 0.03 *vs*. 1.19 ± 0.09 FC, respectively; **Figure 27B**)

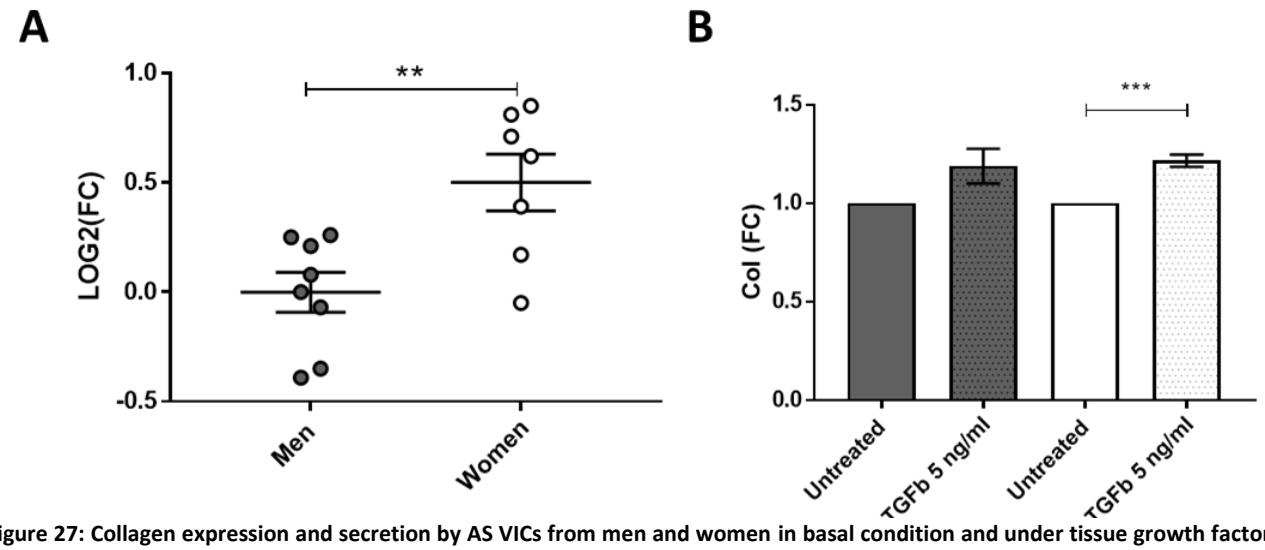

Figure 27: Collagen expression and secretion by AS VICs from men and women in basal condition and under tissue growth factor β1 (TGFb) treatment. (A) Collagen 1A1 mRNA expression in basal condition (n = 8 men vs. 7 women). (B) Collagen secretion under TGFb treatment (n = 4men *vs*. 4 women). ** = p < 0.01; *** = p < 0.001

3.4. Sex-specific analysis of cellular and molecular pathways activated in CAVS patients' valve interstitial cells

In order to explore sex-dependent molecular pathways activated in VICs from CAVS patients, we choose to set a long-read sequencing technique, MinION sequencer, an Oxford Nanopore Technologies (ONT), which offers the ability to generate sequencing data in real time via portable protein nanopore USB devices. The process is based on the passage of DNA/RNA strands through a biological nanopore, generating base-specific changes in electrical conductivity and leading to the identification of specific sequences using a neural network.

3.4.1. Evaluation of Oxford Nanopore MinION RNA-seq performance for human primary cells

To set the technique, three cDNA libraries, obtained from poly-adenosine (poly-A) RNA retrotranscription of six human primary VIC samples ligated with six different barcodes, were sequenced by an ONT MinION sequencer using R9.4 flow cells. The comparison of the gene expression levels, expressed as log2(CPM), showed a strong correlation among these three independent replicates (Pearson's correlation coefficient (rp) = 0.98; **Figure 28**).

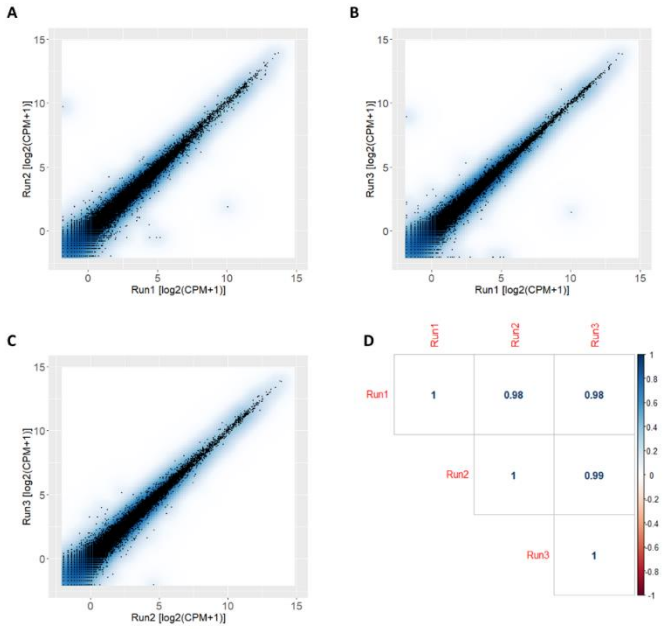

Figure 28: Correlation analysis comparing the three libraries. (**A**) Scatter plot of log2(CPM) values from run1 vs. run2. (**B**) Scatter plot of log2(CPM) values from run1 vs. run3. (**C**) Scatter plot of log2(CPM) values quantified from run2 vs. run3. (D) Correlation matrix with Pearson correlation coefficients

The reliability of the results was evaluated by comparing the quantifications obtained from cDNA sequencing with the dCt values of thirteen selected genes (IL4, MALAT1, COL1A1, DCN, MMP2, H19, CAT, SOD3, BCL2, and BMP2) detected by qPCR. There was a significant correlation between each dataset quantification and the qPCR values ($rp \geq 0.8$ and $p < 0.01$; **Figure 29**).

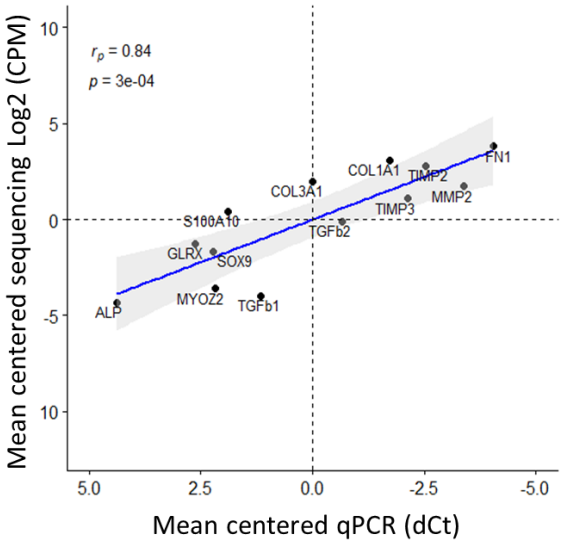

Figure 29: Correlation analysis of gene expression levels obtained from qRT-PCR and ONT sequencing. Alkaline phosphatase (ALP), glutaredoxin (GLRX), myozenin 2 (MYO2), S100 calcium binding protein A10 (S100A10), SRY-box transcription factor 9 (SOX9), tissue growth factor beta1 (TGFb1), collagen type III alpha 1 chain (COL3A1), TGFb2, COL1A1, tissue inhibitor of metallopepdase 2 (TIMP2), TIMP3, matrix metallopeptidase 2 (MMP2), fibronectin 1 (FN1) genes were selected, and qPCR experiments were performed. Pearson correlation coefficients (rp) between log2(CPM) and dCt were computed and reported with the respective p-value (p).

3.4.2. Sex-dependent activated pathways in VICs isolated by stenotic valves

The transcriptome analysis of RNA isolated by ten different AS patient VICs (5 men *vs.* 5 women) showed that there were 65 genes upregulated in men (log (FC) < -1 and adjusted p value <0.05) and 89 genes upregulated in women at basal level (log (FC) >1 and adjusted p value <0,05; **Figure 30**).

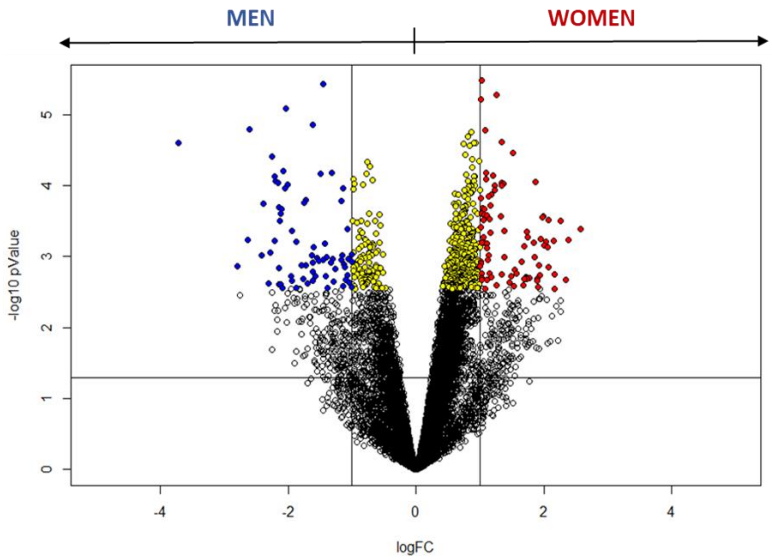

Figure 30: Volcano plot of the differentially expressed genes. Yellow dots represent significant differentially expressed genes at adjusted pValue < 0.05, whereas red and blue dots represent upregulated genes in women and men, respectively, with both the adjusted pValue < 0.05 and the absolute log2 fold change (logFC) > 1.

Starting from data on the gene expression coming from transcriptome sequencing, we perform a functional analysis, to evaluate sex-dependent activated pathways (**Figure 31**). Among pathways regulated by sex, we found the upregulation of mitochondrial gene expression in AS VICs from men and mRNA and protein localization processes. Women showed an upregulation of molecular processes like TGFβ signaling pathway, cell migration and adhesion, inflammation, and regulation of actin polymerization.

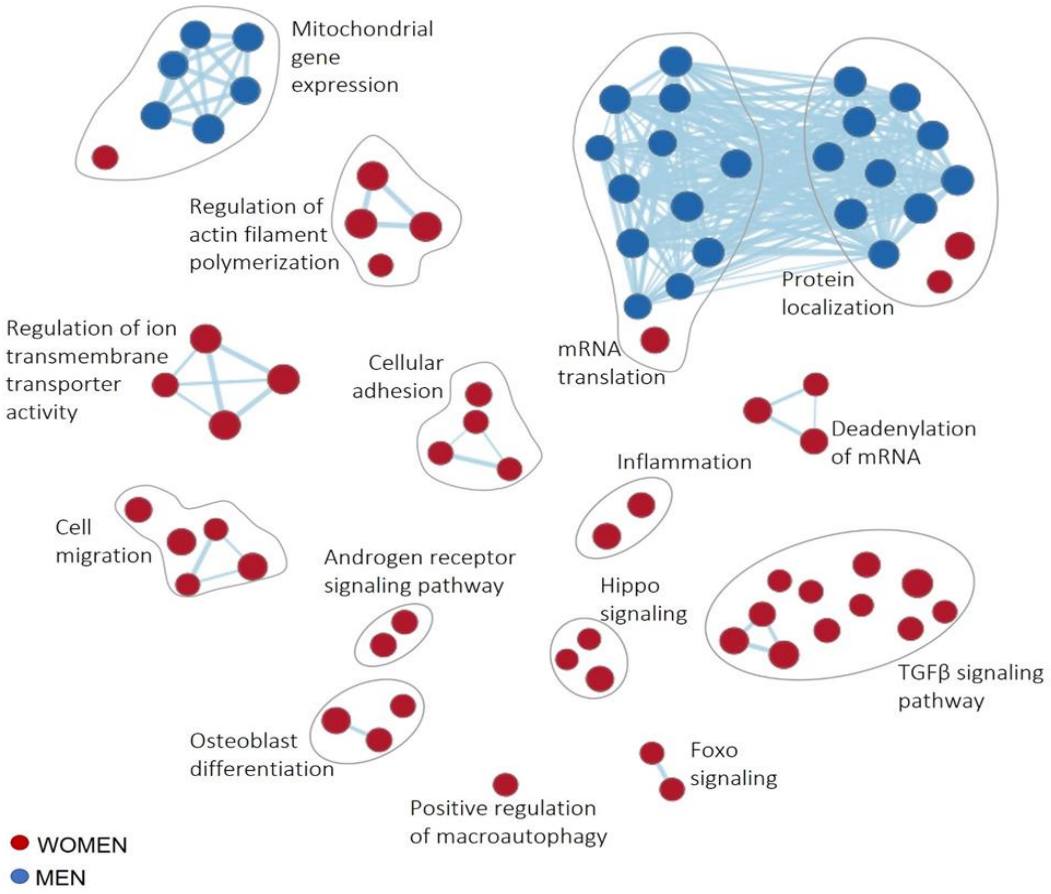

Figure 31: Functional inferences from gene expression analysis of women and men stenotic valve interstitial cells. The enrichment network shows the pathway nodes that are associated (FDR qValue < 0.1) with women (red) and men (blue), where the node size is proportional to the gene-set size.

3.4.3. Mitochondrial damage evaluation

The upregulation of mitochondrial gene expression in men could be due to a higher mitochondrial damage. To validate this hypothesis, we stain cells with mitoSOX, a dye able to stain mitochondrial-derived oxidative stress, and the mitochondrial damage results higher in men than in women (**Figure 32**). In particular, the 51.0 ± 7.3% of VICs from men with CAVS were positive to mitoSOX, while only the 29.5 ± 3.2% of VICs from women showed the mitoSOX staining (n = 12 men *vs.* 12 women; $p < 0.0001$).

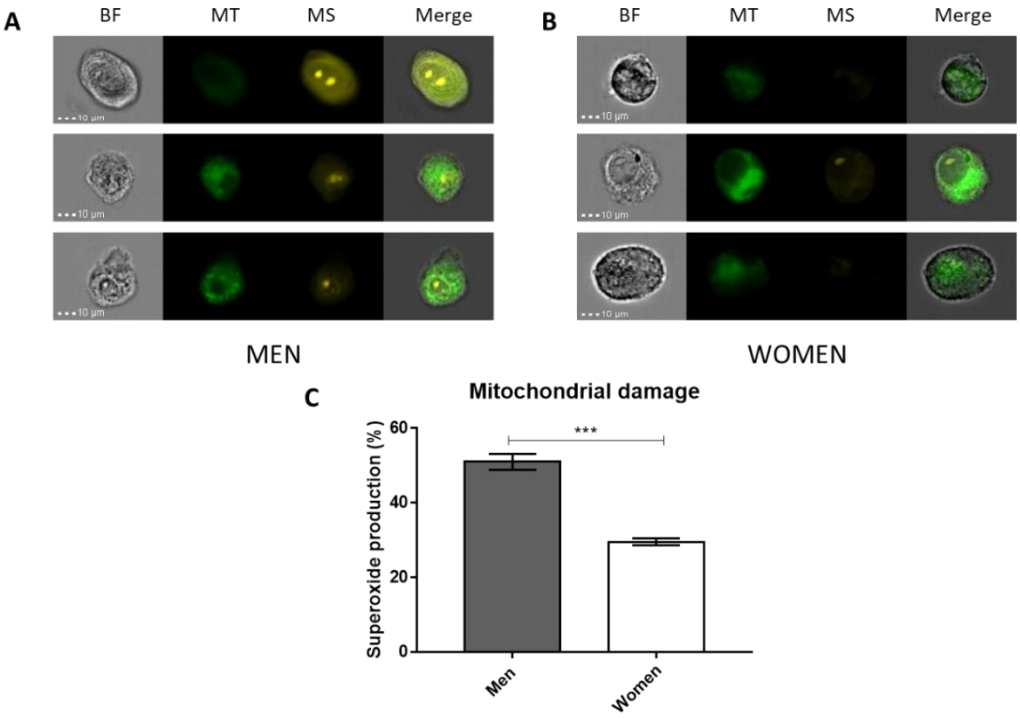

Figure 32: Mitochondrial damage evaluation in man and woman stenotic aortic valve interstitial cells. (**A**-**B**) Representative images of VICs isolated by men and women, respectively, in brightfield (BF) and stained with mitotracker (MT) and mitoSOX (MS). (**C**) Histogram reporting MS positive cell quantification.

3.5. Pharmacological regulation of molecular pathways activated in men with aortic valve stenosis

3.5.1. Extracellular calcium potential and myofibroblastic activation of VICs treated with 2ThioUTP

We verified the P2RY2 expression in isolated VICs in terms of both mRNA, by qPCR (mean Ct: 32.6 ± 0.8; n = 15), and protein, analyzed by capillary Western blot (WES). WES evaluation revealed three different bands at 50, 58, and 65 kDa, probably due to post-translational modifications of P2RY2 [24]. After normalization on GAPDH, the 65 kDa band resulted the most expressed one (ANOVA $p < 0.0001$; n = 12; **Figure 33A-B**), without differences between AVSc and AS patients (2.97 ± 1.34 vs. 3.08 ± 1.21, respectively). The other two bands were not different between AVSc and AS patients (50 kDa 1.08 ± 0.36 vs. 1.15 ± 0.50, respectively, and 58 kDa 1.01 ± 0.37 vs. 0.86 ± 0.63, respectively). However, only a low percentage of cells expressed P2RY2 at the membrane level, as shown by imaging flow cytometry analysis (**Figure 33C**) performed on AVSc (2.1% ± 0.8%; n = 6) and AS patients (3.4% ± 2.3%; n = 11), with no statistical differences between the two groups ($p = 0.21$; **Figure 33D**). Thus, we tested the effects of 2ThioUTP, a potent and selective agonist of P2RY2, on calcium deposition and myofibroblastic activation of human VICs isolated from calcified aortic valve leaflets.

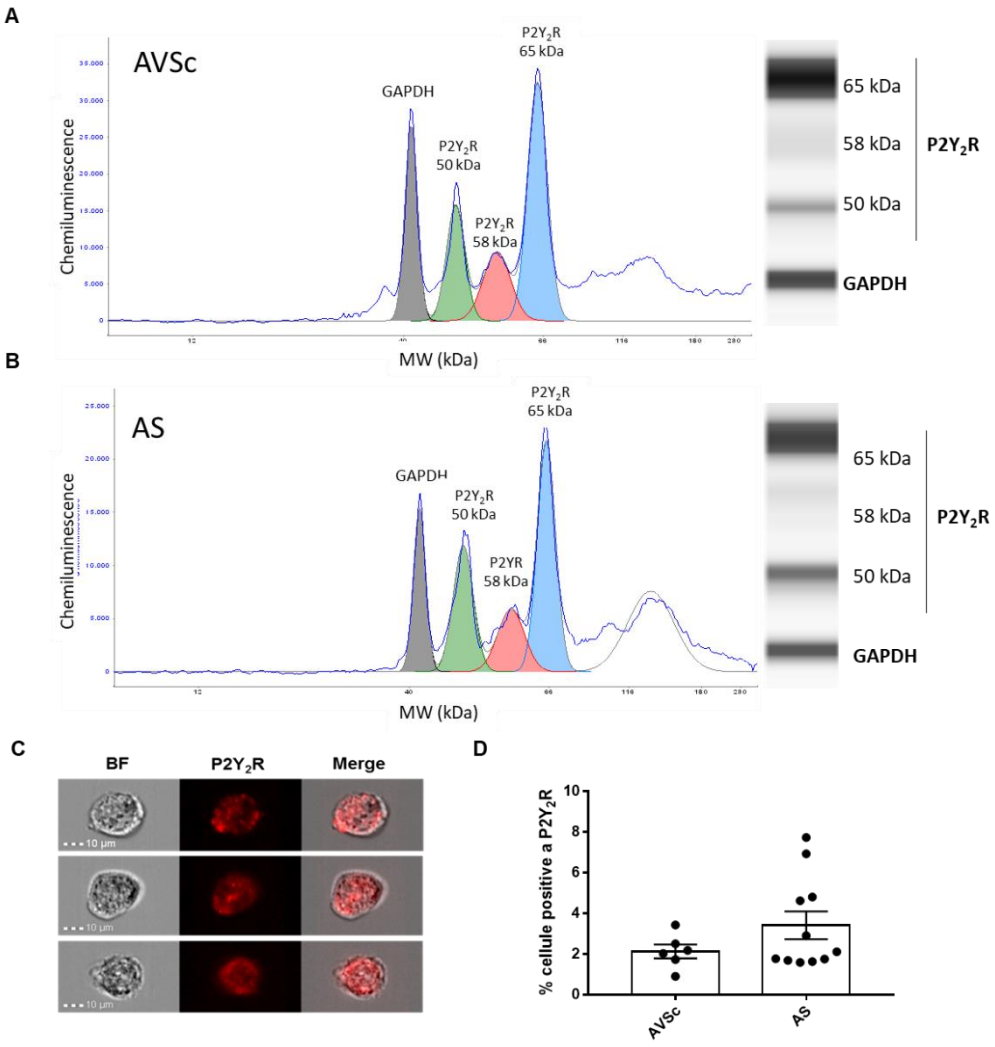

Figure 33: Valve interstitial cells P2RY2 expression. Representative quantification strategy by Compass for SW v3.1.7 (Pro-tein Simple) and illustrative image of capillary Western blot showing P2Y2 receptor (P2RY2) and GAPDH expression of AVSc (n = 6; **A**) and AS (n = 6; **B**) patients. (**C**-**D**) Representative images showing VICs stained for P2RY2 (red) and relative percentage of positive cells in sclerotic (AVSc; n = 6) and stenotic (AS; n = 11) patients Scale bar: 10 µm. BF: bright field.

To verify the extent of extracellular calcification, we employed an in vitro assay with ascorbic acid

AA; 50µg/mL) and inorganic phosphate (Pi; 2mM), widely recognized pro-calcific stimuli. The calcification was induced for 7 days, shown in **Figure 34** as 100%, or 14 days, while 2ThioUTP (10 µM) was administered on the seventh day until the end of the experiment (14 days, n = 6 AVSc and 5 AS). Under continuous pro-calcific stimulus, the activation of P2RY2 led to a mild reduction in VIC extracellular calcification in AVSc patients (AAPi14d + 2ThioUTP: 180% ± 93% vs. AAPi14d: 287% ± 107%; p = 0.09; **Figure 34A**) and to a significant inhibition of VIC calcification potential in AS patients (AAPi14d + 2ThioUTP: 166% ± 43% vs. AAPi14d: 280% ± 80%; p = 0.005; **Figure 34B**). Similarly, when pro-calcific stimulus was interrupted on the seventh day, P2RY2 activation drastically re-duced the extracellular calcification compared to its own control both in AVSc (AAPi7d + 2ThioUTP: 90% ± 51% vs. AAPi7d: 189% ± 67%; p = 0.02; **Figure 34C**) and AS patients (AA-Pi7d + 2ThioUTP: 75% ± 28% vs. AAPi7d: 135% ± 42%; p = 0.03; **Figure 34D**). Of note, the calcification under 2ThioUTP treatment, in pro-calcific medium for 14 days, was comparable to the condition in which calcification was induced only for the first 7 days without 2ThioUTP administration in AVSc (AAPi14d + 2ThioUTP: 180% ± 93% vs. AAPi7d: 189% ± 67%; p = 0.85) and AS patients (AAPi14d + 2ThioUTP: 166% ± 43% vs. AAPi7d: 135% ± 42%; p = 0.28).

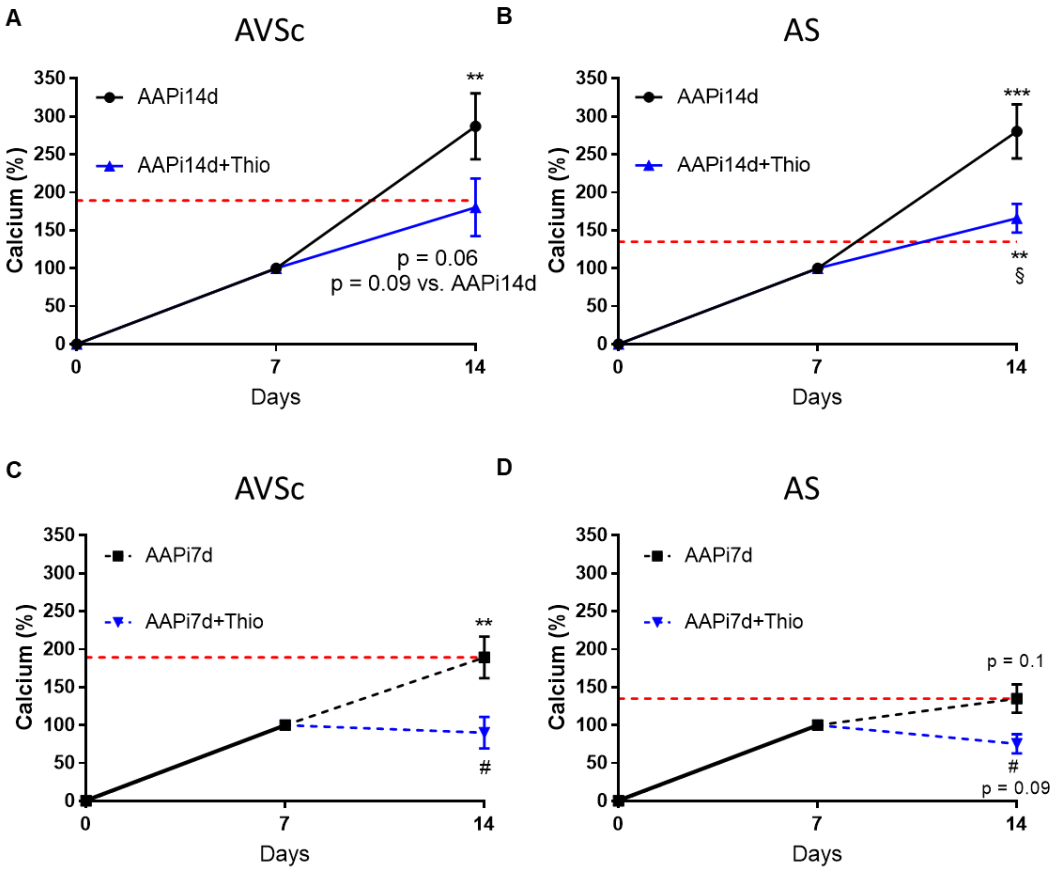

Figure 34: P2RY2 activation reduces extracellular calcification of human valve interstitial cells. Extracellular calcium quantification under pro-calcific condition for 14 days (AAPi14d), with the addition of 2ThioUTP 10 µM (AAPi14d + Thio) in (**A**) sclerotic (AVSc; n = 6) and (**B**) stenotic (AS; n = 5) pa-tients. Extracellular calcium quantification under pro-calcific condition for only the first 7 days (AAPi7d), with the addition of 2ThioUTP 10 µM (AAPi7d + Thio) in (**C**) sclerotic (AVSc; n = 6) and (**D**) stenotic (AS; n = 5) patients. Data were calculated by setting the calcium amount at day 7 in pro-calcific conditions to 100% (n = 11). The red line is set to the mean extracellular calcification of AVSc (**A**-**C**) and AS (**B**-**D**) VICs on the 14th day in pro-calcific conditions for the first 7 days (AAPi7d). Black denotes the inner control; blue denotes treatment with 2thioUTP. Solid line denotes the pro-calcific medium; dashed line denotes normal medium. ** p < 0.01, *** p < 0.001 vs. calcification on day 7; # p < 0.05 vs. AAPi7d; $ p < 0.05 vs. AAPi14d; if not specified, p-values re-ported are vs. calcification on day 7.

Taken together, these data suggested that the activation of P2RY2 by 2ThioUTP pre-vents the extracellular calcium deposition in pathological VICs even under continuous stressed conditions.

In order to evaluate the impact of P2RY2 stimulation on myofibroblastic activation, an important and underestimated feature of CAVS, we treated VICs with 2ThioUTP (10 µM) for 5 days in normal medium. We evaluated the expression of several pro-fibrotic genes by qPCR, and we found that 2ThioUTP treatment was able to significantly reduce their expression (n = 3; **Figure 35A**). In particular, we found that collagen 1A1 (COL1A1) was not significantly reduced by treatment, but we can appreciate a negative trend after the treatment with 2ThioUTP (−0.75 ± 0.5 log2(FC) vs. untreated; p = 0.07). All other screened genes were downregulated by 2ThioUTP: collagen 3A1 (COL3A1 −0.42 ± 0.2 log2(FC); p = 0.03), transforming growth factor β (TGFβ1 −0.53 ± 0.1 log2(FC); p = 0.0006), TGFβ2 (−0.48 ± 0.2 log2(FC); p = 0.02), and actin α2 (ACTA2 −1.28 ± 0.3 log2(FC); p = 0.002). Since the upregulation of ACTA2 mRNA and, thus, αSMA is a widely recognized marker of VIC activation (myofibroblast-like phenotype), we evaluated the protein expression. We found that αSMA expression was significantly downregulated by 2ThioUTP treatment (0.81 ± 0.04 FC vs. untreated; p = 0.004; n = 4; **Figure 35B**).

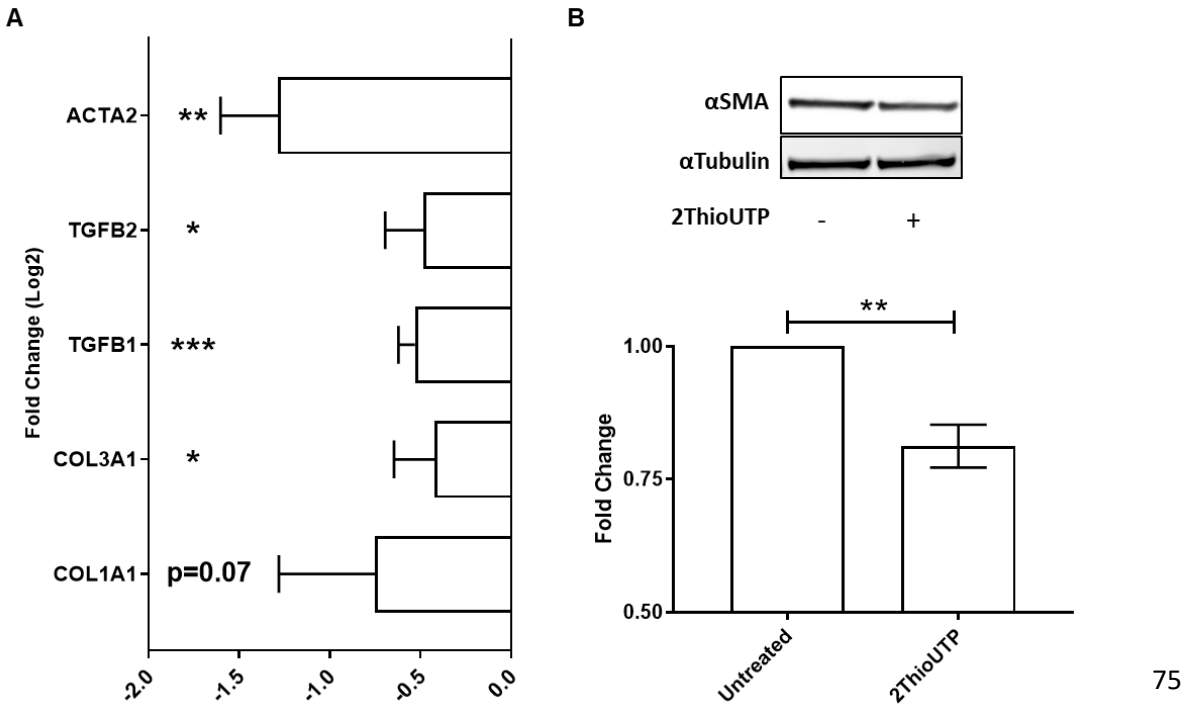

Figure 35: P2RY2 activation reduces human valve interstitial cell fibrosis. (**A**) Relative expression of colla-gen 1A1 and 3A1 (COL1A1 and 3A1), transforming growth factor β1 and 2 (TGFB1 and 2), and ac-tin α2 (ACTA2) genes in VICs treated with 2ThioUTP 10 μM for 5 days (n = 3). (**B**) α-Smooth muscle actin (αSMA) protein expression and relative quantification (n = 4). Data are expressed as logarithm base 2 of the fold change (log2(FC)) or fold change (FC) vs. untreated cells and are shown as the mean ± standard error. * $p < 0.05$, ** $p < 0.01$, *** $p < 0.001$ vs. untreated.

All these data corroborate the hypothesis that P2RY2 stimulation inhibits myofibroblastic gene and protein expression in AS patients.

4. DISCUSSION

Calcific aortic valve stenosis (CAVS) is a slow, progressive, multifactorial disease that leads to impaired movement of the valve leaflets and, consequently, obstruction of blood flow due to calcium deposition on the cusps [3, 110]. The initial phase of CAVS, the aortic valvular sclerosis (AVSc), is characterised by mild cusp thickening and, in some cases, mild calcification. This condition affects approximately 30% of adults over 65 years of age and evolves into aortic stenosis (AS) in 10% of these [111, 112]. The final stage of CAVS, the aortic valve stenosis (AS), is present in 3% of the population. AS is characterised by altered leaflet motion and greatly diminished aortic valve area resulting in resistance to blood flow, causing the hemodynamic changes typical of CAVS [113].

On this basis, it is estimated that by 2050, due to the aging population and increased life expectancy, approximately 25 million people in the US and 1.5 billion people worldwide will suffer from severe AS [114], causing a socio-economic burden. Currently, the only therapeutic option is valve replacement surgery (AVR) or, alternatively, percutaneous aortic valve implantation surgery (TAVI) [115].

In recent years, the presence of calcium in the aortic valve leaflets has become an important prognostic marker for cardiovascular morbidity and mortality [116-119]. In particular, Clavel and colleagues showed that AVC independently predicts mortality after CAVS diagnosis, even after adjustment for hemodynamic characteristics with or without taking into consideration the treatment strategy [109]. Interestingly, guidelines for valve disease underline the role of AVC, measured by CT, in low flow low gradient status, and other challenging situations [120].

Considering all these factors, the study of the molecular and cellular mechanisms activated in the CAVS is fundamental to discover possible pharmacological targets. Emerging evidence reported sexual dimorphism in the development and progression of CAVS.

In 1997, Stewart and colleagues, for the first time, proposed the male gender as an independent risk factor for CAVS, showing that men had a twofold increased risk of CAVS presence compared to women, measured by echocardiography [37]. In CAVS patients, the difference between genders starts with the discrepancy in clinical manifestation. Women, more often than men, show absence or later manifestation of the symptoms that lead to a lower referral rate to surgery [121]. However, when symptoms appear, women present higher NYHA class [122].

The first study showing differences in men's and women's AVC load was performed by Agrawal et al. in a cohort of 665 patients (427 men and 238 women) [80]. Criteria of AVC, for aortic valve severity, are markedly different in men and women (e.g. severe aortic stenosis very likely: men ≥ 3000 AU; women ≥ 1600 AU). Indeed, recently published studies already apply these criteria for the likelihood categorization of patients into different aortic stenosis categories stratified by gender and using AVC Agatston scores [123, 124]. Sex-specific features were observed in AVC load and AVC density with the same severity of CAVS. In particular, women presented significantly lower AVC load compared to men, even after normalization of AVC load for body surface area (BSA) and cross-sectional aortic annulus area [80, 125]. Recently, it has been shown that surgically excised aortic valve weight (AVW) correlates well with both AVC load and hemodynamic indices of CAVS severity [126]. Thaden et al. noted that AVW, as well as AVC load, were lower in women than men, even after indexed to BSA or LVOT, regardless of valve morphology [84]. Nguyen and colleagues, studying a prospective cohort of AS patients, highlighted that women had a faster AVC progression and thus a higher AS-related event rate than men [108]. Another study, evaluating AVC load by CT, found similar results showing that women have less AVC and faster hemodynamic progression than men [127].

Our results obtained with the systemic review and meta-analysis of 7 studies including more than 2900 patients with several degrees of AS, confirmed sex-differences in AVC load and density in CAVS patients [128]. In particular, our analysis reported that men with AS have a higher amount of calcium deposition than women with AS, even considering the smaller aortic annulus area and body surface area of women and the severity of the pathology. All these results support that AS pathophysiology may differ between sexes and closer follow-up time may be advised in women with AS at early stages [108]. The same results came from the analysis of computed tomography aortic valve images performed on our population by different human operators and by the U-net artificial intelligence analysis. Men with AS showed a 2-fold increase in calcium deposition than women with AS.

Recent studies, for the first time, evaluated the fibrocalcific remodelling of the aortic valve, specifically looking at gender differences. Indeed, it has been reported that women, with respect to men, had a higher amount of fibrosis within the aortic valve leaflets, even if there were no differences in valve weight, density, and hemodynamic severity between the two groups. The presence of a higher fibrosis score in women may partially explain the AVC hemodynamic severity

disproportion between men and women [85, 86]. Our data on the measurement of fibrosis amount by the CT scan images supported the previous results showing higher fibrosis levels in women with AS with respect to men. Our deep learning analysis revealed a useful non-invasive imaging tool to predict the fibrosis level in CAVS patients with a routine exam. The fibrosis quantification in a semi-automated fashion could be introduced in the clinical practice, as support to the AVC score, in order to improve diagnostic and prognostic accuracy in the stratification of patients.

In order to deeper explore the influence of sex in the molecular mechanisms involved in the progression of CAVS, we took advantage of a public microarray dataset on 240 stenotic valves (120 men and 120 women). The whole tissue analysis revealed several sex-dependent activated pathways, among which there is a strong involvement of adaptive and innate immunity, and inflammation in men and pro-fibrotic pathways in women. These data were corroborated by the cell-type enrichment analysis, which revealed that mesenchymal cells (e.g. fibroblasts) were over-represented in woman AS valves, whereas transcriptional signatures for immune cells such as monocytes, macrophages, T and B cells were enriched in men ones, in line with recent studies [129, 130]. In addition, it has been shown that the crosstalk between these immune cell infiltrates and VICs plays a pivotal role in CAVS development and progression [131, 132]. Our results on the circulating expression of cytokines support data on the upregulation of inflammatory genes in men because sclerotic and stenotic men showed a higher secretion of pro-inflammatory cytokines such as IL1β, IL1α, TNFα, INFγ (in AVSc), and TNFα and INFβ (in AS).

Since the fibro-calcification processes are mainly due to VICs, we performed *in vitro* experiments to test their fibro-calcification potential and their possible use as a tool to investigate sex-differences *in vitro*. As expected, VICs isolated from stenotic and sclerotic valves showed sex-dimorphism: VICs from stenotic men calcified more under pro-calcific conditions and secreted less collagen at basal level than VICs from women. According to our findings, some studies showed that human and animal male VICs, under osteogenic conditions, had a significantly higher calcification potential than female cells [133, 134], while female VICs were more prone to differentiate into myofibroblasts, in line with the upregulation of fibrosis in women VICs [135]. What is interesting is the opposite behaviour of VICs from sclerotic men, which calcified less than ones from sclerotic women. This data suggests that men's AVSc VICs could have some molecular pathways activated able to buffer the higher pro-calcific stimulus, not already present in woman's

AVSc VICs. Indeed, at basal level, AVSc VICs from men calcify more than the ones from AVSc women. This hypothesis needs to be validated by RNA sequencing of AVSc VICs.

Taken together, these data suggest that VICs influence the progression of the pathology in a sex-dependent way. In order to evaluate sex-dependent activated pathways, we performed the transcriptome sequencing of AS VICs from men and women. We found several molecular pathways differentially expressed by sex. Among these, there was an up-regulation of TGFβ signalling, cellular migration, and adhesion in female VICs, all molecular pathways related to fibrosis. Male AS VICs reported an upregulation of mitochondrial gene expression compared to female ones. This finding suggested involvement of mitochondria in the progression of the pathology in men. To validate this hypothesis, we evaluated the mitochondrial damage and it resulted to be higher in men than in women. Côté et al., in a previous study, reported that ATP signal prevented the extracellular mineralization of the aortic valve, by promoting cell survival [136]. We hypothesized that the mitochondrial damage could cause lower ATP bioavailability and extracellular secretion. This condition could bring to lower activation of the purinergic receptor 2Y type 2 (P2RY2). Previous authors reported that the activation of P2RY2 by 2ThioUTP has been reported to prevent extracellular calcification, and its administration has already been tested in a mouse model, proving its safety (e.g., no effects on bone mineral density, inflammation, and lipid profile). The same authors showed that the depletion of P2RY2 resulted in the ineffectiveness of 2ThioUTP on ectopic calcification of mouse and healthy human VICs [66]. Our results showed for the first time in our knowledge the that the stimulation of P2RY2 by 2ThioUTP attenuates the extracellular calcification and myofibroblastic activation of male VICs isolated from human calcified aortic valve leaflets (AVSc and AS). Thus, P2RY2 stimulation could be implemented at the earliest stage of CAVS, the AVSc, which is an essential step toward the end-stage disease [27, 137]. AVSc is an echocardiographic finding not well understood, which remains a very controversial topic considering it has no clinical symptoms but is linked to increased cardiovascular risk and associated mortality [32, 138, 139]. Taken together, these data suggest that P2RY2 selective activation should be further investigated as a pharmacological target for the prevention of CAVS progression, acting on both calcification and myofibroblastic activation of VICs. These data could also be of high importance for the future development of tissue engineering. Indeed, 2ThioUTP administration could be proposed in multiple applications, such as maintaining an inactive VIC phenotype and reducing aortic valve fibro-calcification while seeding in a decellularized scaffold for the generation of new tissue-engineered aortic valves.

5. CONCLUSION

Although calcific aortic valve stenosis is a debilitating disease, no pharmacological treatments are available. Surgical or transcatheter aortic valve substitution are the only available options to arrest the disease progression. For this reason, the search for pharmacological targets is of critical importance to reduce the costs for the national health system and to have an alternative to the surgery. In the last decade, several studies reported sex dimorphism in the progression of the pathology. The principal aim of this work is to better define the sex-dependent molecular mechanisms activated in the onset and progression of CAVS.

Are there sex-differences in the development and progression of CAVS?

We performed a meta-analysis to provide strong evidences on a large number of AS patients of the higher amount of calcium deposition in men than in women. Moreover, the analysis of computed tomography images confirmed that the fibrotic fibres deposition was higher in women than in men with AS. Circulating inflammatory cytokines were differently expressed during the development of the pathology, in particular men with AVSc and AS expressed more pro-inflammatory cytokines than women.

Could CAVS be driven by sex-dependent molecular pathways?

As showed by our data, the cellular composition of VICs was different between sexes: AS man VICs are mostly represented by inflammatory cells derived from the circulation, while AS woman VICs are mostly fibroblastic-like resident cells. The RNA sequencing revealed that the molecular pathways activated in the last stage of the pathology were different between sexes. This data confirmed the hypothesis that there are sex-dependent activated molecular pathways in the progression of CAVS. The study of these molecular ways could shed light on the pharmacological targets to study to arrest and/or revert CAVS phenotype.

Considering the high mitochondrial damage seen in the AS man VICs and, thus, the possible decrement of ATP production, the physiological activation of P2RY2 could be lower in men patients with CAVS respect to women and this could be linked to the higher extracellular calcification measured with man VICs. Our data suggest that P2RY2 activation should be further investigated as a pharmacological target for the prevention of CAVS progression, acting on both calcification and myofibroblastic activation. Our findings reveal the potential therapeutic effects of 2ThioUTP in CAVS patients, even at the early stage of the pathology. Its ability to prevent calcium

deposition could be of interest to fill the absence of pharmacological treatments for patients with AVSc and avoid the CAVS onset, thus reducing the need for more invasive approaches such as surgery or transcatheter aortic valve replacement.

6. REFERENCES

1. Sacks, M.S., W. David Merryman, and D.E. Schmidt, *On the biomechanics of heart valve function.* J Biomech, 2009. **42**(12): p. 1804-24.
2. Anderson, R.H., *The surgical anatomy of the aortic root.* Multimed Man Cardiothorac Surg, 2007. **2007**(102): p. mmcts 2006 002527.
3. Perrucci, G.L., et al., *Pathophysiology of Aortic Stenosis and Mitral Regurgitation.* Compr Physiol, 2017. **7**(3): p. 799-818.
4. Chen, J.H. and C.A. Simmons, *Cell-matrix interactions in the pathobiology of calcific aortic valve disease: critical roles for matricellular, matricrine, and matrix mechanics cues.* Circ Res, 2011. **108**(12): p. 1510-24.
5. Gould, S.T., et al., *Hemodynamic and cellular response feedback in calcific aortic valve disease.* Circ Res, 2013. **113**(2): p. 186-97.
6. Mongkoldhumrongkul, N., M.H. Yacoub, and A.H. Chester, *Valve Endothelial Cells - Not Just Any Old Endothelial Cells.* Curr Vasc Pharmacol, 2016. **14**(2): p. 146-54.
7. Tao, G., J.D. Kotick, and J. Lincoln, *Heart valve development, maintenance, and disease: the role of endothelial cells.* Curr Top Dev Biol, 2012. **100**: p. 203-32.
8. Butcher, J.T. and R.M. Nerem, *Valvular endothelial cells and the mechanoregulation of valvular pathology.* Philos Trans R Soc Lond B Biol Sci, 2007. **362**(1484): p. 1445-57.
9. Deck, J.D., *Endothelial cell orientation on aortic valve leaflets.* Cardiovasc Res, 1986. **20**(10): p. 760-7.
10. Gendron, N., et al., *Human Aortic Valve Interstitial Cells Display Proangiogenic Properties During Calcific Aortic Valve Disease.* Arterioscler Thromb Vasc Biol, 2021. **41**(1): p. 415-429.
11. Lis, G.J., et al., *Identification of CD34+/PGDFRalpha+ Valve Interstitial Cells (VICs) in Human Aortic Valves: Association of Their Abundance, Morphology and Spatial Organization with Early Calcific Remodeling.* Int J Mol Sci, 2020. **21**(17).
12. Liu, A.C., V.R. Joag, and A.I. Gotlieb, *The emerging role of valve interstitial cell phenotypes in regulating heart valve pathobiology.* Am J Pathol, 2007. **171**(5): p. 1407-18.
13. Xu, K., et al., *Cell-Type Transcriptome Atlas of Human Aortic Valves Reveal Cell Heterogeneity and Endothelial to Mesenchymal Transition Involved in Calcific Aortic Valve Disease.* Arterioscler Thromb Vasc Biol, 2020. **40**(12): p. 2910-2921.
14. Goody, P.R., et al., *Aortic Valve Stenosis: From Basic Mechanisms to Novel Therapeutic Targets.* Arterioscler Thromb Vasc Biol, 2020. **40**(4): p. 885-900.
15. Chen, J.H., et al., *beta-catenin mediates mechanically regulated, transforming growth factor-beta1-induced myofibroblast differentiation of aortic valve interstitial cells.* Arterioscler Thromb Vasc Biol, 2011. **31**(3): p. 590-7.
16. Gould, S.T., N.J. Darling, and K.S. Anseth, *Small peptide functionalized thiol-ene hydrogels as culture substrates for understanding valvular interstitial cell activation and de novo tissue deposition.* Acta Biomater, 2012. **8**(9): p. 3201-9.
17. Balachandran, K., et al., *Elevated cyclic stretch alters matrix remodeling in aortic valve cusps: implications for degenerative aortic valve disease.* Am J Physiol Heart Circ Physiol, 2009. **296**(3): p. H756-64.
18. Butcher, J.T. and R.M. Nerem, *Valvular endothelial cells regulate the phenotype of interstitial cells in co-culture: effects of steady shear stress.* Tissue Eng, 2006. **12**(4): p. 905-15.
19. Ma, H., et al., *Myofibroblastic activation of valvular interstitial cells is modulated by spatial variations in matrix elasticity and its organization.* Biomaterials, 2017. **131**: p. 131-144.
20. Liu, Z., et al., *IL-21 promotes osteoblastic differentiation of human valvular interstitial cells through the JAK3/STAT3 pathway.* Int J Med Sci, 2020. **17**(18): p. 3065-3072.
21. Wang, B., et al., *Abeta40 Promotes the Osteoblastic Differentiation of Aortic Valve Interstitial Cells through the RAGE Pathway.* Curr Med Sci, 2020. **40**(5): p. 931-936.
22. Li, F., et al., *Oxidized low-density lipoprotein promotes osteoblastic differentiation of valvular interstitial cells through RAGE/MAPK.* Cardiology, 2015. **130**(1): p. 55-61.
23. Zhou, T., et al., *Factors influencing osteogenic differentiation of human aortic valve interstitial cells.* J Thorac Cardiovasc Surg, 2021. **161**(2): p. e163-e185.

24. Lindman, B.R., et al., *Calcific aortic stenosis.* Nat Rev Dis Primers, 2016. **2**: p. 16006.
25. Pazianas, M., *Calcific aortic stenosis.* N Engl J Med, 2009. **360**(1): p. 85; author reply 85-6.
26. Peeters, F., et al., *Calcific aortic valve stenosis: hard disease in the heart: A biomolecular approach towards diagnosis and treatment.* Eur Heart J, 2018. **39**(28): p. 2618-2624.
27. Myasoedova, V.A., et al., *Novel pharmacological targets for calcific aortic valve disease: Prevention and treatments.* Pharmacol Res, 2018. **136**: p. 74-82.
28. Poggio, P., et al., *MiRNA profiling revealed enhanced susceptibility to oxidative stress of endothelial cells from bicuspid aortic valve.* J Mol Cell Cardiol, 2019. **131**: p. 146-154.
29. Abdelbaky, A., et al., *Early aortic valve inflammation precedes calcification: a longitudinal FDG-PET/CT study.* Atherosclerosis, 2015. **238**(2): p. 165-72.
30. Buttner, P., et al., *Dissecting Calcific Aortic Valve Disease-The Role, Etiology, and Drivers of Valvular Fibrosis.* Front Cardiovasc Med, 2021. **8**: p. 660797.
31. Santoro, R., et al., *Activation of human aortic valve interstitial cells by local stiffness involves YAP-dependent transcriptional signaling.* Biomaterials, 2018. **181**: p. 268-279.
32. Gharacholou, S.M., et al., *Aortic valve sclerosis and clinical outcomes: moving toward a definition.* Am J Med, 2011. **124**(2): p. 103-10.
33. Agmon, Y., et al., *Aortic valve sclerosis and aortic atherosclerosis: different manifestations of the same disease? Insights from a population-based study.* J Am Coll Cardiol, 2001. **38**(3): p. 827-34.
34. Kanwar, A., J.J. Thaden, and V.T. Nkomo, *Management of Patients With Aortic Valve Stenosis.* Mayo Clin Proc, 2018. **93**(4): p. 488-508.
35. Bakaeen, F.G., T.K. Rosengart, and B.A. Carabello, *Aortic Stenosis.* Ann Intern Med, 2017. **166**(1): p. ITC1-ITC16.
36. Katz, R., et al., *Relationship of metabolic syndrome with incident aortic valve calcium and aortic valve calcium progression: the Multi-Ethnic Study of Atherosclerosis (MESA).* Diabetes, 2009. **58**(4): p. 813-9.
37. Stewart, B.F., et al., *Clinical factors associated with calcific aortic valve disease. Cardiovascular Health Study.* J Am Coll Cardiol, 1997. **29**(3): p. 630-4.
38. Conte, M., et al., *The role of inflammation and metabolic risk factors in the pathogenesis of calcific aortic valve stenosis.* Aging Clin Exp Res, 2021. **33**(7): p. 1765-1770.
39. Yousry, M., et al., *Aortic valve type and calcification as assessed by transthoracic and transoesophageal echocardiography.* Clin Physiol Funct Imaging, 2015. **35**(4): p. 306-13.
40. Baumgartner, H.C., et al., *Recommendations on the echocardiographic assessment of aortic valve stenosis: a focused update from the European Association of Cardiovascular Imaging and the American Society of Echocardiography.* Eur Heart J Cardiovasc Imaging, 2017. **18**(3): p. 254-275.
41. Miller, J.D., R.M. Weiss, and D.D. Heistad, *Calcific aortic valve stenosis: methods, models, and mechanisms.* Circ Res, 2011. **108**(11): p. 1392-412.
42. Hutcheson, J.D., E. Aikawa, and W.D. Merryman, *Potential drug targets for calcific aortic valve disease.* Nat Rev Cardiol, 2014. **11**(4): p. 218-31.
43. Goldstone, A.B., et al., *Mechanical or Biologic Prostheses for Aortic-Valve and Mitral-Valve Replacement.* N Engl J Med, 2017. **377**(19): p. 1847-1857.
44. Sun, J.C., et al., *Antithrombotic management of patients with prosthetic heart valves: current evidence and future trends.* Lancet, 2009. **374**(9689): p. 565-76.
45. Kiyose, A.T., et al., *Comparison of Biological and Mechanical Prostheses for Heart Valve Surgery: A Systematic Review of Randomized Controlled Trials.* Arq Bras Cardiol, 2019. **112**(3): p. 292-301.
46. Head, S.J., M. Celik, and A.P. Kappetein, *Mechanical versus bioprosthetic aortic valve replacement.* Eur Heart J, 2017. **38**(28): p. 2183-2191.
47. Vitanova, K., et al., *Surgical Aortic Valve Replacement-Age-Dependent Choice of Prosthesis Type.* J Clin Med, 2021. **10**(23).
48. Malvindi, P.G., et al., *Aortic valve replacement with biological prosthesis in patients aged 50-69 years.* Eur J Cardiothorac Surg, 2021. **59**(5): p. 1077-1086.
49. David, T.E., *Surgical treatment of aortic valve disease.* Nat Rev Cardiol, 2013. **10**(7): p. 375-86.

50. Schmiegelow, M.D.S., et al., *Reintervention rates following bioprosthetic surgical aortic valve replacement-a Danish Nationwide Cohort Study.* Eur J Cardiothorac Surg, 2022. **61**(3): p. 614-622.
51. Hwang, Y.M., et al., *Conduction disturbance after isolated surgical aortic valve replacement in degenerative aortic stenosis.* J Thorac Cardiovasc Surg, 2017. **154**(5): p. 1556-1565 e1.
52. Leon, M.B., et al., *Transcatheter or Surgical Aortic-Valve Replacement in Intermediate-Risk Patients.* N Engl J Med, 2016. **374**(17): p. 1609-20.
53. Montaigne, D., et al., *Daytime variation of perioperative myocardial injury in cardiac surgery and its prevention by Rev-Erbalpha antagonism: a single-centre propensity-matched cohort study and a randomised study.* Lancet, 2018. **391**(10115): p. 59-69.
54. Auensen, A., et al., *Morbidity outcomes after surgical aortic valve replacement.* Open Heart, 2017. **4**(1): p. e000588.
55. Nielsen, H.H., *Transcatheter aortic valve implantation.* Dan Med J, 2012. **59**(12): p. B4556.
56. Siontis, G.C.M., et al., *Transcatheter aortic valve implantation vs. surgical aortic valve replacement for treatment of symptomatic severe aortic stenosis: an updated meta-analysis.* Eur Heart J, 2019. **40**(38): p. 3143-3153.
57. Smith, J.G., et al., *Association of low-density lipoprotein cholesterol-related genetic variants with aortic valve calcium and incident aortic stenosis.* JAMA, 2014. **312**(17): p. 1764-71.
58. Dichtl, W., et al., *Prognosis and risk factors in patients with asymptomatic aortic stenosis and their modulation by atorvastatin (20 mg).* Am J Cardiol, 2008. **102**(6): p. 743-8.
59. Rossebo, A.B., et al., *Intensive lipid lowering with simvastatin and ezetimibe in aortic stenosis.* N Engl J Med, 2008. **359**(13): p. 1343-56.
60. Cowell, S.J., et al., *A randomized trial of intensive lipid-lowering therapy in calcific aortic stenosis.* N Engl J Med, 2005. **352**(23): p. 2389-97.
61. Parolari, A., et al., *Do statins improve outcomes and delay the progression of non-rheumatic calcific aortic stenosis?* Heart, 2011. **97**(7): p. 523-9.
62. Poggio, P., et al., *Antihypertensive Treatments in Patients Affected by Aortic Valve Stenosis.* Curr Pharm Des, 2017. **23**(8): p. 1188-1194.
63. Capoulade, R., et al., *Impact of hypertension and renin-angiotensin system inhibitors in aortic stenosis.* Eur J Clin Invest, 2013. **43**(12): p. 1262-72.
64. Bull, S., et al., *A prospective, double-blind, randomized controlled trial of the angiotensin-converting enzyme inhibitor Ramipril In Aortic Stenosis (RIAS trial).* Eur Heart J Cardiovasc Imaging, 2015. **16**(8): p. 834-41.
65. Choi, B., et al., *Dipeptidyl Peptidase-4 Induces Aortic Valve Calcification by Inhibiting Insulin-Like Growth Factor-1 Signaling in Valvular Interstitial Cells.* Circulation, 2017. **135**(20): p. 1935-1950.
66. Bouchareb, R., et al., *Carbonic anhydrase XII in valve interstitial cells promotes the regression of calcific aortic valve stenosis.* J Mol Cell Cardiol, 2015. **82**: p. 104-15.
67. von Kugelgen, I., *Pharmacology of P2Y receptors.* Brain Res Bull, 2019. **151**: p. 12-24.
68. Abe, M., et al., *Homodimer formation by the ATP/UTP receptor P2Y2 via disulfide bridges.* J Biochem, 2018. **163**(6): p. 475-480.
69. Abbracchio, M.P., et al., *International Union of Pharmacology LVIII: update on the P2Y G protein-coupled nucleotide receptors: from molecular mechanisms and pathophysiology to therapy.* Pharmacol Rev, 2006. **58**(3): p. 281-341.
70. Leipziger, J., *Control of epithelial transport via luminal P2 receptors.* Am J Physiol Renal Physiol, 2003. **284**(3): p. F419-32.
71. Cressman, V.L., et al., *Effect of loss of P2Y(2) receptor gene expression on nucleotide regulation of murine epithelial Cl(-) transport.* J Biol Chem, 1999. **274**(37): p. 26461-8.
72. Potthoff, S.A., et al., *P2Y2 receptor deficiency aggravates chronic kidney disease progression.* Front Physiol, 2013. **4**: p. 234.
73. Rieg, T., et al., *P2Y(2) receptor activation decreases blood pressure and increases renal Na(+) excretion.* Am J Physiol Regul Integr Comp Physiol, 2011. **301**(2): p. R510-8.
74. Cohen, R., et al., *UTP reduces infarct size and improves mice heart function after myocardial infarct via P2Y2 receptor.* Biochem Pharmacol, 2011. **82**(9): p. 1126-33.

75. Ajit, D., et al., *Loss of P2Y(2) nucleotide receptors enhances early pathology in the TgCRND8 mouse model of Alzheimer's disease.* Mol Neurobiol, 2014. **49**(2): p. 1031-42.
76. Lazarowski, E.R., et al., *Pharmacological selectivity of the cloned human P2U-purinoceptor: potent activation by diadenosine tetraphosphate.* Br J Pharmacol, 1995. **116**(1): p. 1619-27.
77. Ivanov, A.A., et al., *Molecular modeling of the human P2Y2 receptor and design of a selective agonist, 2'-amino-2'-deoxy-2-thiouridine 5'-triphosphate.* J Med Chem, 2007. **50**(6): p. 1166-76.
78. Xu, P., et al., *Current knowledge on the nucleotide agonists for the P2Y2 receptor.* Bioorg Med Chem, 2018. **26**(2): p. 366-375.
79. Messika-Zeitoun, D., et al., *Evaluation and clinical implications of aortic valve calcification measured by electron-beam computed tomography.* Circulation, 2004. **110**(3): p. 356-62.
80. Aggarwal, S.R., et al., *Sex differences in aortic valve calcification measured by multidetector computed tomography in aortic stenosis.* Circ Cardiovasc Imaging, 2013. **6**(1): p. 40-7.
81. Diederichsen, A., et al., *Sex Differences in Factors Associated With Progression of Aortic Valve Calcification in the General Population.* Circ Cardiovasc Imaging, 2022. **15**(1): p. e013165.
82. Thomassen, H.K., et al., *Echocardiographic aortic valve calcification and outcomes in women and men with aortic stenosis.* Heart, 2017. **103**(20): p. 1619-1624.
83. Clavel, M.A., et al., *The complex nature of discordant severe calcified aortic valve disease grading: new insights from combined Doppler echocardiographic and computed tomographic study.* J Am Coll Cardiol, 2013. **62**(24): p. 2329-38.
84. Thaden, J.J., et al., *Sex-related differences in calcific aortic stenosis: correlating clinical and echocardiographic characteristics and computed tomography aortic valve calcium score to excised aortic valve weight.* Eur Heart J, 2016. **37**(8): p. 693-9.
85. Simard, L., et al., *Sex-Related Discordance Between Aortic Valve Calcification and Hemodynamic Severity of Aortic Stenosis: Is Valvular Fibrosis the Explanation?* Circ Res, 2017. **120**(4): p. 681-691.
86. Voisine, M., et al., *Age, Sex, and Valve Phenotype Differences in Fibro-Calcific Remodeling of Calcified Aortic Valve.* J Am Heart Assoc, 2020. **9**(10): p. e015610.
87. Shen, M., et al., *Effect of age and aortic valve anatomy on calcification and haemodynamic severity of aortic stenosis.* Heart, 2017. **103**(1): p. 32-39.
88. Summerhill, V.I., et al., *Sex-Specific Features of Calcific Aortic Valve Disease.* Int J Mol Sci, 2020. **21**(16).
89. Rathan, S., A.P. Yoganathan, and C.W. O'Neill, *The role of inorganic pyrophosphate in aortic valve calcification.* J Heart Valve Dis, 2014. **23**(4): p. 387-94.
90. Annoni, A.D., et al., *CT angiography prior to TAVI procedure using third-generation scanner with wide volume coverage: feasibility, renal safety and diagnostic accuracy for coronary tree.* Br J Radiol, 2018. **91**(1090): p. 20180196.
91. Moher, D., et al., *Preferred reporting items for systematic reviews and meta-analyses: the PRISMA statement.* PLoS Med, 2009. **6**(7): p. e1000097.
92. Clavel, M.A., et al., *Aortic valve area calculation in aortic stenosis by CT and Doppler echocardiography.* JACC Cardiovasc Imaging, 2015. **8**(3): p. 248-257.
93. Higgins, J.P., et al., *Measuring inconsistency in meta-analyses.* BMJ, 2003. **327**(7414): p. 557-60.
94. de Vaan, J., et al., *The 3mensio Valves multimodality workstation.* EuroIntervention, 2012. **7**(12): p. 1464-9.
95. Schneider, C.A., W.S. Rasband, and K.W. Eliceiri, *NIH Image to ImageJ: 25 years of image analysis.* Nat Methods, 2012. **9**(7): p. 671-5.
96. Theriault, S., et al., *A transcriptome-wide association study identifies PALMD as a susceptibility gene for calcific aortic valve stenosis.* Nat Commun, 2018. **9**(1): p. 988.
97. Subramanian, A., et al., *GSEA-P: a desktop application for Gene Set Enrichment Analysis.* Bioinformatics, 2007. **23**(23): p. 3251-3.
98. Merico, D., et al., *Enrichment map: a network-based method for gene-set enrichment visualization and interpretation.* PLoS One, 2010. **5**(11): p. e13984.
99. Shannon, P., et al., *Cytoscape: a software environment for integrated models of biomolecular interaction networks.* Genome Res, 2003. **13**(11): p. 2498-504.

100. Aran, D., *Cell-Type Enrichment Analysis of Bulk Transcriptomes Using xCell.* Methods Mol Biol, 2020. **2120**: p. 263-276.
101. Li, H., *Minimap2: pairwise alignment for nucleotide sequences.* Bioinformatics, 2018. **34**(18): p. 3094-3100.
102. Li, H., et al., *The Sequence Alignment/Map format and SAMtools.* Bioinformatics, 2009. **25**(16): p. 2078-9.
103. Liao, Y., G.K. Smyth, and W. Shi, *featureCounts: an efficient general purpose program for assigning sequence reads to genomic features.* Bioinformatics, 2014. **30**(7): p. 923-30.
104. Robinson, M.D., D.J. McCarthy, and G.K. Smyth, *edgeR: a Bioconductor package for differential expression analysis of digital gene expression data.* Bioinformatics, 2010. **26**(1): p. 139-40.
105. Kechin, A., et al., *cutPrimers: A New Tool for Accurate Cutting of Primers from Reads of Targeted Next Generation Sequencing.* J Comput Biol, 2017. **24**(11): p. 1138-1143.
106. Ritchie, M.E., et al., *limma powers differential expression analyses for RNA-sequencing and microarray studies.* Nucleic Acids Res, 2015. **43**(7): p. e47.
107. Abramowitz, Y., et al., *Severe aortic stenosis with low aortic valve calcification: characteristics and outcome following transcatheter aortic valve implantation.* Eur Heart J Cardiovasc Imaging, 2017. **18**(6): p. 639-647.
108. Nguyen, V., et al., *Sex Differences in the Progression of Aortic Stenosis and Prognostic Implication: The COFRASA-GENERAC Study.* JACC Cardiovasc Imaging, 2016. **9**(4): p. 499-501.
109. Clavel, M.A., et al., *Impact of aortic valve calcification, as measured by MDCT, on survival in patients with aortic stenosis: results of an international registry study.* J Am Coll Cardiol, 2014. **64**(12): p. 1202-13.
110. Wu, B., et al., *Developmental Mechanisms of Aortic Valve Malformation and Disease.* Annu Rev Physiol, 2017. **79**: p. 21-41.
111. Mishra, S. and D.A. Kass, *Cellular and molecular pathobiology of heart failure with preserved ejection fraction.* Nat Rev Cardiol, 2021. **18**(6): p. 400-423.
112. Faggiano, P., et al., *Progression of aortic valve sclerosis to aortic stenosis.* Am J Cardiol, 2003. **91**(1): p. 99-101.
113. Otto, C.M., *Calcific aortic valve disease: outflow obstruction is the end stage of a systemic disease process.* Eur Heart J, 2009. **30**(16): p. 1940-2.
114. Lui, C.Y. and N. Alexander, *Prolonged survival in 2 nonagenarians with heart failure and severe aortic stenosis.* Tex Heart Inst J, 2008. **35**(3): p. 321-2.
115. Nishimura, R.A., et al., *2017 AHA/ACC Focused Update of the 2014 AHA/ACC Guideline for the Management of Patients With Valvular Heart Disease: A Report of the American College of Cardiology/American Heart Association Task Force on Clinical Practice Guidelines.* Circulation, 2017. **135**(25): p. e1159-e1195.
116. Blaha, M.J., et al., *Relation of aortic valve calcium detected by cardiac computed tomography to all-cause mortality.* Am J Cardiol, 2010. **106**(12): p. 1787-91.
117. Di Minno, M.N.D., et al., *Cardiovascular morbidity and mortality in patients with aortic valve sclerosis: A systematic review and meta-analysis.* Int J Cardiol, 2018. **260**: p. 138-144.
118. Nchimi, A., et al., *Predicting Disease Progression and Mortality in Aortic Stenosis: A Systematic Review of Imaging Biomarkers and Meta-Analysis.* Front Cardiovasc Med, 2018. **5**: p. 112.
119. Pradelli, D., et al., *Impact of aortic or mitral valve sclerosis and calcification on cardiovascular events and mortality: a meta-analysis.* Int J Cardiol, 2013. **170**(2): p. e51-5.
120. Baumgartner, H., et al., *2017 ESC/EACTS Guidelines for the management of valvular heart disease.* Eur Heart J, 2017. **38**(36): p. 2739-2791.
121. Genereux, P., et al., *Natural History, Diagnostic Approaches, and Therapeutic Strategies for Patients With Asymptomatic Severe Aortic Stenosis.* J Am Coll Cardiol, 2016. **67**(19): p. 2263-2288.
122. Chandrasekhar, J., et al., *Sex-Based Differences in Outcomes With Transcatheter Aortic Valve Therapy: TVT Registry From 2011 to 2014.* J Am Coll Cardiol, 2016. **68**(25): p. 2733-2744.
123. Eberhard, M., et al., *Reproducibility of aortic valve calcification scoring with computed tomography - An interplatform analysis.* J Cardiovasc Comput Tomogr, 2019. **13**(2): p. 92-98.

124. Guimaraes, L., et al., *Transcatheter aortic valve replacement with the balloon-expandable SAPIEN 3 valve: Impact of calcium score on valve performance and clinical outcomes.* Int J Cardiol, 2020. **306**: p. 20-24.
125. Choi, B.H., et al., *Association between aortic valvular calcification and characteristics of the aortic valve in patients with bicuspid aortic valve stenosis.* Acta Radiol, 2019. **60**(4): p. 468-477.
126. Boulif, J., et al., *Assessment of aortic valve calcium load by multidetector computed tomography. Anatomical validation, impact of scanner settings and incremental diagnostic value.* J Cardiovasc Comput Tomogr, 2017. **11**(5): p. 360-366.
127. Tastet, L., et al., *Impact of Aortic Valve Calcification and Sex on Hemodynamic Progression and Clinical Outcomes in AS.* J Am Coll Cardiol, 2017. **69**(16): p. 2096-2098.
128. Myasoedova, V.A., et al., *Sex-specific differences in age-related aortic valve calcium load: A systematic review and meta-analysis.* Ageing Res Rev, 2020. **61**: p. 101077.
129. Matilla, L., et al., *Sex-Differences in Aortic Stenosis: Mechanistic Insights and Clinical Implications.* Front Cardiovasc Med, 2022. **9**: p. 818371.
130. Peeters, F., et al., *Biomarkers Associated With Aortic Valve Calcification: Should We Focus on Sex Specific Processes?* Front Cell Dev Biol, 2020. **8**: p. 604.
131. Lee, S.H. and J.H. Choi, *Involvement of Immune Cell Network in Aortic Valve Stenosis: Communication between Valvular Interstitial Cells and Immune Cells.* Immune Netw, 2016. **16**(1): p. 26-32.
132. Raddatz, M.A., et al., *Macrophages Promote Aortic Valve Cell Calcification and Alter STAT3 Splicing.* Arterioscler Thromb Vasc Biol, 2020. **40**(6): p. e153-e165.
133. Parra-Izquierdo, I., et al., *Calcification Induced by Type I Interferon in Human Aortic Valve Interstitial Cells Is Larger in Males and Blunted by a Janus Kinase Inhibitor.* Arterioscler Thromb Vasc Biol, 2018. **38**(9): p. 2148-2159.
134. McCoy, C.M., D.Q. Nicholas, and K.S. Masters, *Sex-related differences in gene expression by porcine aortic valvular interstitial cells.* PLoS One, 2012. **7**(7): p. e39980.
135. Aguado, B.A., et al., *Genes That Escape X Chromosome Inactivation Modulate Sex Differences in Valve Myofibroblasts.* Circulation, 2022. **145**(7): p. 513-530.
136. Cote, N., et al., *ATP acts as a survival signal and prevents the mineralization of aortic valve.* J Mol Cell Cardiol, 2012. **52**(5): p. 1191-202.
137. Towler, D.A., *Molecular and cellular aspects of calcific aortic valve disease.* Circ Res, 2013. **113**(2): p. 198-208.
138. Myasoedova, V.A., et al., *Aortic Valve Sclerosis in High-Risk Coronary Artery Disease Patients.* Front Cardiovasc Med, 2021. **8**: p. 711899.
139. Myasoedova, V.A., et al., *Aortic Valve Sclerosis as an Important Predictor of Long-Term Mortality in Patients With Carotid Atheromatous Plaque Requiring Carotid Endarterectomy.* Front Cardiovasc Med, 2021. **8**: p. 653991.

7. Appendix A

Overview of sex differences in the experimental models of CAVS.

Experimental model		Experiment description/Molecular pathway	Tested in females	Tested in males	References (PMID)
In vitro	**Ex vivo**				
Human aortic VICs		IFN-α–mediated inflammation and calcification		Observed to a higher degree	18671964
Human aortic VICs		PI3K/Akt/cell signaling survival pathway matrix-Gla protein expression BCL-2 gene expression	Upregulated		18671964
Human aortic VICs		IFN-γ-mediated pro-angiogenic, inflammatory, and calcific effects		Upregulated	27761653
Porcine aortic VICs		Angiogenesis Lipid accumulation MAPK/ERK-1/2 pathway Inflammation		Upregulated	18665344
Rat and porcine aortic VICs		Osteogenic differentiation Calcification		Upregulated	10760546
Porcine aortic VICs		Angiogenesis, lipid management and deposition, CNP, MAPK/ERK-1/2 pathways, and inflammation		Upregulated	22808080
	Human excised aortic valve leaflets	Fibrosis	Upregulated		27879282 32384012
	Human excised aortic valve leaflets	Calcification		Upregulated	27879282 32384012 25803964
Porcine and human aortic VICs	Human aortic VICs	Myofibroblastic activation	Upregulated		35000411
	Human aortic VICs	JAK/STAT, NF-kB mediated calcification and inflamation, BMP2 secretion, apoptosis		Upregulated	30026273